CREEP OF HI-NICALON S CERAMIC FIBER TOWS AT

ELEVATED TEMPERATURE IN AIR AND IN STEAM

THESIS

Benjamin R. Steffens, Captain, USAF

AFIT/GMS/ENY/12-M03

DEPARTMENT OF THE AIR FORCE
AIR UNIVERSITY

AIR FORCE INSTITUTE OF TECHNOLOGY

Wright-Patterson Air Force Base, Ohio

CREEP OF HI-NICALON S CERAMIC FIBER TOWS AT

ELEVATED TEMPERATURE IN AIR AND IN STEAM

THESIS

Presented to the Faculty

Department of Aeronautical and Astronautical Engineering

Graduate School of Engineering and Management

Air Force Institute of Technology

Air University

Air Education and Training Command

In Partial Fulfillment of the Requirements for the

Degree of Master of Science (Materials Science)

Benjamin R. Steffens

Captain, USAF

March 2012

CREEP OF HI-NICALON S CERAMIC FIBER TOWS AT

ELEVATED TEMPERATURE IN AIR AND IN STEAM

Benjamin R. Steffens

Captain, USAF

Approved:

_____	_____
Marina Ruggles-Wrenn, PhD (Chairman)	Date
_____	_____
Geoff Fair, PhD (Member)	Date
_____	_____
Thomas Eason, PhD (Member)	Date

Abstract

Structural aerospace components require materials to have superior long-term mechanical properties that can withstand severe environmental conditions, such as high temperatures, high pressures and moisture, whilst enduring the loads they are designed for. Ceramic-matrix composites (CMCs) are capable of maintaining excellent strength and creep resistance at high temperatures, which make them attractive candidate materials for aerospace applications, particularly in propulsion. Silicon Carbide (SiC) ceramic fibers have been used as constituent materials in CMCs, although oxidation of the SiC to SiO_2 has been a known degradation mechanism. Recently developed near stoichiometric SiC fibers have shown significant improvements in thermochemical stability; however performance of the new fibers at elevated temperatures in steam environments has not been studied thoroughly. The objective of this thesis is to investigate creep of near stoichiometric SiC fiber tows at elevated temperatures in air and in steam environments.

The creep response of Hi-Nicalon™-S SiC fiber tows was investigated at 800°C and 1100°C in laboratory air and in steam environments. The creep stresses ranged from 76 MPa to 1560 MPa. Creep run-out was defined as 100 h at creep stress. The presence of steam significantly degraded the creep performance of the fiber tows both at 800°C and at 1100°C. The creep lifetimes of the Hi-Nicalon™-S SiC fiber tows were reduced by approximately an order of magnitude due to steam.

Acknowledgements

Table of Contents

List of Figures

List of Tables

CREEP OF HI-NICALON S CERAMIC FIBER TOWS AT ELEVATED TEMPERATURE IN AIR AND IN STEAM

I. Introduction

Materials development has set the pace for much of our technological advancements and continues to do so. Examining history and how the eras have been labeled, (i.e. Stone age, Bronze age, Iron age), can effectively represent the evolution of mankind by the materials used at the time. The world is currently at a time where technology is driven by harnessing the individual performance characteristics of two or more constituent materials in a synergistic mass, hence what may be called the "The Composite Age".

Composite materials have been used in various ways throughout history. However, research and development of composite materials for use in engineering applications has grown dramatically since the turn of the 20th century. Honeycomb structures, powder metallurgy, and glass reinforced plastic were the advanced structural material technologies in the 1930s and 1940. Continuous glass fibers were first produced commercially in 1939 [36]. Advanced fibers such as boron and carbon were developed in the 1950's and 1960's [19]. From 1965 to 1973, the United States Air Force led 80% of the research and development effort to bring high performance fiber composites to practical applications [7].

Composite materials made their appearance in commercial airplanes with the introduction of the Boeing 707 in the 1950s. Composites comprise 9% of the aircraft structural weight in the Boeing 777. Fighter aircraft produced in the late 1970s such as the F-15 and F-16 incorporated about 1-2% composites into the airframe of by weight. The use of composites increased greatly in the next generation of fighter aircraft (Figure 1), so much so that the F/A-18E/F and F-22A are

approximately 25% composites by weight [12]. Today, composites make up a large percentage of aircraft components, for example the fuselage and wings of the Boeing 787 Dreamliner consist mostly of composites which make up 50% of the aircraft by weight [1].

Figure 1 : USAF F/A-22 multi-role aircraft [2]

Traditional metal alloys found in the power plants of aircraft today are now being replaced by ceramic matrix composites (CMC). This has raised the limitations on the operating temperatures that the propulsion systems can attain. In turbine engines, operating at higher temperatures allows for increased power, reduced fuel consumption, and a reduction in emissions. [10]. Figure 2 demonstrates that CMCs have far surpassed the temperature limits of the previously used aerospace materials.
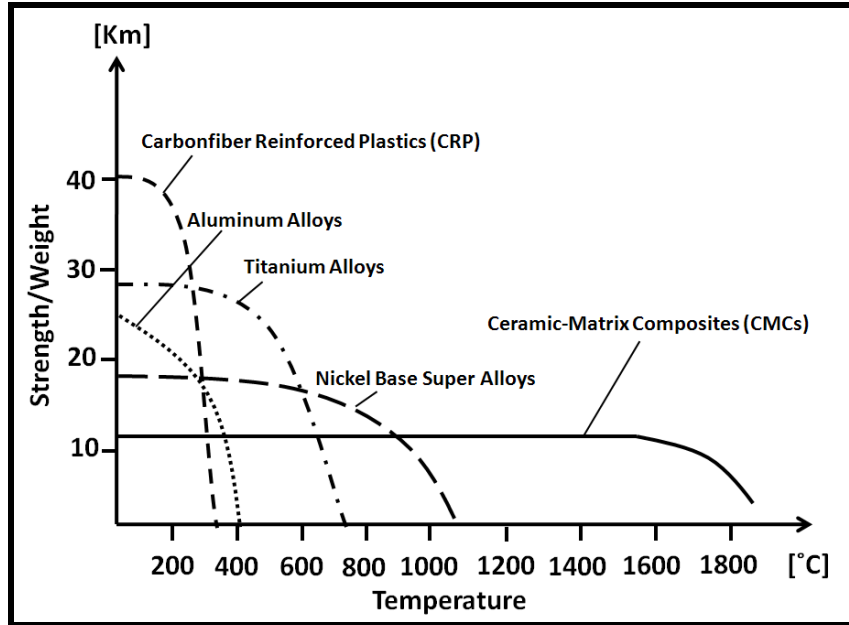
Figure 2 : Strength to weight ratio as a function of temperature for select aerospace materials [31].

II. Background

2.1 Ceramic Matrix Composites

In the recent decades many active material science and engineering research efforts have been directed towards ceramic matrix composites (CMC). CMCs are designed to withstand high temperatures and extreme environments, while remaining load carrying members of a structure. Structural components for hypersonic vehicles, rockets, jet engines, power plants, space vehicles, and furnaces are some of the candidate uses for CMCs [29].

Ceramic-matrix composites are currently being evaluated for use in aerospace turbine engines and are likely to be incorporated in combustion chambers and nozzle extensions of the advanced rocket propulsion systems. The lower densities of CMCs and their higher use temperatures, together with a reduced need for cooling air, allow for improved high-temperature performance when compared to conventional nickel-based superalloys. Table 1 provides additional examples of military and commercial applications of CMCs.

Table 1 : CMC Applications [1]

Applications / Sectors	Continuous Fiber CMCs		
MILITARY	• F414 and F110 Nozzle Flaps and Seals • F117 Aft Deck Heat Shields • Engine Vanes • Flame Holders	• Orbital Transfer Engine Thrusters • Low Cost Large Rocket Thruster (Million Pound) Heavy Lift Launch • Tactical Missile Combustors, Rotors • Divert and Attitude Control Thrusters	• Turboramjet Variable Area Nozzles • Surveillance OTV Thrusters • Hypersonic Leading Edges, Inlet Cowlings and Nozzles • Linear Aerospike Engine, Thrust Cells and Ramp
Commercial/Dual Use	• Heat Exchangers • Radiant Burner Tubes • Land-Based Gas Turbines • Candle Filters	• MDH Air Preheater Tubes • Immersion Heaters • Seal-less Magnetic Pumps • Motorcycle Brakes	• Diesel Components • Valve Guides • Pistons • Turbocharger Rotors

Attempts to emphasize the favorable properties while minimizing the undesirable properties of ceramic materials led to significant developments in the area of CMCs. One of the inherent limitations of ceramic materials is their brittle nature. Monolithic ceramics tend to have low toughness, low ductility and unanticipated catastrophic failure. Therefore, in order to use ceramic materials in structural applications, the CMCs were developed. The objective of the CMC design is to retain the desirable mechanical, thermal, and environmental properties of ceramics while providing a mechanism for a more graceful failure. To be useful for engineering applications the CMCs must exhibit high strength and fracture toughness at high temperatures. Therefore the main advantages of CMCs over monolithic ceramics are their superior toughness, tolerance to the presence of defects, and non-catastrophic mode of failure. Figure 3 shows typical tensile stress-strain curves for a monolithic ceramic material and for a CMC.
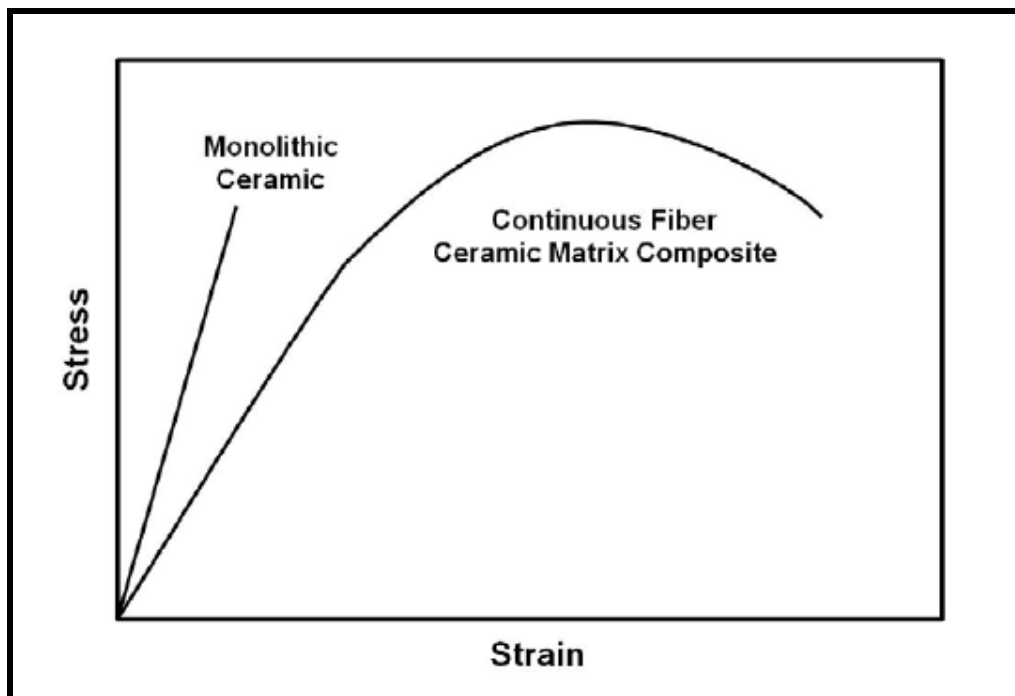
Figure 3 : Stress-Strain Curves, Monolithic ceramic vs. CMC [3]

5

In order to improve the fracture toughness of a CMC, cracks must be allowed to propagate within the material before catastrophic failure. Propagating matrix cracks must be deflected at the fiber-matrix interface while allowing the fiber to bear load in order to avoid brittle failure in a CMC. Crack deflection around the fibers leads to formation of the fiber bridged matrix cracks as loads are progressively transferred to fibers, and finally to uncorrelated fiber fracture and subsequent fiber pullout [13, 23]. Therefore, the fibers are able to maintain load-carrying capability upon matrix cracking before the entire system gradually fails as is shown in Figure 4.
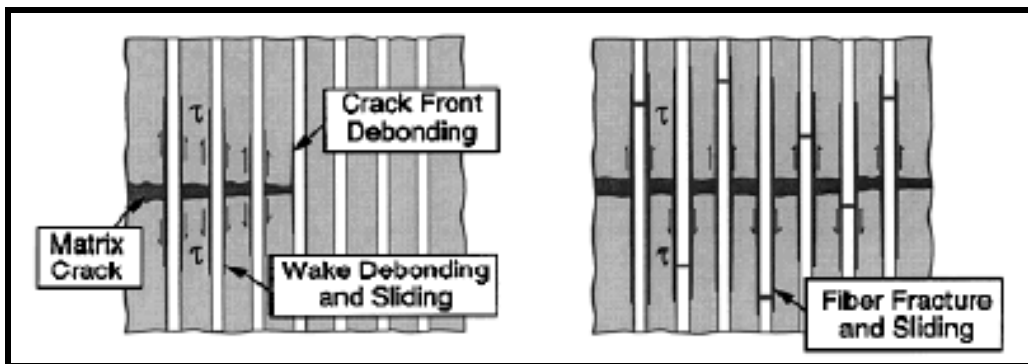
Figure 4 : Fiber/matrix interface [38]

CMCs offer superior long-term mechanical properties and retained properties under high temperature. Yet, because in many engineering applications the CMCs are exposed to oxidizing environments at high temperatures, the thermodynamic stability and oxidation resistance of CMCs are vital issues. As CMCs emerged, one of the limitations of the early SiC–based fibers, like Nicalon and Hi-Nicalon, was degradation by oxidation. Oxidation of SiC-based fibers severely degrades their mechanical properties and performance. In order to use CMCs in combustion environments, like jet engines, their environmental resistance and mechanical performance in such environment must be assured [25, 27, 32, 33, 35].

2.2 Silicon Carbide Based Fibers

SiC-based fibers have been produced since the mid-1960s by chemical vapor deposition (CVD) onto a tungsten or carbon filament core. Resulting filaments had large diameter (100–140 μm) diameter, which together with the lack of flexibility limited their use as the reinforcement for metals such as aluminum, titanium, and intermetallics. In the 1980s fine SiC-based fibers with diameters of 10 μm were developed. This development opened the possibility of reinforcing ceramic materials with ceramic fibers in order to produce high-temperature structural composites. Schematic in Figure 5 shows the process of producing fine silicon carbide fibers by the melt spinning, crosslinking, and pyrolysis of an organosilicon polymer.
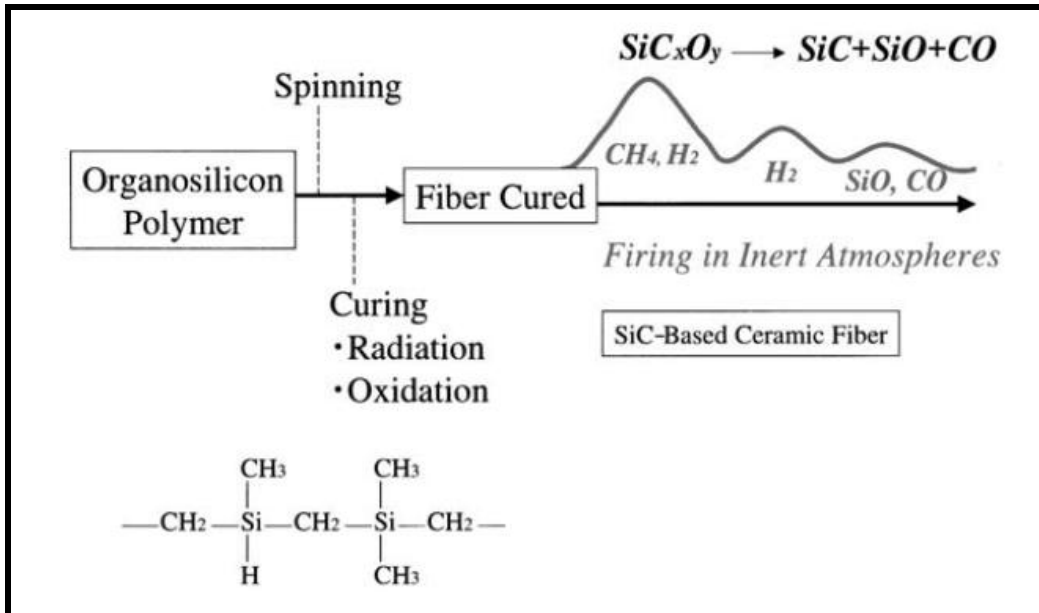
Figure 5 : Fundamental production process of SiC-based fibers using PCS precursor [21]

It is recognized that all SiC-based fibers are not pure SiC. The Si-based fibers of first generation such as Nicalon fiber (manufactured by Nippon Carbon, Japan), consist of SiC-

nanocrystals (1–2nm in size) and free carbon embedded in an amorphous SiCxOy matrix. Consequently, their stiffness (220 GPa) is much lower than that of pure SiC (400 GPa), while their strain at failure is fairly high (~1.4%). Furthermore, these fibers suffer severe strength degradation at temperatures above 1200 °C. Hence, SiC/SiC composites reinforced with these fibers must be processed at low temperatures (i. e. using CVI or PIP techniques) and the use of these composites would be limited in temperature.

Numerous studies performed on the first generation SiC-based fibres led to the conclusion that it the non-stoichiometric composition of the fibres was limiting their performance and physical characteristics. The oxygen which remained in the fibres after pyrolysis formed an amorphous intergranular Si–O–C phase [5]. The presence of this amorphous phase was responsible for the loss of fiber strength and creep at temperatures around 1000-1100°C, where bulk SiC be expected to exhibit excellent strength and creep resistance. The fact that the Young's modulus of the fibers was only half of that of bulk SiC could be accounted by a low fraction of a granular SiC phase in the fibers. These findings demonstrated that in order to produce improved fibers, it was necessary to achieve a more stoichiometric composition and to considerably reduce the oxygen content in the fiber.

SiC-based fibers of second generation, such as Hi-Nicalon, are oxygen-free. They consist of SiC-nanocrystals (average size ~5 nm) and free carbon [C/Si (at) ratio=1.39]. Because these fibers do not contain significant amounts of SiCxOy phase they do not undergo decomposition at high temperature. The SiC-based fibers of second generation creep at ~1200 °C. However, heat treating them at 1400-1600°C stabilizes the microstructure and improves their creep resistance. It was found that the Hi-Nicalon fiber did not creep at temperatures below 1000°C. Furthermore, Hi-Nicalon fiber was shown to possess the highest creep threshold and to produce the lowest

strain rate among the first and second generation SiC-based fibers. However, at 1400°C all first and second generation SiC fibers produced very similar creep rates ($\sim$5 $\times$ 10^{-7} s^{-1} under a stress of 0.3 GPa) [5]. The activation energy for the creep of Hi-Nicalon fibers was determined to be ~360 kJ/mol and the predominant creep mechanism was identified as grain boundary sliding accommodated by interface-controlled diffusion. It was recognized that the carbon layers located between the grains could facilitate the grain boundary sliding. It was found that the ultimate failure of the fibers in creep was not to be due to a lack of accommodation, as is the case for bulk ceramics. It was concluded that the ultimate failure in creep was caused by surface defects, such as cavities or porous zones growing from local chemical heterogeneities [5].

The development of the small diameter SiC fibers was primarily driven by the need of the gas turbine generator industry for materials capable of withstanding higher temperatures than the nickel based superalloys which are limited to a maximum temperature of 1150°C. The development of ceramic matrix composites based on first generation or second generation fibers did not meet all the high temperature requirements. Further improvements in the high temperature stability of the fibers were needed. Industry needs drove the development of more stoichiometric fibers which would be stable in air at temperatures up to 1400°C. Nippon Carbon recognized that to achieve near stoichiometry the excess carbon in the Hi-Nicalon fiber had to be reduced. The radiation cured precursor route utilized to produce the Hi-Nicalon fiber became an intermediate step in producing a near stoichiometric SiC fiber without the use of sintering aids. The Hi-Nicalon fiber was then heated to ~1500°C in a hydrogen rich atmosphere to reduce the excess carbon from a C/Si ratio of 1.39 to 1.05 to achieve the near stoichiometric fiber called Hi-Nicalon-Type-S [20].

Microstructures of Nicalon, Hi-Nicalon and Hi-Nicalon S fibers are shown schematically in Figure 6.
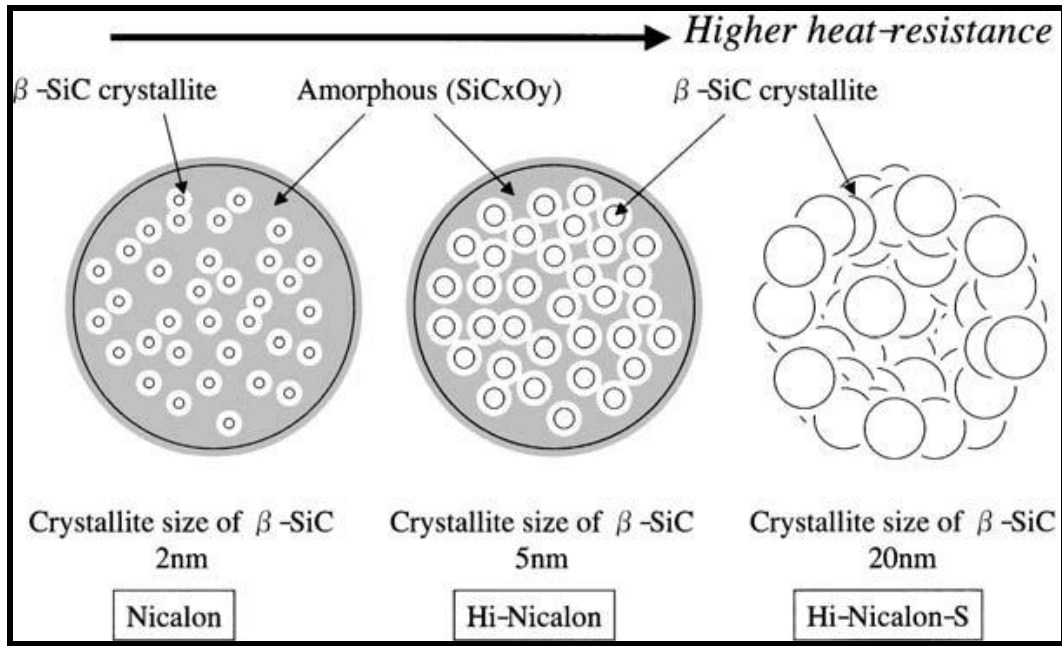
Figure 6 : Schematic Showing Microstructures of Nicalon, Hi-Nicalon and Hi-Nicalon S Fibers [21]

Efforts to reduce the oxygen content by processing in inert atmospheres and crosslinking by radiation have produced fibers with very low oxygen contents and nearly stoichiometric chemical composition. Hi-Nicalon S is formed from a polycarbosilane (PCS) precursor. The fundamental process that the fiber undergoes during fabrication is outlined in Figure 5. The filaments are cured by electron irradiation and pyrolyzed by a modified Hi-Nicalon process in a closely controlled atmosphere from 1600 – 2000°C [30]. They primarily consist of relatively large (20 – 200nm) SiC grains and several phases, which considerably influence the thermal stability of the fibers. As a result excess carbon from processing is reduced and an almost 1 to 1 ratio of Carbon to Silicon is achieved, which enhances the fiber material by making it more

chemically stable and therefore more oxidation resistant and consequently more thermally

resistant [30].

Table 2 : Specifications and Material Properties of various SiC Fiber Tows [21]

☐ : Nearly stoichiometric SiC fiber

	SiC Fibers							
	Nicalon			Tyranno				Sylramic
	NL-200	Hi-Nicalon	Hi-Nicalon–s	Lox M	ZMI	ZE	SA*	
Atomic Composition	$SiC_{1.34}$ $O_{0.36}$	$SiC_{1.39}$ $O_{0.01}$	$SiC_{1.05}$	$SiTi_{0.02}$ $C_{1.37}O_{0.32}$	$SiZr_{<0.01}$ $C_{1.44}O_{0.24}$	$SiZr_{<0.01}$ $C_{1.52}O_{0.05}$	SiC $O,Al_{<0.008}$	$SiCTi_{0.02}$ $B_{0.09}O_{0.02}$
Tensile Strength (GPa)	3.0	2.8	2.6	3.3	3.4	3.5	2.8	3.0
Tensile Modulu (GPa)	220	270	410	187	200	233	410	420
Elongation (%)	1.4	1.0	0.6	1.8	1.7	1.5	0.7	0.7
Density (g·cm⁻³)	2.55	2.74	3.10	2.48	2.48	2.55	3.02	>3.1
Diameter (µm)	14	14	12	8 & 11	8 & 11	11	8 & 10	10
Specific Resistivity (Ω · cm)	10^3-10^4	1.4	0.1	30	2.0	0.3	—	—
Thermal Expansion coeff. (10^{-6}/K)	3.2 (25-500℃)	3.5 (25-500℃)	—	3.1	4.0	—	4.5 (20-1320℃)	—
Thermal Conductivity (W/mK)	2.97(25℃) 2.20(500℃)	7.77(25℃) 10.1(500℃)	18.4 (25℃) 16.3 (500℃)	—	2.52	—	64.6	40-45

Continuous fiber reinforced ceramic composites are potential candidates for use at

temperatures. SiC fiber-reinforced SiC matrix composites are currently being evaluated for use

in various applications, including aircraft jet engines, gas turbines for electrical power/steam

cogeneration, as well as nuclear power plant components. It is recognized that the structural

performance of the CMCs is controlled by the strength of the fibers. Therefore, the sensitivity of

fibers to temperature and environmental effects is a critical factor in development of composites

with load carrying capacity and environmental durability. Multifilament tows, which comprise

several hundreds of single filaments, represent a fundamental unit in textile composites. Fiber

tows progressively carry the load as the matrix becomes more and more damaged and control the

ultimate failure of the composite. Multifilament tows are damage tolerant, while single fibers are brittle. The ultimate failure of the fiber tows is preceded by breaks of individual fibers.

Lamon and co-workers studied the delayed failure of SiC fiber tows at intermediate temperatures (600°C-800°C) in air [14, 15, 16]. Forio et al [14] subjected Nicalon fiber tows to static fatigue at temperatures in the 600°C-700°C range. The delayed failure of the fiber tows was attributed to the phenomenon of slow crack growth activated by oxidation. Gauthier and Lamon [15] investigated static fatigue of Hi-Nicalon and Hi-Nicalon S multifilament tows at temperatures in the 500°C-800°C range in air. Static fatigue of single filaments was also examined. A thorough analysis of the stress–rupture time data was presented. A model based on slow crack growth in single filaments was shown to successfully represent delayed failure of fiber tows. Gauthier et al [16] examined oxidation of SiC-based fibers (Nicalon, Hi-Nicalon, and Hi-Nicalon S) during static fatigue at temperatures in the 500°C-800°C range. The results demonstrated that the delayed failure of the fiber tows was caused by subcritical crack growth of the surface defects by oxidation of the grain boundaries (free carbon) and the SiC nanograins or silicon oxicarbide at the crack tip.

2.3 Research Objectives

The main focus of this research effort is on mechanical performance of SiC-based fibers at elevated temperatures in air and steam. In order for SiC/SiC CMCs to be safely used in advanced aerospace applications such as jet engines, their environmental durability at elevated temperatures in operating environments must be assured. Therefore, a thorough understanding and analysis of the performance of SiC-based fibers at elevated temperature in oxidizing

environment is required. The main objective of this research is to evaluate the effects of steam on creep performance of Hi-Nicalon S fiber tows at 800 and 1100°C.

An experimental facility had been designed and a test method had been developed previously by Major Clint Armani for the testing of oxide fibers in air and steam [3]. In the course of the present effort the experimental facility was adapted to testing of higher strength SiC fiber tows. In addition, several adjustments were made in order to achieve more consistent heating of the test specimens. The test method employed in the present effort permitted accurate load control and, most importantly, accurate strain measurement. Creep strains were measured and creep rates were determined.

III. Material and Test Specimen

3.1 Material

This research studied Hi Nicalon^{TM} Type-S fiber tows, the SiC-based fiber tows manufactured by Nippon Carbon Co. (Tokyo, Japan). The fiber tow consisted of approximately 500 filaments with an average diameter of 12 μm [34]. Based on this data, a cross sectional area of 5.655×10^{-8} m^2 was used for all engineering stress calculations.

3.2 Test Specimen

The first group of fiber tow specimens was prepared using the tabs designed by Armani for testing of the oxide fiber tows [3]. That tab design included a 0.75 in. x 1.50 in. primary tab and a 0.75 in. x 0.75 in. secondary tab (see tab design labeled First Iteration in Figure 7). This tabbing method worked well for the oxide fiber tows, which have lower filament count and lower tensile strength, and consequently were tested at lower creep stress level. However, when the higher strength Hi-Nicalon S fiber tows containing a larger number of filaments were tested in creep, this tabbing method proved inadequate. Fiber tow pulled out from the tab at all but the lowest creep stress levels rendering the creep tests unsuccessful. Hence an alternative tabbing method was attempted.

The second tabbing method still utilized a primary tab and a secondary tab, but increased the adhesion area from 0.75 in. x 0.75 in. to 1.00 in. x 1.00 in. The second tab design is shown in Figure 7, where it is labeled Second Iteration. This tabbing design also proved inadequate as it resulted in fiber pullout at higher creep stress levels.

The third method was developed that utilized a primary tab, a secondary tab and a tertiary tab. In this method, the excess tail of the fiber tow was folded over the secondary tab, then a tertiary tab was bonded to the secondary tab effectively capturing the folded over portion of the tow. This method was demonstrated to perform well for all required creep stress levels. The third tab design is shown in Figure 7, where it is labeled Third Iteration and in Figure 8.
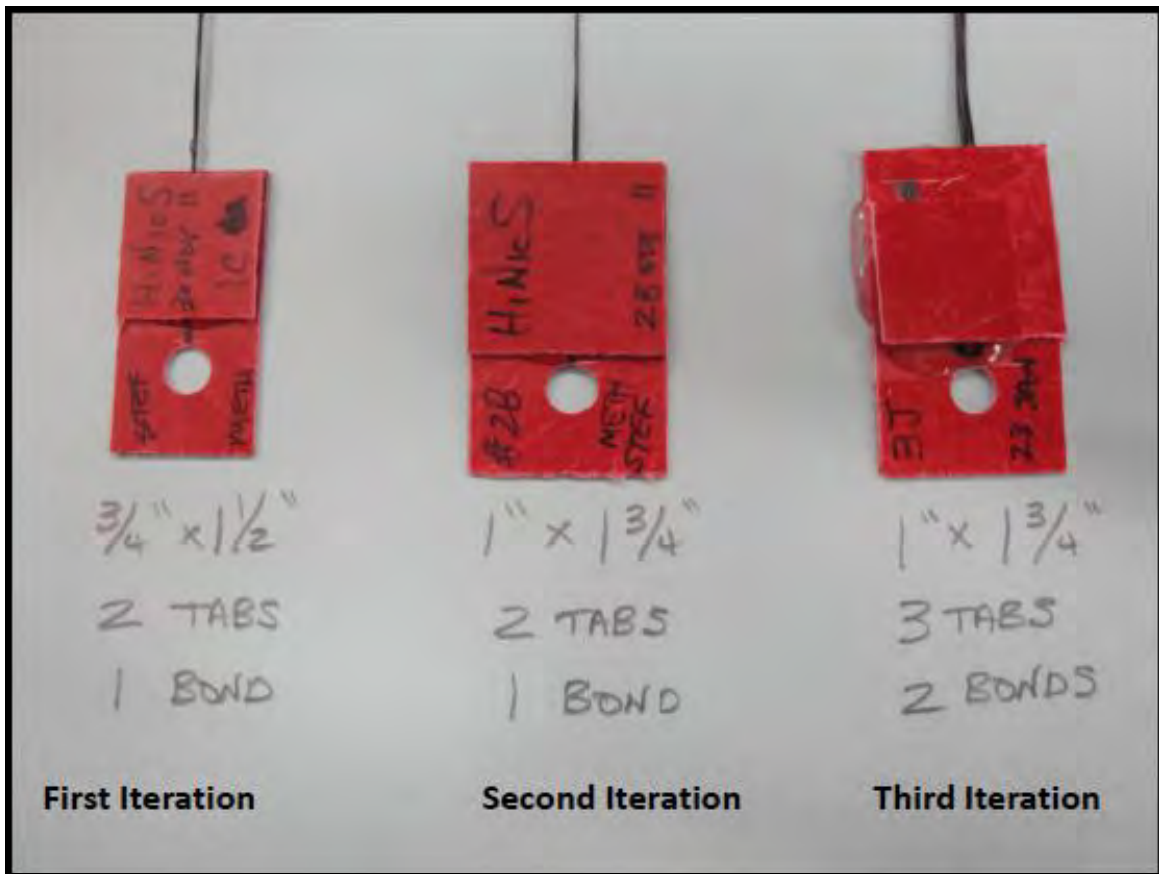
Figure 7 : Three tab designs used in the current research.
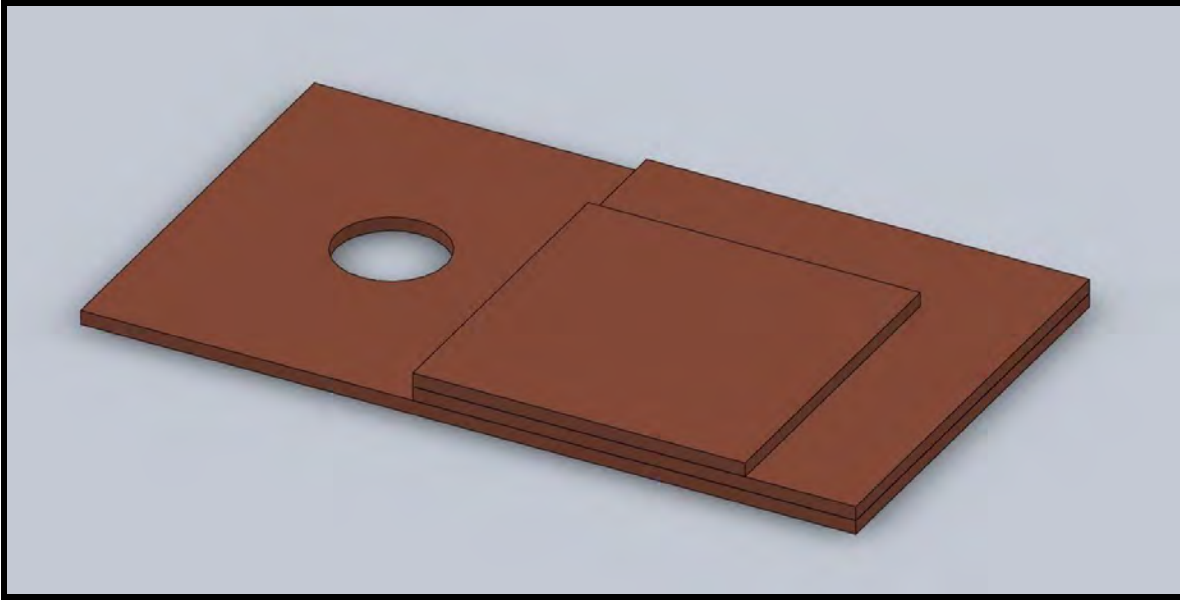
Figure 8 : A solid model of the third iteration tab.

In preparing the fiber tows for testing, excess lengths of tow were taken from the manufacturer's spool. Areas of the tow that contained obvious damage, to include broken filaments and curled fibers were discarded. Each tow section was taped onto a cutting board utilizing grid lines for alignment. Fiberglass tabs were prepositioned seven inches apart on the grid section. A two part epoxy (Hardman Double Bubble Epoxy, 04001) was then applied to the tow section on top of the primary tab, and the secondary fiberglass tab was applied in order to sandwich the tow and the epoxy between the fiberglass tabs. Once the adhesive had thickened (after 5 minutes), the excess tow protruding beyond the tabs was folded forward toward the test section. A second application of two part epoxy was then applied to the folded tow section on top of the secondary tab, and a tertiary fiberglass tab was applied in order to sandwich the folded portion of the tow between the secondary and tertiary fiberglass tabs. After letting the adhesive fully cure, the excess tail that remains beyond the tertiary tab is cut with a razor blade. The final tow length measured between tabs was seven inches for all experiments. For installation into the

16

creep testing equipment, a centerline hole was punched in the fiberglass tabs to permit hanging the fiber tow specimen on the hook fixtures. The primary tab dimensions were 1.75 in. x 1.0 in., the secondary sandwiching tab had dimensions of 1.00 in. x 1.00 in. and the tertiary sandwiching tab had dimensions of 0.75 in. x 0.75 in.

A detailed description of the specimen preparation procedure is given in Appendix A1.

IV. Experimental Arrangements and Procedures

The experimental facility for testing fiber tows at elevated temperature in air and in steam environment was designed and assembled by Major Clint Armani in the Mechanics of Advanced Aerospace Materials Laboratory of the Department of Aeronautics and Astronautics at the Air Force Institute of Technology. Additionally, the methods for testing ceramic fiber tows under monotonic tension and creep loadings at elevated temperature in air and in steam environments were developed by Major Clint Armani [ref Armani dissertation].

It has been established that the tensile strength of ceramic fiber tows is generally less than the mean strength of fiber filaments [6, 8, 26]. Nevertheless, it was concluded that because composites utilize fiber tows, the experiments conducted on fiber tows were more representative of the actual service conditions than those conducted on single filaments. Additionally, Dassios et al. [9] and Calard et al. [6] also concluded that experiments conducted on fiber tows were more representative of actual composites containing the fiber tows rather than single filaments. These results and observations support the decision to investigate the creep response of fiber tows rather than that of the single filaments in this work.

The creep performance of HI-Nicalon S fiber tows was investigated in air and in steam at the temperatures of 800°C and 1100°C. Creep experiments were performed at stresses ranging from 76 to 1560 MPa in order to establish dependence of creep behavior on the applied stress. Creep run-out was set to 100 hours. All creep tests were performed in air and in steam in order to evaluate the effects of steam environment on creep behavior. In each test, load-displacement data were recorded during the initial heating, during loading to the creep stress level, and during the actual creep period. Thus applied stress, thermal strain, the total mechanical strain, and the creep strain could be calculated and examined. In all tests, a heating rate of 1.0°C/s was used, and the

targeted temperature was maintained for a minimum of 45 minutes before beginning each test in order to achieve thermal equilibrium. During heat-up and heat-soak each specimen was subjected to a small weight of 10 to 20 grams in order to keep the fiber tow taut. It is noteworthy that in all tests the failures occurred in the heated gauge section of the specimen. Analysis of the experimental data provided insight into the creep and the environmental degradation occurring in the fiber tows at elevated temperatures.

An experimental facility for testing fiber tows at elevated temperature in air and in steam environment was designed and configured at AFIT. An MTS FlexTest 40 digital controller was used for data acquisition. High temperature environment was provided by an MTS 653.03A two-zone furnace, shown in Figure 9, with silicon carbide heating elements and two R-type control thermocouples, which supplied feedback to an MTS 409.83 temperature controller. The furnace had a 3.5 inch (90 mm) hot zone. Temperature profiles were measured throughout the length of the furnace using an S-type thermocouple. Once the temperature profile throughout the length of the furnace was established, an effective gauge length of the fiber tow specimen was calculated, which enabled the calculation of engineering strain from recorded displacement measurements. This technique is discussed in detail in Section 4.2 All tests on fiber tows employed an alumina susceptor (ceramic tube with endcaps) designed to fit inside the furnace. The use of the susceptor resulted in a more uniform and repeatable temperature distribution along the fiber tow specimen. Therefore the susceptor was used for all fiber tow testing. The gauge section of the fiber tow specimen was located inside the susceptor with the ends of the fiber tow specimen passing through slots in the susceptor end caps. Additionally, a hole was cut in the side of the susceptor in order to inject steam through a feeding tube. Figure 10 shows the susceptor set in one half of

the furnace with the steam injection tube entering the susceptor at the bottom and a fiber tow specimen suspended from an extendable fixture of the creep test setup.

A model HGA-H from MHI steam generator (see Figure 11) generated steam at 50 mL/hr using deionized water. Steam was supplied to the susceptor through a ceramic feeding tube (see Figure 10) in a continuous flow with a slightly positive pressure, expelling the dry air and creating a near 100% steam environment inside the susceptor.
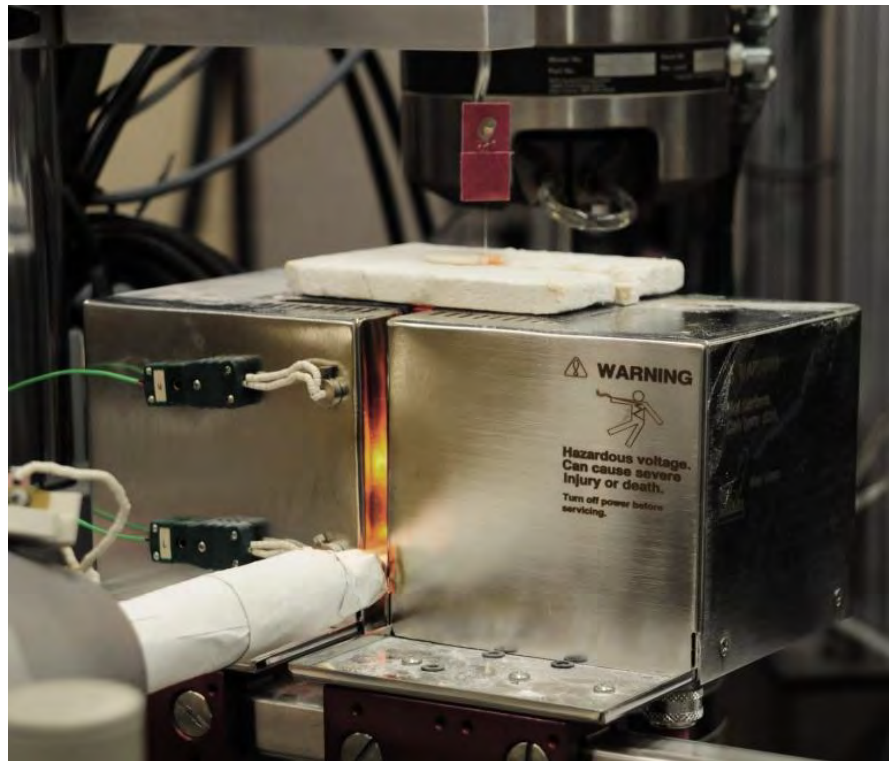
Figure 9 : MTS 653.03A two-zone furnace used for fiber tow testing. Reproduced from [3].
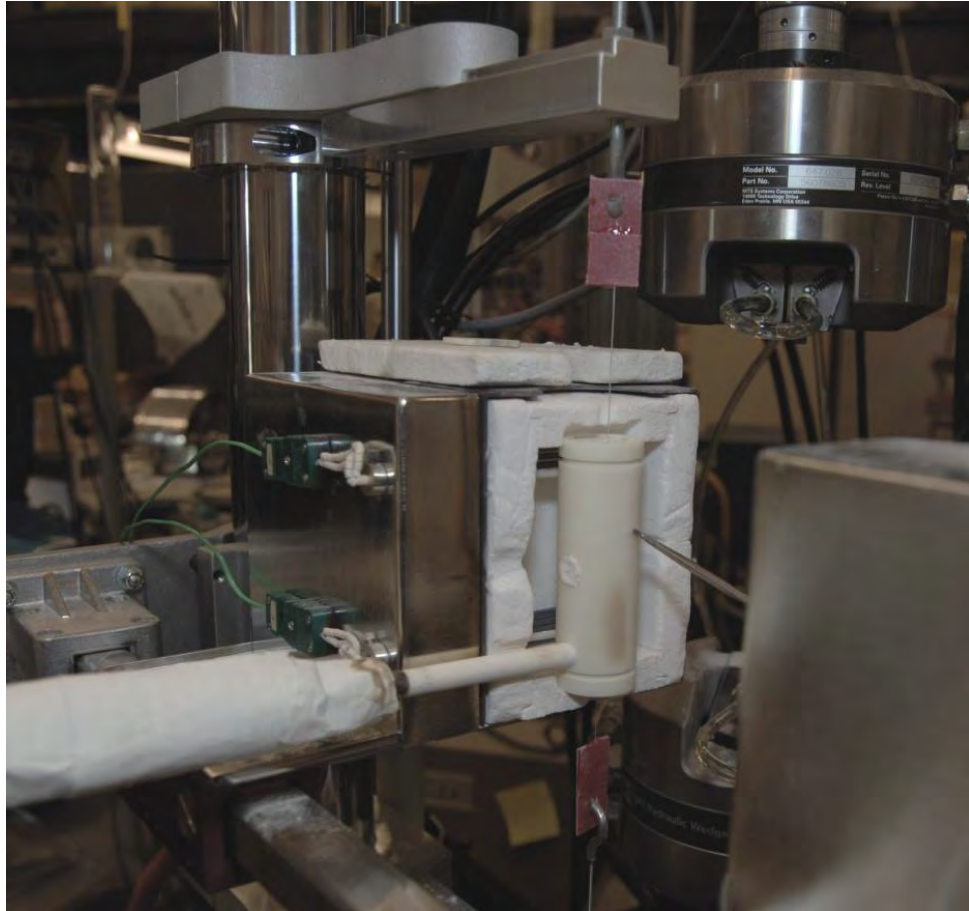
Figure 10 : Experimental setup for creep testing of fiber tows with susceptor and steam feeding tube. Reproduced from [3].
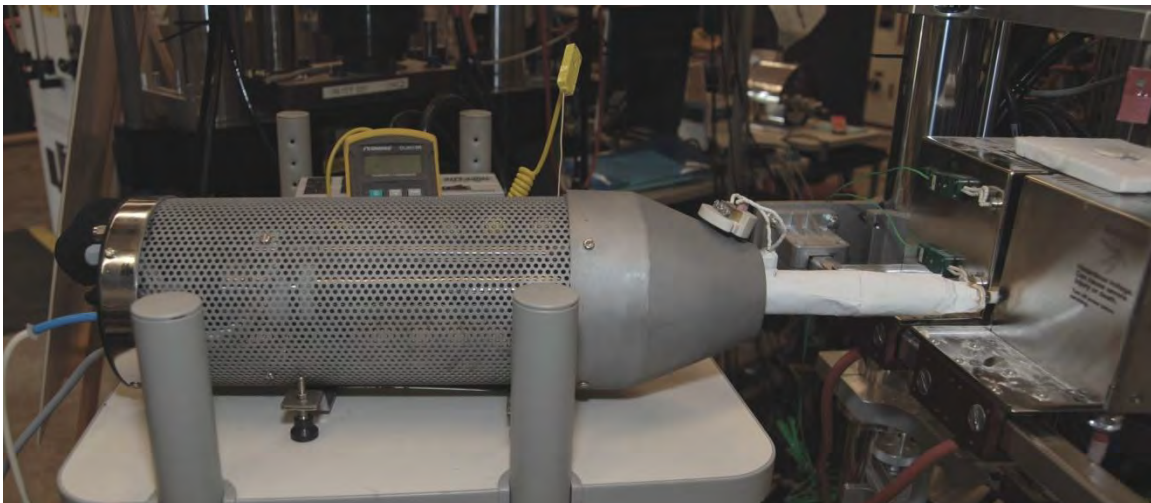
Figure 11 : MHI model HGA-H steam generator. Reproduced from [3].

A dead weight setup developed by Armani [3] was used for creep testing of the Hi-Nicalon S fiber tows at elevated temperatures in air and in steam. Two extendable fixtures for suspending the test specimens are an integral part of the dead weight creep testing facility. The upper fixture contains a hook for hanging the upper tab of the specimen. The lower fixture holds a Schaevitz M12-30 LVDT, which measures the elongation of the fiber tow specimen. The LVDT extension rod hooks onto the bottom tab of the fiber tow specimen. A second LVDT extension rod extends from the bottom of the LVDT core and contains nuts and washers at the bottom for applying the desired load. Finally, a hand-driven screw elevator is used to slowly apply the load to the fiber tow specimen. Slow application of the load is essential to prevent damage to the tow during the initial loading. Figure 20 shows a fiber tow specimen mounted in the dead weight creep testing facility. The fiber tow specimen is suspended from the upper fixture hook through the furnace. The LVDT is held by a phenolic block mounted on the end of the lower fixture, and the weights are stacked on the LVDT lower extension rod.

A detailed description of the specimens mounting procedure and of the creep test procedures is given in Appendix A1 and A2 respectively. A stress-weight index for the stackable weights is provided in Appendix A3
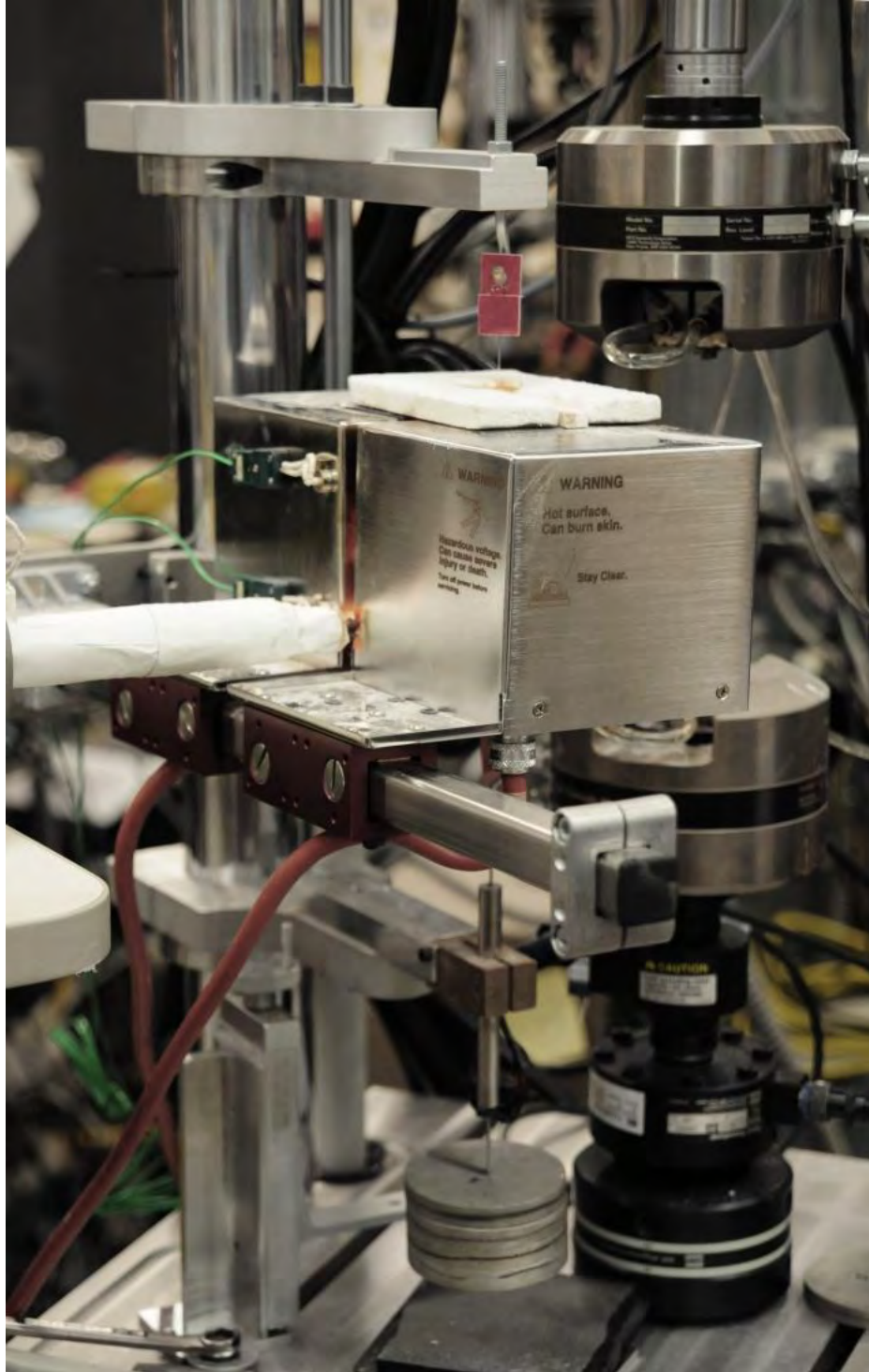
Figure 12 : Fiber tow specimen mounted in the dead weight creep testing facility. Reproduced from [3].

4.1 Temperature Profiles

Temperature profiles for fiber tow testing were determined by measuring the temperature vertically along the centerline of the furnace with an S-type thermocouple. The S-type thermocouple was approximately 6 inches in length and comprised of an unshielded tip with 1/8 in. diameter ceramic insulation used to protect the lead wires. A CL3515R model thermometer was used for temperature readings. The accuracy of these components was ±1.5°C for the S-type thermocouple and ±1.5°C for the thermometer. During the temperature measurements, the thermocouple was attached to a magnetic v-block fixture, which was attached to the ram of the servo-hydraulic machine. This allowed for convenient probing throughout the length of furnace.

In order to improve thermal insulation of the furnace and to shield the upper grip and the specimen tab, a 0.5-in. thick piece of oxide insulation board was placed on top of the furnace. In order to determine the furnace controller temperature setpoints, the thermocouple was positioned in the center of the furnace as the temperature was increased. To obtain the desired temperature setpoints of the upper and lower temperature controllers, an iterative process was performed by moving the thermocouple up and down from the center point of the furnace and adjusting the setpoints. The heating elements and furnace control couples were approximately 6 cm apart vertically. Therefore, initial observations of the temperature profile were obtained in the vertical region located within ±3 cm from the center of the furnace. Once the desired setpoints for the temperature controllers were determined, a detailed temperature profile was obtained by taking measurements every 5 mm along the vertical axis of the furnace starting at the bottom inner surface of the susceptor and ending at the top inner surface of the susceptor.

Temperature profiles obtained for 800°C, 900°C, 1000°C, 1100°C, and 1200°C in air and in steam are provided in Figures 13, 14, 15, 16 and 17, respectively.
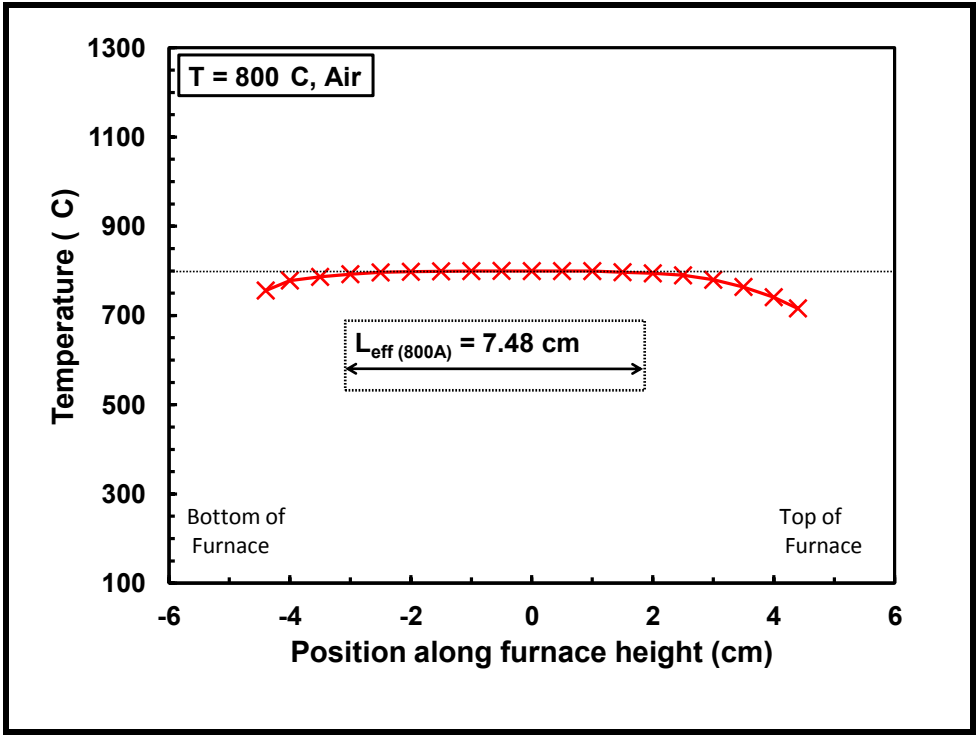
(a)
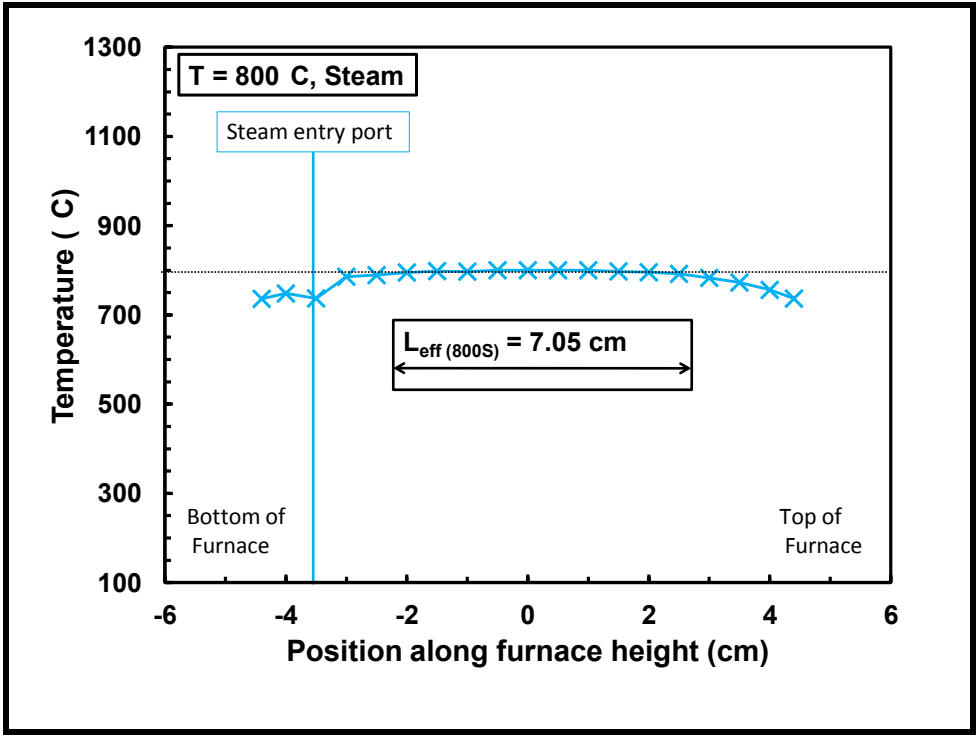
(b)

Figure 13 : Temperature profile obtained for Hi Nicalon^{TM} Type-S fiber tow specimen at 800°C: (a) in air and (b) in steam.
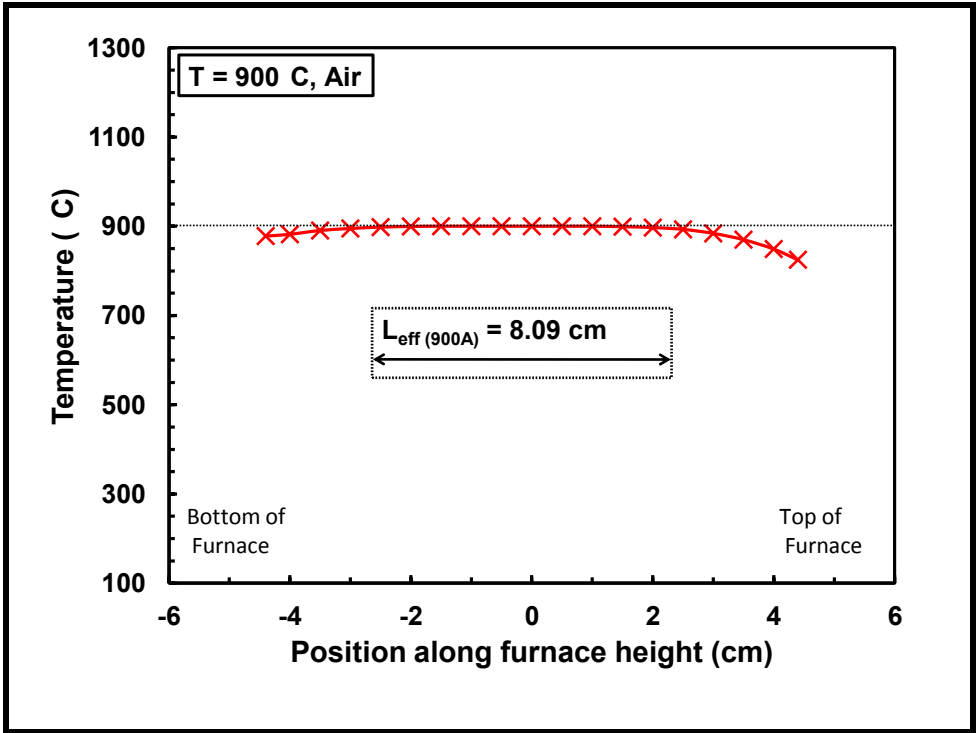
(a)
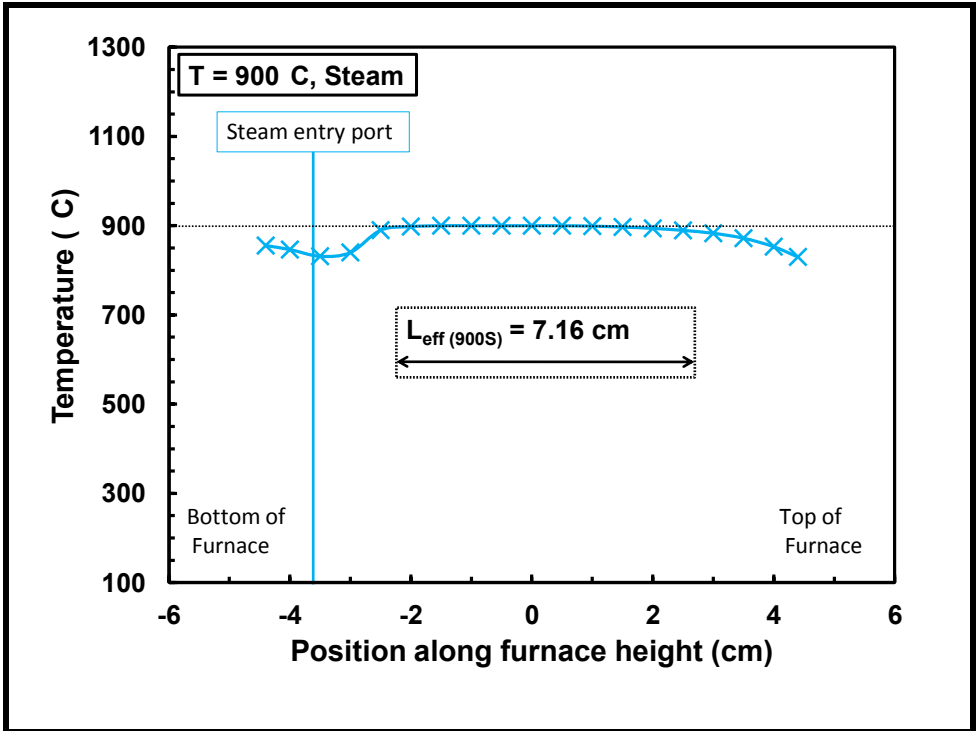
(b)

Figure 14 : Temperature profile obtained for Hi Nicalon[TM] Type-S fiber tow specimen at 900°C: (a) in air and (b) in steam.
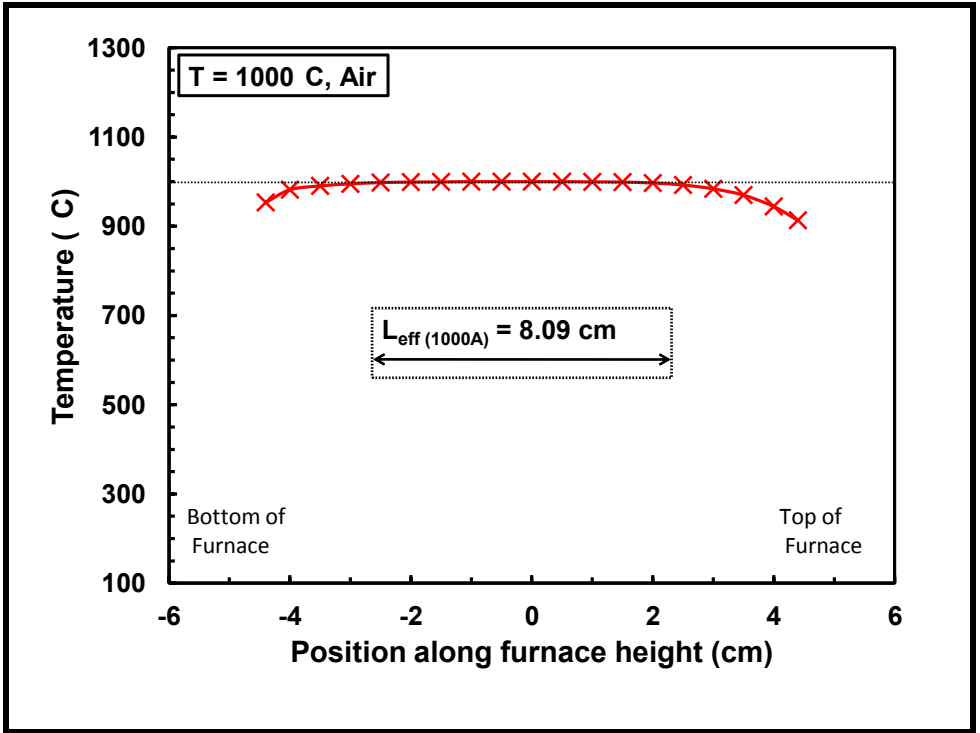
(a)
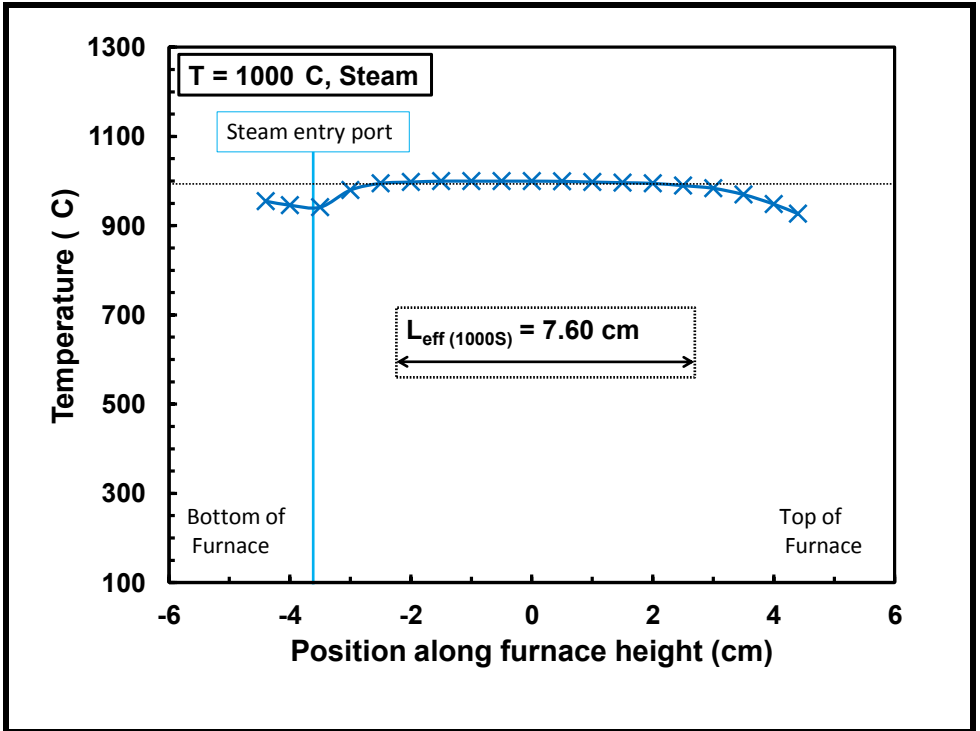
(b)

Figure 15 : Temperature profile obtained for Hi Nicalon^{TM} Type-S fiber tow specimen at 1000°C: (a) in air and (b) in steam.
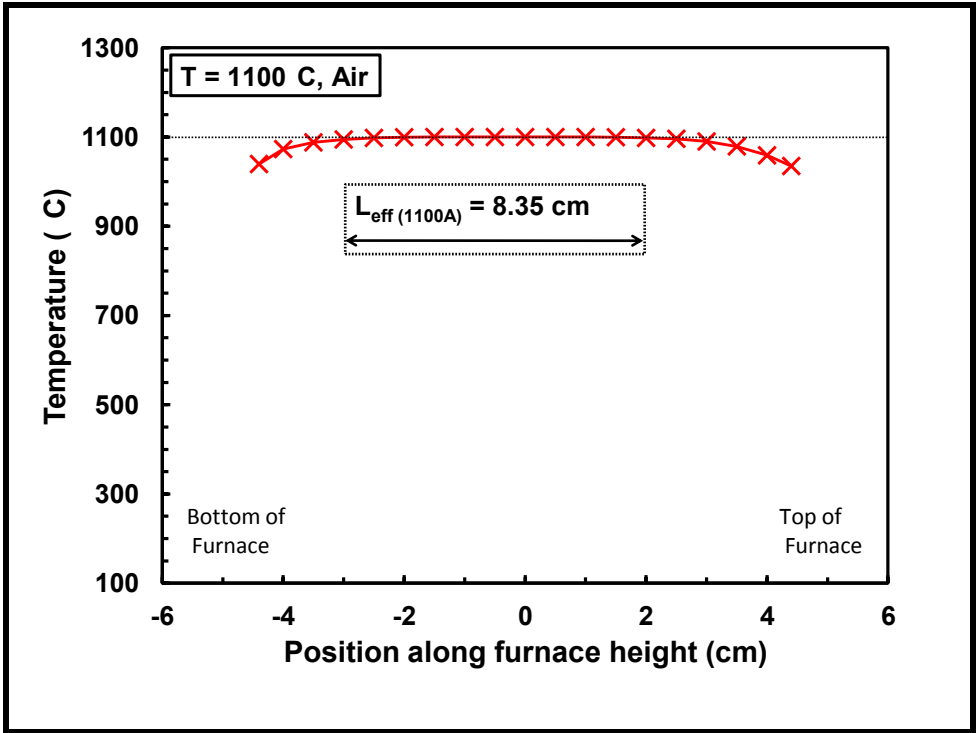
(a)
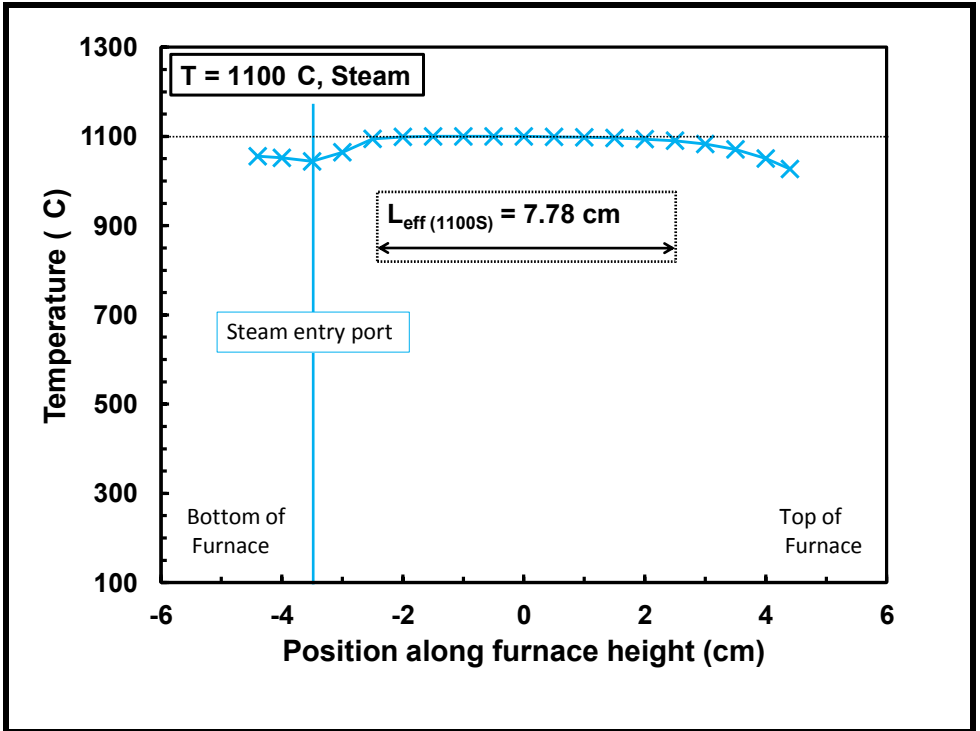
(b)

Figure 16 : Temperature profile obtained for Hi Nicalon[TM] Type-S fiber tow specimen at 1100°C: (a) in air and (b) in steam.
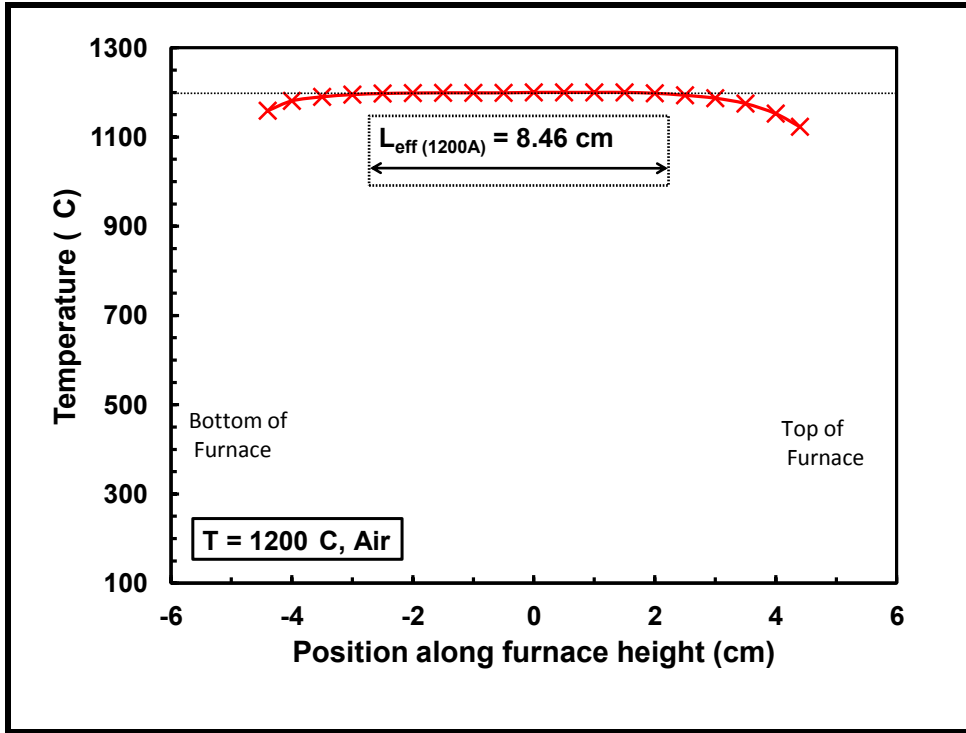
(a)
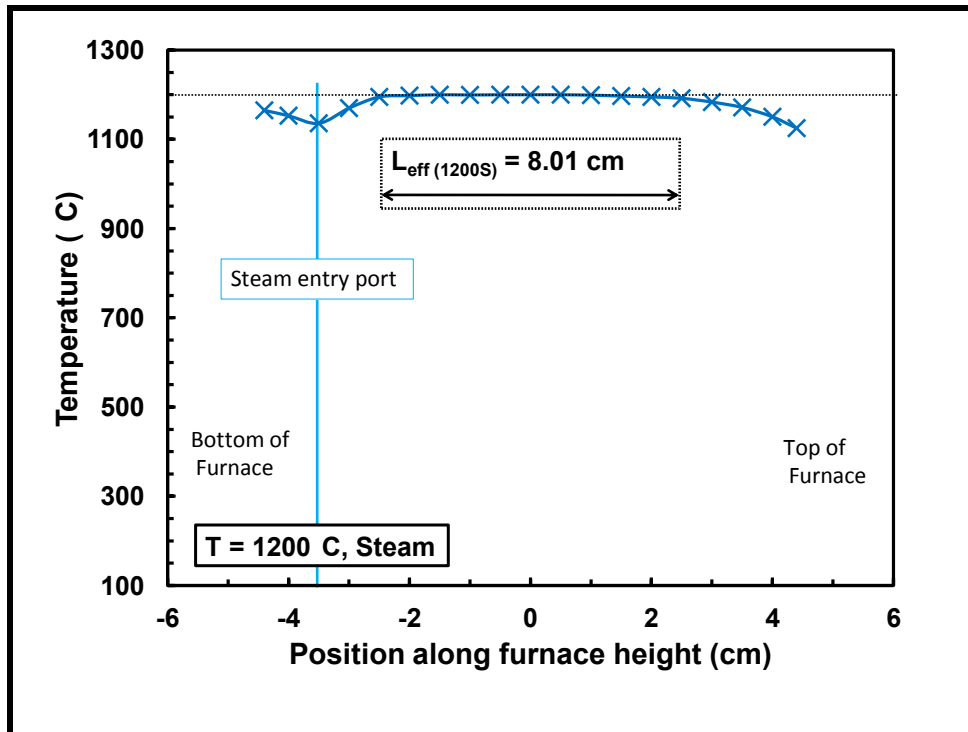
(b)

Figure 17 : Temperature profile obtained for Hi Nicalon[TM] Type-S fiber tow specimen at 1200°C: (a) in air and (b) in steam.

Note the "dips" in the temperature profiles in Figures 13-17 correspond to the locations where the steam was injected into the susceptor.

4.2 Strain Measurement

Because a strain measurement device could not be placed directly on a bundle of fibers inside a furnace, an indirect method of obtaining strain measurements detailed by Armani [3] was employed. Extension of the fiber tow specimen was measured by linear variable displacement transducers outside the furnace. The initial strain measurements were calculated using the effective gauge length described below and the average displacement value of the fiber tow length upon thermal equilibrium during the heat-soak. Machine compliance correction was accomplished for each test during post-processing by subtracting the strain value immediately upon the load application from the subsequent strain data.

An indirect method detailed by Armani [3] was also utilized in this research to calculate strain and the strain rate of the specimen in the hot test section. Extension of the fiber tow specimen was measured outside the furnace by linear variable displacement transducers and consisted of an amalgamation of extensions produced over the entire specimen length throughout the temperature profile. In order to convert the LVDT measurement into a representative strain at the desired test temperature, the amount of displacement along the length of the test specimen subjected to the temperature profile must be determined. Consider that the section of a fiber tow specimen subjected to a specific load at a higher temperature would displace more than another section of the same fiber tow specimen subjected to the same load but at a lower temperature in the temperature profile. In order to convert the overall displacement of the fiber tow specimen to strain at the desired temperature, the distribution of displacement along the temperature profile

30

must be established. The method for calculating strain and strain rate from displacement measurements proposed below is similar to that of Morrell [28], Kandil and Dyson [22], and DiCarlo [11]. This calculation of the effective gauge length takes into account the varying compliance along the fiber tow subjected to a temperature profile. Equation 1 is the general power-law creep equation.

$$\dot{\varepsilon} = A\sigma^n \exp\left(\frac{-Q}{RT}\right)$$

(1)

Consider a test specimen of constant cross section with a length 2L. From the center of the specimen gauge section, creep occurs over a total length –L to L. Beyond these boundaries creep is negligible. Therefore, the total measured strain and total measured strain rate are:

$$\varepsilon_m = \frac{\Delta l}{2L} = \int_0^t \dot{\varepsilon}_m \, dt$$

(2)

$$\dot{\varepsilon}_m = \frac{\text{measured extension rate}}{2L} = \frac{1}{2L}\int_{-L}^{L} \dot{\varepsilon} \, dl$$

(3)

Note that the total measured strain and strain rate account for variations in strain and strain rate along the specimen subject to a temperature profile. At the hottest sections, the amount of strain or strain rate will be greater than at a lower temperature.

Now, consider the strain and strain rate at the desired maximum temperature at the center of the furnace. Let subscript O denote quantities obtained at the center of the specimen gauge section. The strain at the center of the furnace can be calculated as the time integral of the strain

rate at the center of the furnace. It can also be described by the same overall change in length of the entire specimen divided by a hypothetical length called the effective gauge length, $(2L)_{eff}$. The effective gauge length can also be thought of as the gauge length obtained under a hypothetical step-function temperature profile, in which all the strain was accumulated under the peak temperature and zero strain is achieved under the lower temperature.

$$\varepsilon_o = \int_0^t \dot{\varepsilon}_o \, dt = \frac{\Delta l}{(2L)_{eff}} \tag{4}$$

Similarly, the strain rate at the maximum temperature (i.e. strain rate at the center of the furnace) can be expressed by using the effective gauge length as:

$$\dot{\varepsilon}_o = \frac{\text{measured extension rate}}{(2L)_{eff}} = \frac{1}{(2L)_{eff}} \int_{-L}^{L} \dot{\varepsilon} \, dl \tag{5}$$

Taking the ratio of Equations 3 and 5 obtain:

$$\frac{\dot{\varepsilon}_m}{\dot{\varepsilon}_o} = \frac{(2L)_{eff}}{2L} \tag{6}$$

Recall the general power-law creep equation given in Equation 3 and reproduced here considering that stress is uniform and that temperature is a function of location along the fiber tow specimen:

$$\dot{\varepsilon} = A\sigma^n \exp\left(\frac{-Q}{RT(l)}\right) \tag{7}$$

Using Equations 3, 6 and 7, the ratio of the measured strain rate to the actual strain rate becomes only a function of temperature, given by:

$$\frac{\dot{\varepsilon}_m}{\dot{\varepsilon}_o} = \frac{1}{2L} \int_{-L}^{L} \exp\left\{ \frac{-Q}{R}\left(\frac{1}{T(l)} - \frac{1}{T_o} \right) \right\} dl$$

(8)

Utilizing a numerical summation of increments of length h, such that $L = kh$ where k is an integer, the ratio of the measured strain rate to the actual strain rate is:

$$\frac{\dot{\varepsilon}_m}{\dot{\varepsilon}_o} = \frac{1}{2k} \sum_{i=-k}^{k} \exp\left\{ \frac{-Q}{R}\left(\frac{1}{T_i} - \frac{1}{T_o} \right) \right\}$$

(9)

As a result, an effective gauge length can be calculated such that:

$$(2L)_{\mathit{eff}} = 2L\left(\frac{\dot{\varepsilon}_m}{\dot{\varepsilon}_o} \right)$$

(10)

The effective gauge length can be used to calculate strain as well as strain rate from displacement measurements made outside the hot zone of the furnace.

Using this approach together with the temperature profiles established in Section 4.1, and creep activation energy of 177 kJ/mol from literature [15], effective gauge lengths were calculated for Hi-Nicalon S fiber tow specimens at temperatures of interest in air and in steam. Figures 13-17 schematically show the effective gauge lengths of the Hi-Nicalon S fiber tow specimens next to the respective temperature profiles.

Hammond [17] and Yun, et al. [37] applied a simpler approach by assuming the main creep deformation occurred only in the hot zone of the furnace and approximated the gauge length by the flat portion of the temperature profile. This approach is subjective in defining the gauge length of the specimen and is dependent on how flat the maximum temperature profile

33

was and how sharply the temperature drops at the edges of the furnace – the flatter and sharper, the better the estimate.

The calculated effective gauge lengths presented in Figures 13-17 are physically representative of the flat portion of the temperature profile. Furthermore, notice that the effective gauge lengths essentially compensates for changes in the temperature profile. For example the inflow of steam as represented by the dips in the profiles. Using this calculated effective gauge lengths is a more systematic approach to obtaining strain from extension measurements for a specimen subjected to a temperature profile regardless of the shape of the profile.

V. Results and Discussion

5.1 Creep of Hi-Nicalon S fiber tows at elevated temperature

Creep tests on Hi-Nicalon S ceramic fiber tows were performed at 800°C and at 1100°C in laboratory air and in steam. Results of the creep-rupture tests performed in air are summarized in Table 3.

Table 3 : Summary of creep results for Hi-Nicalon S ceramic fiber tows at 800°C and at 1100 °C in air and in steam

Test Environment	Creep Stress (MPa)	Creep Lifetime (h)	Steady-State Creep Rate (s⁻¹)	Creep Strain (%)
Tests at 800°C				
Air	467	100†	1.05×10^{-9}	0.17 †
Air	780	100†	1.70×10^{-9}	0.27†
Air	936	5.63	1.80×10^{-8}	0.27
Air	1248	1.04	1.24×10^{-7}	0.27
Steam	76	100†	4.00×10^{-10}	0.05
Steam	115	100†	5.70×10^{-10}	0.08
Steam	139	100†	8.35×10^{-10}	0.12
Steam	154	0.03	1.38×10^{-8}	0.05
Tests at 1100°C				
Air	154	100†	4.60×10^{-11}	0.04
Air	467	17.12	2.03×10^{-9}	0.18
Steam	154	0.33	6.92×10^{-8}	0.03

† Runout defined as 100 h at creep stress. Failure of specimen did not occur when the test was terminated.

Creep curves obtained at 800°C in laboratory air are shown in Figure 18. It is seen that creep curves produced in all tests conducted in air exhibit primary and secondary creep regimes, but no tertiary creep. Transition from primary to secondary creep occurred fairly early in the

creep life. The accumulated creep strain increased as the applied stress increased from 467 to 780 MPa, but remained unchanged as the applied stress increased from 780 to 1248 MPa. Creep run-out of 100 hours was achieved at 467 MPa and at 780 MPa.

Figure 18 : Creep strain vs. time curves for Hi-Nicalon S fiber tows at 800°C in laboratory air: (a) scale 0-400000 s, (b) 0-30000 s.

36

Creep curves obtained at 800°C in steam are shown in Figure 19. Creep curves produced in all tests conducted in steam exhibit primary and secondary creep regimes. No tertiary creep is observed. Creep run-out of 100 hours was achieved at 76, 115, and 139 MPa. However, when the applied stress was increased to 154 MPa, creep lifetime decreased dramatically to 0.03h. The accumulated creep strain increased from 0.05% to 0.12% as the applied stress increased from 76 MPa to 139 MPa, then dropped to 0.05% as the applied stress increased to 154 MPa.

It is recognized that creep performance of Hi-Nicalon S fiber tows at 800°C in steam (and to a lesser degree in air) may be degraded and creep lifetimes shortened as a result of subcritical crack growth of the surface defects due to oxidation. Recent studies [15, 16, 24] found that during static fatigue of SiC fibers and SiC fiber-reinforced CMCs at temperatures above 1000°C grain growth of SiC due to oxidation took place. A formation of a uniform silicon oxide layer on the surface of fibers was observed [15, 16, 24]. This "protective" silica scale was reported to have a beneficial effect on the creep performance of the SiC fibers at elevated temperatures in oxidizing environments provided the material was not subjected to temperature cycling [24, 30]. Hence, it was decided to test the Hi-Nicalon S fiber tows in creep at 1100°C in order to assess whether the fiber tow performance would indeed improve at this higher temperature.

Figure 19 : Creep strain vs. time curves for Hi-Nicalon S fiber tows at 800°C in steam.

Creep curves obtained at 1100°C in laboratory air and in steam are shown in Figures 20 and 21, respectively. Creep curves produced in all tests conducted at 1100°C exhibit primary and secondary creep regimes, but no tertiary creep. In all tests primary creep rapidly transitions into secondary creep. In the case of tests performed at 1100°C in air, the accumulated creep strain increases from 0.04% to 0.18% as the applied stress increased from 154 to 467 MPa. Note that the strain accumulated in the 467 MPa test at 1100°C in air is very close to that accumulated at the same stress level at 800°C in air. However, while the 467 MPa test performed at 800°C in air achieved a 100 h run-out, the test performed at 1100°C in air failed after 17.12 h. Apparently, the increase in temperature had a detrimental effect on the creep performance of the Hi-Nicalon S fiber tow in air. Conversely, results obtained in steam suggest a different conclusion. Note that similar creep strains were also accumulated in the 154 MPa tests performed in steam at 800°C and at 1100°C. In contrast, the creep lifetimes produced in these two tests differ by an order of

38

magnitude. Specimen tested in steam survived 0.33 h under load, while specimen tested in air failed after mere 0.03 h. This result indicates that a protective silica scale may indeed have formed, which serves to improve creep performance of the Hi-Nicalon S fiber tow at elevated temperature in steam.
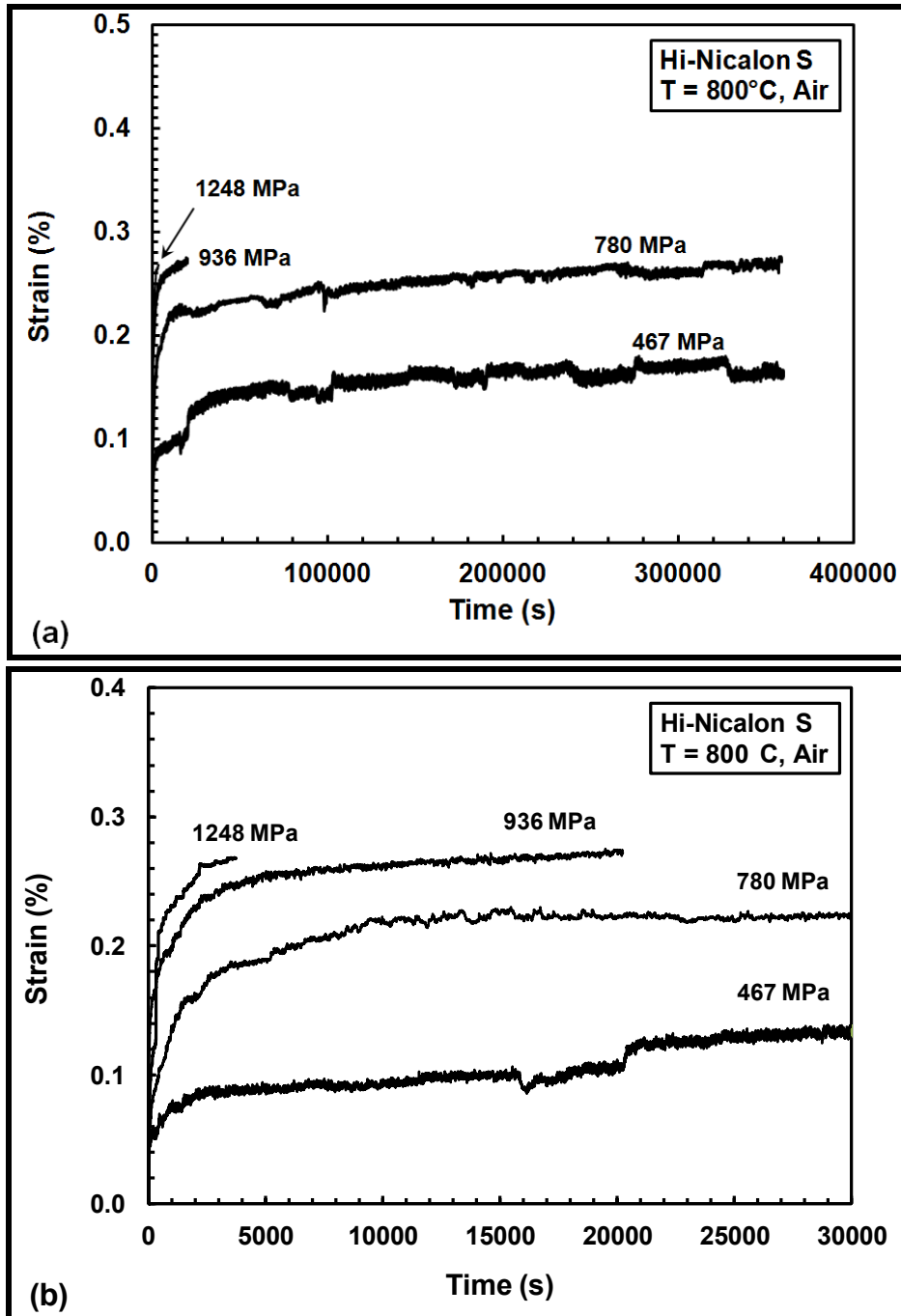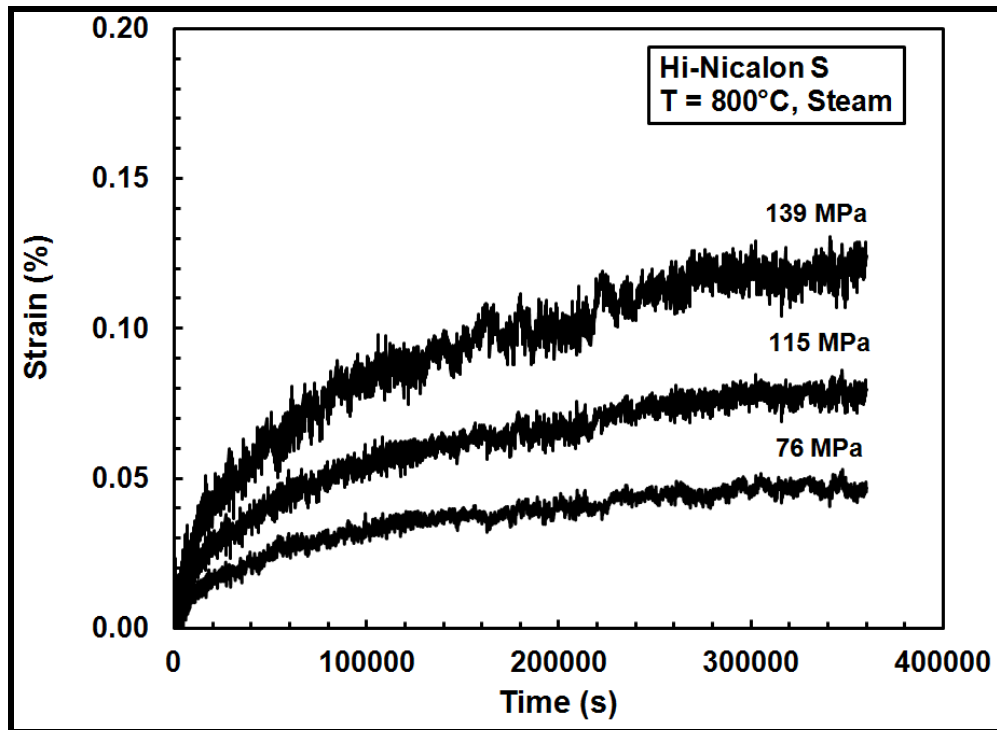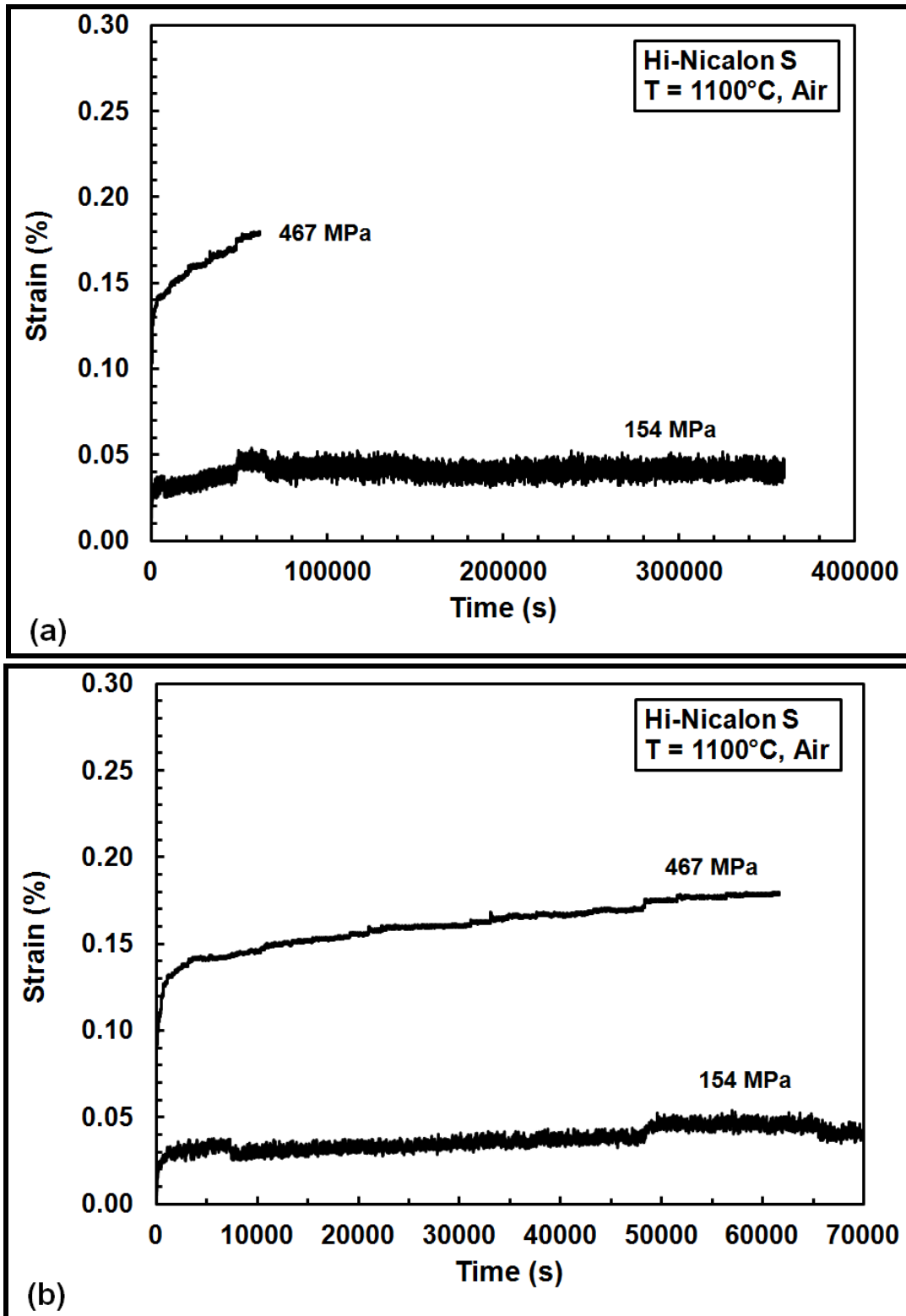
Figure 20 : Creep strain vs. time curves for Hi-Nicalon S fiber tows at 1100°C in laboratory air: (a) scale 0-400000 s, (b) 0-70000 s.
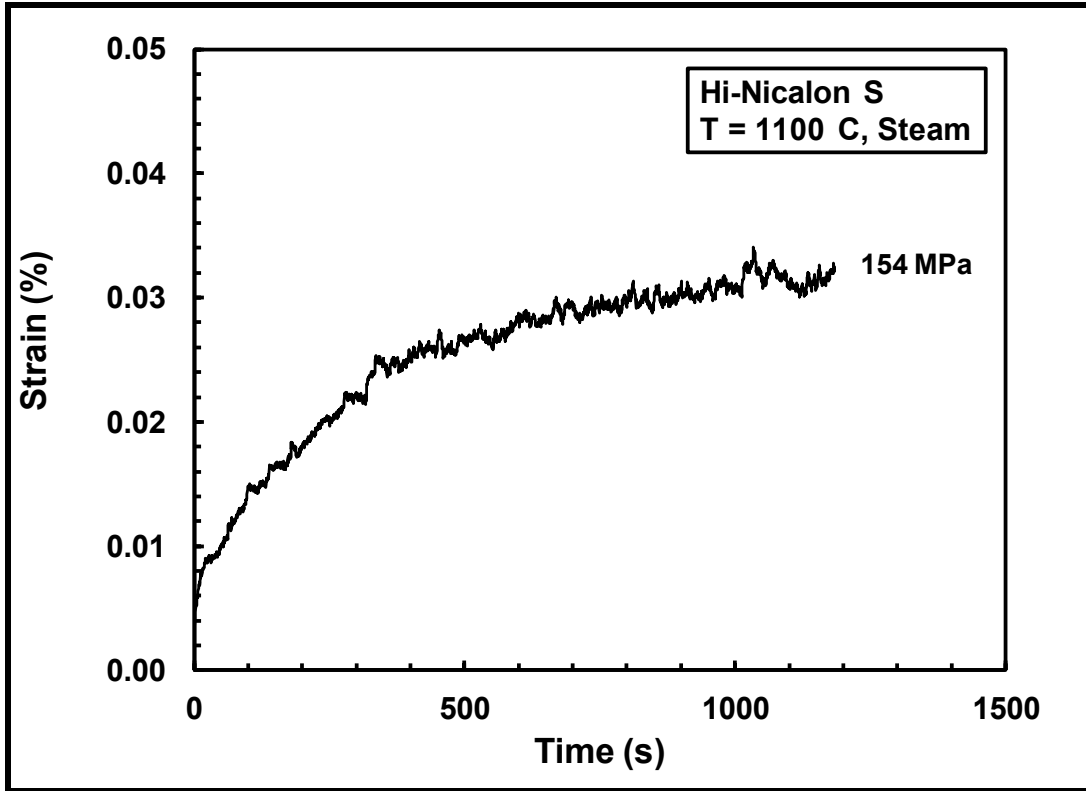
Figure 21 : Creep strain vs. time curves for Hi-Nicalon S fiber tows at 1100°C in steam.

Steady-state creep rate was reached in all tests and dominated the majority of the creep lifetime. Creep rate as a function of applied stress is presented in Figure 22. It was possible to fit the creep results obtained at 800°C in air and in steam with a temperature-independent Norton-Bailey equation of the form

$$\dot{\varepsilon} = A\sigma^n \tag{11}$$

Here $\dot{\varepsilon}$ is the minimum creep rate, A is a temperature-dependent coefficient that accounts for the activation energy, grain size and other variables in the full form of the power law, and σ is the applied stress. Using a log-log plot of the creep rate as a function of stress, the stress exponent n was determined for Hi-Nicalon S fiber tows at 800°C in air and in steam by linear regression. The stress exponent, n, was 4.8 in laboratory air and 3.8 in steam.

41

Theoretically, the predominant creep mechanism can be identified from the analysis of experimental creep data. Different creep mechanisms have been correlated to different values of the stress exponent n, obtained from the experimental creep data [4,13]. The stress exponent, $n \approx$ 5, obtained for Hi-Nicalon S fiber tows at 800°C in air appears to be consistent with the climb controlled dislocation creep mechanism. The stress exponent, $n \approx 4$, obtained for Hi-Nicalon S fiber tows at 800°C in steam appears to be consistent with the grain boundary sliding and cavity growth creep mechanism. However, extensive analysis of the microstructure of the tested specimens would be required before a definitive conclusion regarding creep mechanisms operating at 800°C in air and in steam could be reached. It is recognized that in the full form of the Equation 11 the steady-state creep rate is proportional to the applied stress σ raised to a stress exponent, n, and inversely proportional to the grain size d raised to a grain size exponent, m, such that:

$$\dot{\varepsilon} \propto \frac{\sigma^n}{d^m} \tag{12}$$

Therefore the grain size of the tested fiber tows would have to be determined before a conclusion regarding creep mechanisms can be reached.

Results in Figure 22 reveal that at 800°C the presence of steam significantly accelerated creep rates for stress levels $\geq$ 154 MPa. It is noteworthy that the creep rate produced at 154 MPa in steam is an order of magnitude higher than that produced at a higher stress of 467 MPa in air. Recall that a much shorter creep lifetime (0.03 h) was produced at 154 MPa in steam while a 100-h runout was achieved at 467 MPa in air.

42

Increase in temperature from 800°C to 1100°C appeared to have little effect on creep rates obtained in laboratory air or in steam. For example, at 467 MPa creep rate obtained at 1100°C was not very different from that obtained at 800°C. Similar observation can be made regarding creep rates obtained at 154 MPa in air and in steam. Yet creep lifetimes obtained in these tests differed dramatically. Hence additional testing should be performed to further explore this phenomenon.
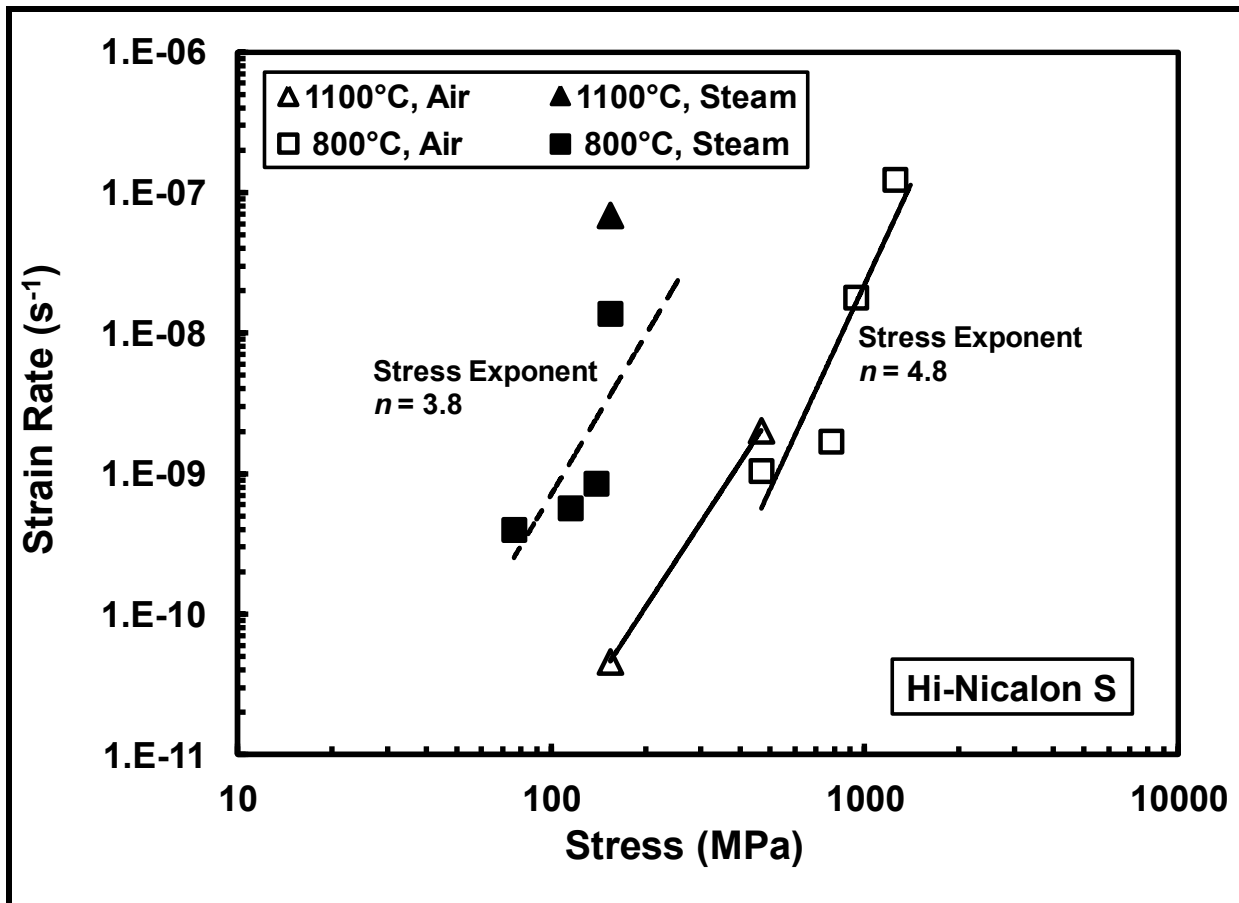

Figure 22 : Steady-state creep rate vs applied stress for Hi-Nicalon S fiber tows at 800°C and 1100°C in laboratory air and in steam.

The stress-rupture behavior of Hi-Nicalon S fiber tows at 800°C and at 1100°C in air and steam is summarized in Figure 23. As expected, the creep lifetime decreases with increasing applied stress at both temperatures investigated. At 800°C in air, creep runout of 100 h was achieved at 780 MPa. Creep lifetimes reduced drastically as the applied stress increased above 780 MPa. It is noteworthy that the creep lifetimes obtained in this study for the Hi-Nicalon S fiber tows at 800°C in air are consistent, see Figure 23, with those reported by Gauthier and Lamon [15]. At 800°C in steam, creep runout was achieved at 139 MPa. Creep lifetime dropped to 0.03 h when the applied stress was raised to 154 MPa. Further testing is required to explore this threshold. At 800°C the presence of steam had a profound influence on creep performance of the HI-Nicalon S fiber tows. Creep lifetime appears to be dramatically reduced due to steam.

At 1100°C in air, creep runout of 100 h was achieved at 154 MPa. Creep runout was not achieved in steam. Results in Table 3 indicate that in steam the creep run-out stress would lie below 150 MPa. At 1100°C the presence of steam significantly degraded creep lifetime of the fiber tow at 154 MPa. However, creep lifetime obtained in steam at 1100°C significantly exceeded that obtained at 800°C in steam. This result supports the hypothesis that at higher temperatures in an oxidizing environment, a protective silica scale forms on the surface of the fiber, thus improving creep performance of the fiber. Additional testing at temperatures in the 800-1200°C range is recommended to assess the effects of steam on creep performance of the Hi-Nicalon S fiber tows at different temperatures in the aforementioned range.
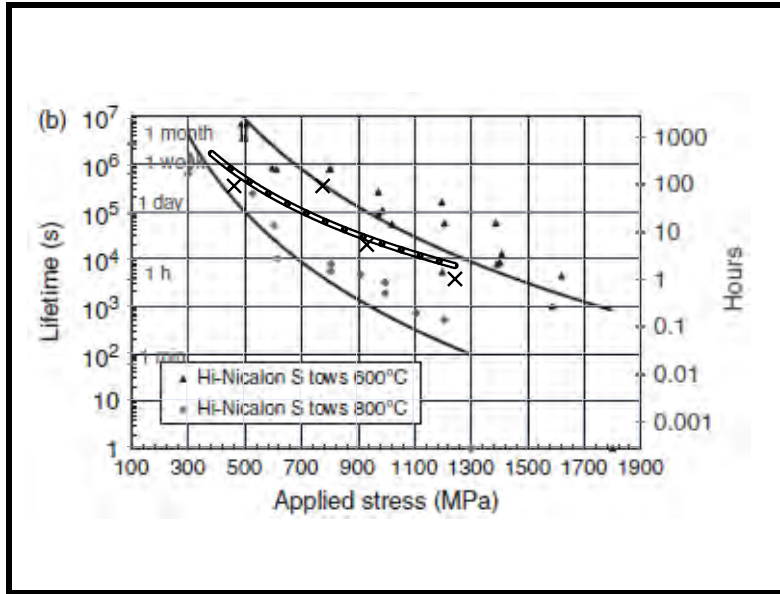
Figure 23 : Gauthier and Lamon data for 800°C in air [15] with actual 800°C in air experimental results overlaid (shown with X for data points and dashed line curve)
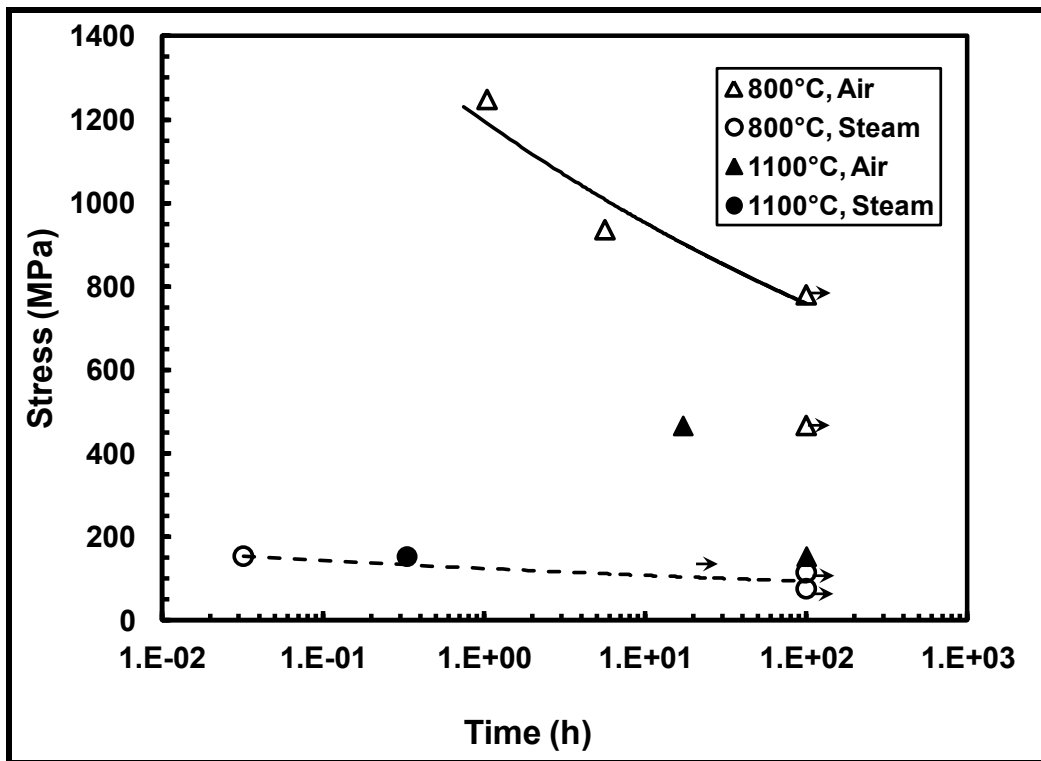
Figure 24 : Creep stress vs. time to rupture for Hi-Nicalon S fiber tows at 800°C and 1100°C in laboratory air and in steam. Arrow indicates that failure of specimen did not occur when the test was terminated.

Figure 24 shows Hi-Nicalon S fiber tow specimens tested at 800 °C in laboratory air. Note that all failures occurred approximately in the middle of the specimen gauge section. A different result is seen in Figure y, which shows Hi-Nicalon S fiber tow specimens tested at 800 °C in steam. Recall that in these tests, steam enters the susceptor through the feeding tube at the bottom of the susceptor. Figure 25 demonstrates that in the case of all specimens tested at 800°C steam, failures occurred near the point of steam entry into the susceptor. Recall that steam is introduced into the susceptor in a continuous flow with a slightly positive pressure in order to expell the dry air and to create a steam-rich environment inside the susceptor. Apparently, the part of the fiber tow, which comes in contact with steam as it first enters the susceptor, suffers the most degradation due to steam.
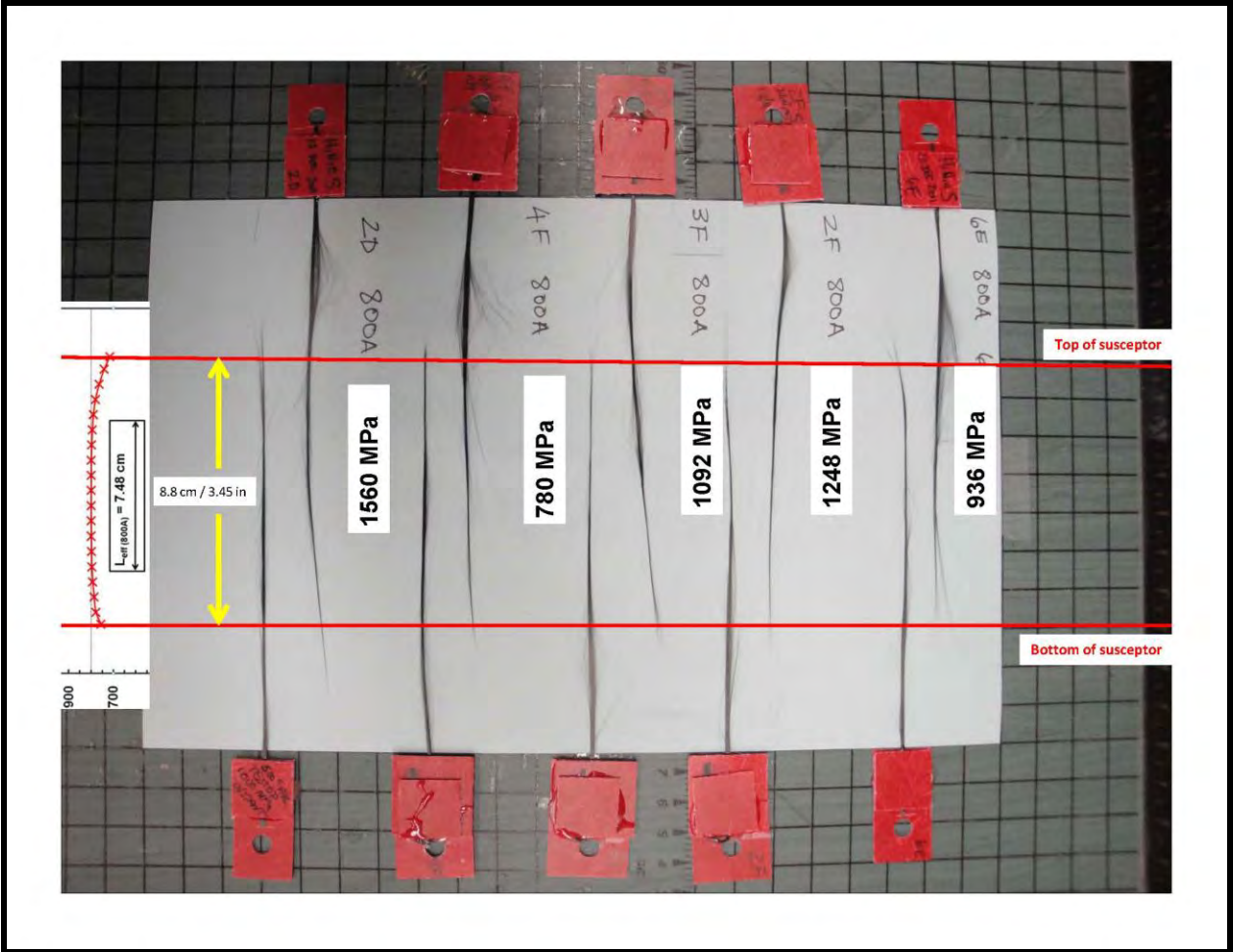
Figure 25 : Hi-Nicalon S fiber tow specimens tested at 800 °C in laboratory air. It is seen that all failures occur approximately in the middle of the gauge section.

Figure 26 : Hi-Nicalon S fiber tow specimens tested at 800 °C in steam. It is seen that all failures occur approximately at or just above the point of steam entry into the susceptor.
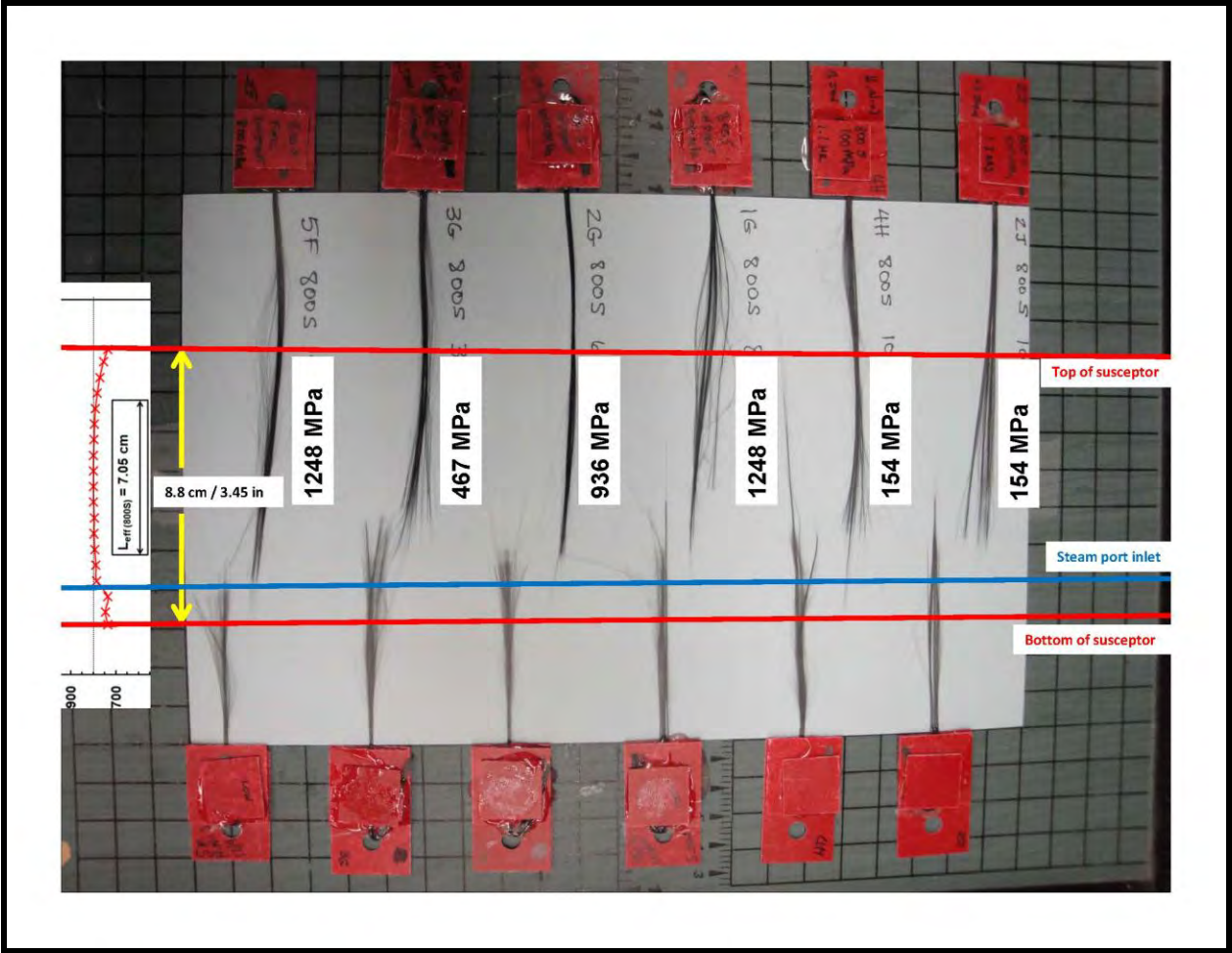
VI. Conclusion and Recommendations

6.1 Conclusions

The effect of steam on creep performance of the Hi-Nicalon S fiber tows was investigated at 800°C. Creep results revealed that the presence of steam had a degrading effect on the creep lifetimes and steady-state creep rates of the Hi-Nicalon S fiber tows at 800°C. In the presence of steam, the creep rates of the Hi-Nicalon S fiber tows increased by at least one order of magnitude, while the creep lifetimes decreased by more than three orders of magnitude. In air creep run-out of 100 h was achieved at 780 MPa. In steam creep run-out was achieved only at 139 MPa. At 800°C in air, the stress exponent was determined as $n \approx 5$, suggesting climb controlled dislocation creep mechanism as the responsible creep mechanism. At 800°C in steam, the stress exponent was determined as $n \approx 4$, suggesting grain boundary sliding and cavity growth creep mechanism as the responsible creep mechanism.

Results of the additional creep tests performed at 1100°C revealed that the increase in temperature had a degrading effect on creep performance of the Hi-Nicalon S fiber tows in laboratory air. At 1100°C in laboratory air, the creep lifetimes of the Hi-Nicalon S fiber tows decreased by approximately one order of magnitude. Contrastingly, the increase in temperature from 800°C to 1100°C had a beneficial effect on creep performance of the Hi-Nicalon S fiber tows in steam. At 1100°C in the presence of steam, the creep lifetimes of the Hi-Nicalon S fiber tows increased by at least one order of magnitude. Improvement in creep performance noted at 1100°C in steam was attributed to the formation of a "protective" silica scale. At 800°C in steam, the slow growth of surface defects is likely the dominant failure mechanism. At 1100°C in steam, a uniform silicon oxide layer (known to form on the surface of the SiC-based fibers at

temperatures above 1000°C in oxidizing environments) decelerates the growth of surface defects thereby delaying fiber failure.

6.2 Recommendations

A thorough analysis of the microstructure of the tested fiber tow specimens should be performed. The surface of the fibers should be analyzed using scanning electron microscopy (SEM) and Auger electron spectroscopy (AES). Examination of the fiber tows with SEM could identify two important features: (1) multiple crack tips on the fracture surface of the fibers, which would indicate slow crack growth, and (2) formation of a thin oxide film on the exterior surface of the fibers. The AES analysis could provide additional information about the oxide layer that may have formed on the surface of the fibers. Detecting higher atomic concentration of oxygen on the exterior surface of the fiber than in the fiber interior would indicate the presence of the oxide layer. A decrease in the atomic concentration of oxygen at some distance from the exterior surface would identify the limits of the oxide layer. Thus the thickness of the silica scale could be measured and, possibly, correlated with the applied load and test duration.

Results of this research revealed a dramatic drop in creep lifetime when the applied stress increased from 139 MPa to 154 MPa at 800°C in steam. Additional creep tests should be performed at 800°C in steam in order to thoroughly investigate the stress-rupture behavior for applied stresses ranging from 130 MPa to 160 MPa.
Additional creep tests should be performed in air and in steam at 900, 1000, 1100, and 1200°C in order to evaluate the effect of steam on creep performance of the Hi-Nicalon S fiber tows at different temperatures. It is important to identify the temperature range where the presence of

steam degrades creep resistance. It is likely that between 1000°C and 1200°C there is a

temperature range where the presence of steam has beneficial effect (or no effect) on creep

Appendix A1

PROCEDURE 1 : Fiber Tow Specimen Layup for Creep or Tensile Testing
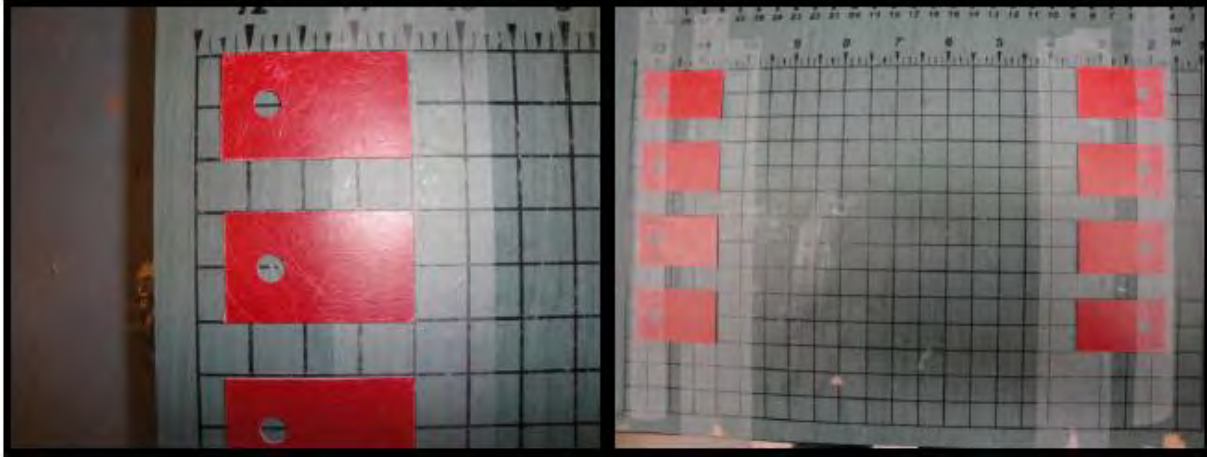
1. <u>CLEAN FIXTURE BOARD</u>

Clean fixture board using Isopropyl Alcohol. Apply two widths of tape (side-by-side) vertically centered on each of the 10 ½" and 3 ½" gridlines. This protects the fixture board from epoxy that may contact it during this procedure.
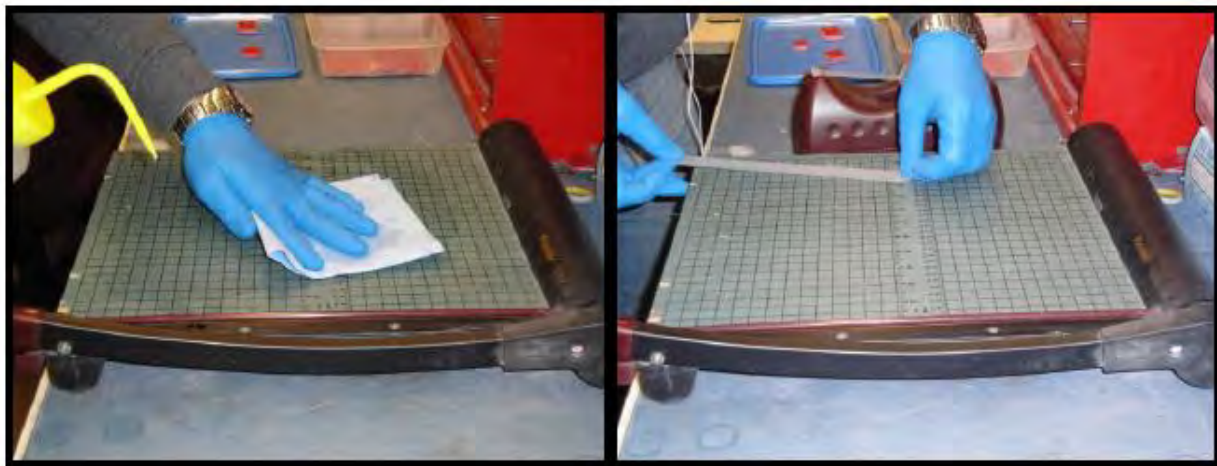
Figure 27 : Cleaning fixture board and applying tape.

2. <u>ARRANGE TABS ON GRID</u>

Arrange the primary tabs on the gridlines with the base edge of the tab on the 10 ½" and 3 ½" gridlines and the holes on center of a common horizontal gridline. Affix tabs by using a long vertically oriented strip of tape that just covers the holes.

Figure 28 : Arranging tabs on fixture board and fastening tabs with tape.

3. <u>PREPARE FIBER TOWS</u>

Cut 4 lengths of fiber tows to approximately 16" lengths, paying special attention for irregularities or breakages on the fiber. (Do not touch fibers with bare hands or damage the fiber on the spool in any way.)

Figure 29 : Cutting fiber tows.
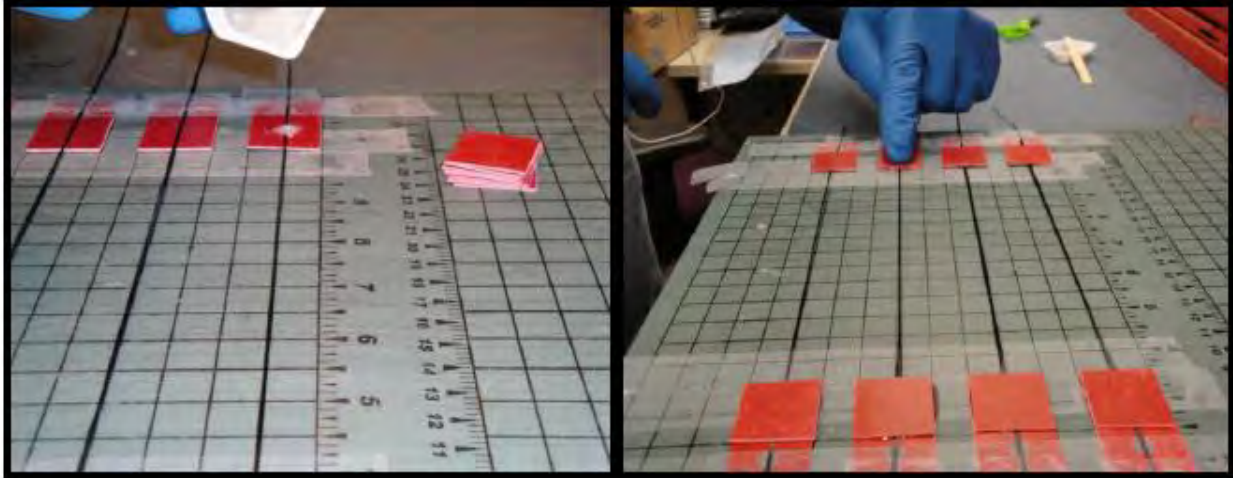
4. ALIGN FIBER TOWS

Align the fiber tows across the tabs making sure that the tow is stretched taut and is following the gridline that bisects the two hook holes on the tabs. Affix the fiber tows to the tabs with a small piece of tape at each tab outside of the adhesion area.
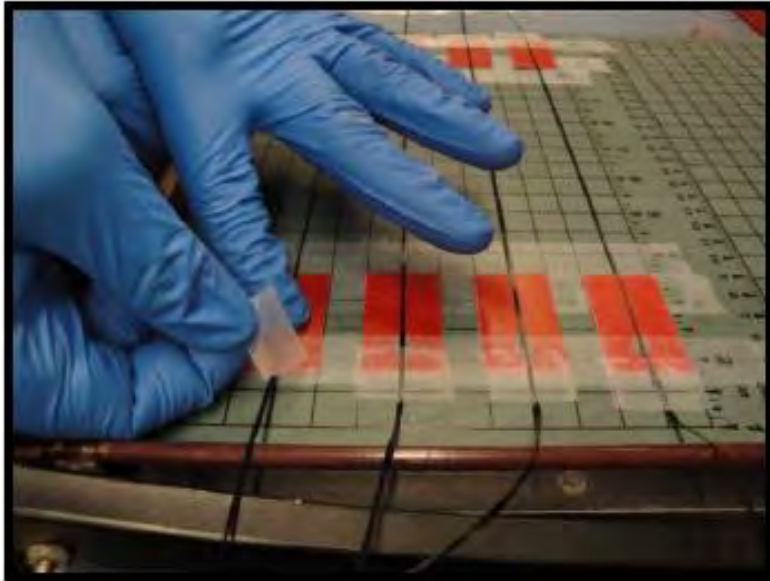
Figure 30 : Align the fiber tow sections on the tabs.
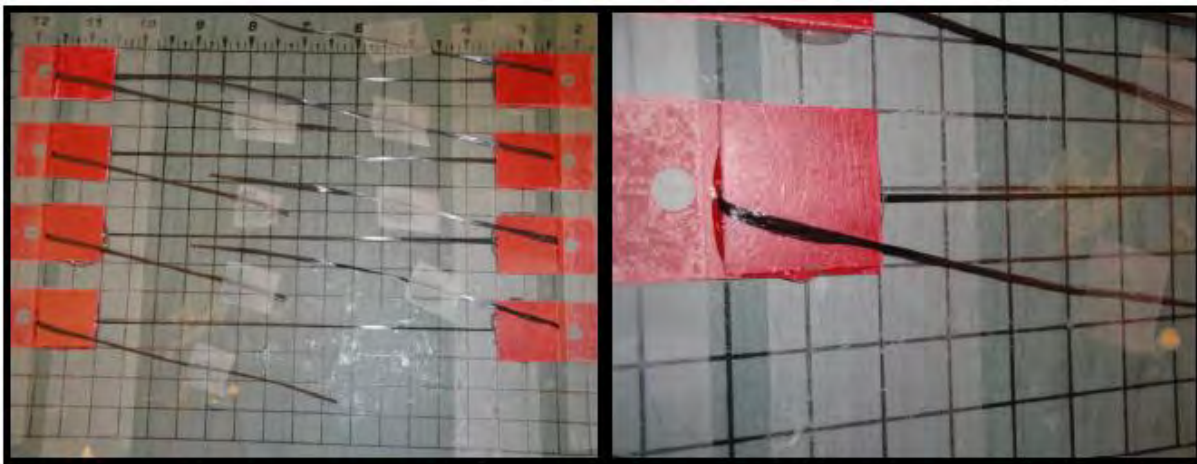
5. SECONDARY TAB TO PRIMARY TAB

Stage the secondary tabs (1" x 1") for easy application while the epoxy is workable. Mix an epoxy blister pack as per directions and apply a pea size quantity to each tab. Apply the secondary tab to the primary tab so that edges are coincident and push on tab until epoxy squeeze-out is detected. One blister pack will secure 8 secondary tabs (4 fiber tow specimens).

Figure 31 : Applying epoxy to primary tab/fiber tow and adding secondary tab.

6. ALLOW 5 MINUTES FOR EPOXY TO START HARDENING

7. RE-ALIGN FIBER TOW FOR TERTIARY TAB

Carefully pull the excess tail of the fiber tow up and unstuck the small piece of tape that was previously holding it. Fold the fiber tow over the secondary tab and affix it to the fixture board with the piece of tape. Be careful when folding the fiber, there should be an approximate 1/8" radius formed at the fold point. Do not make this a sharp fold, or the fiber will break. Repeat this for all of the tabs and alternate the folding direction as shown in the figure.


Figure 32 : Preparing excess of fiber tow for tertiary tab application.

8. TERTIARY TAB TO TAB ASSEMBLY

Stage the tertiary tab (¾" x ¾") for easy application while the epoxy is workable. Mix an epoxy

blister pack as per directions and apply a pea size quantity to each tab. Affix the tertiary tab in

the corner of the secondary tab as to most securely hold the fiber tow. Push the tab down and

look for epoxy squeeze-out.   Key Point: Ensure that the bend in the fiber is completely engulfed

in epoxy.
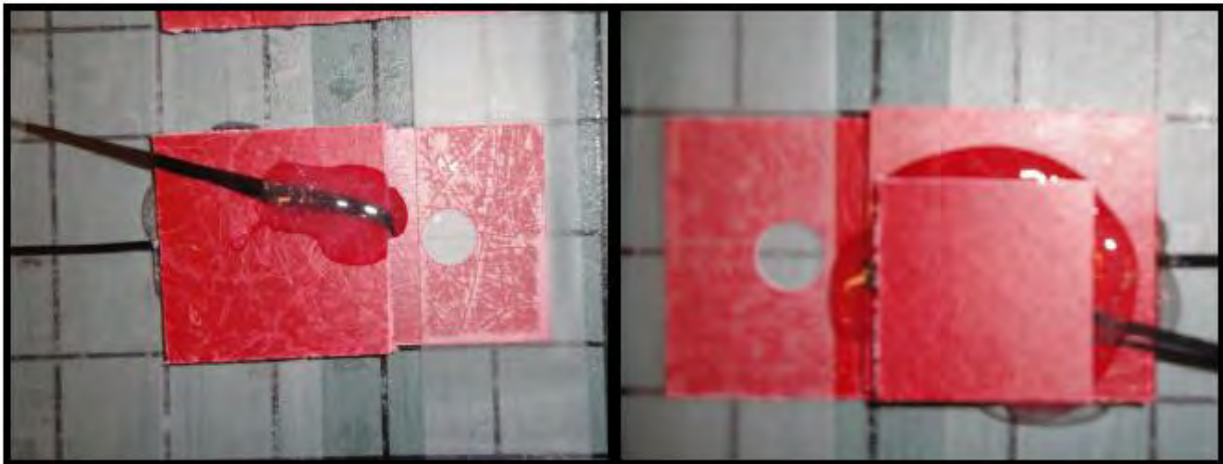
Figure 33 : Adding epoxy for tertiary tab application and illustrating epoxy placement engulfing folded portion of fiber.

9. WAIT 1 HOUR FOR EPOXY TO CURE

Wait an hour to detach specimens from the fixture board. Use a razor blade to cut the excess

fiber tow against the secondary tab. This will leave a witness mark so that any fiber pullout

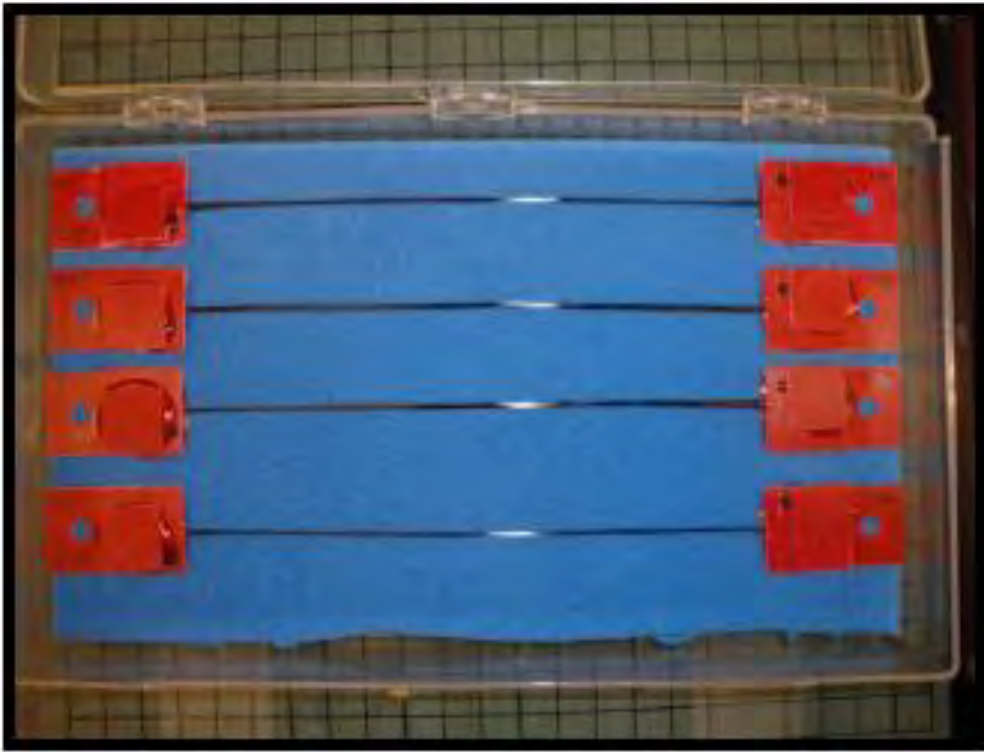during testing will be evident.
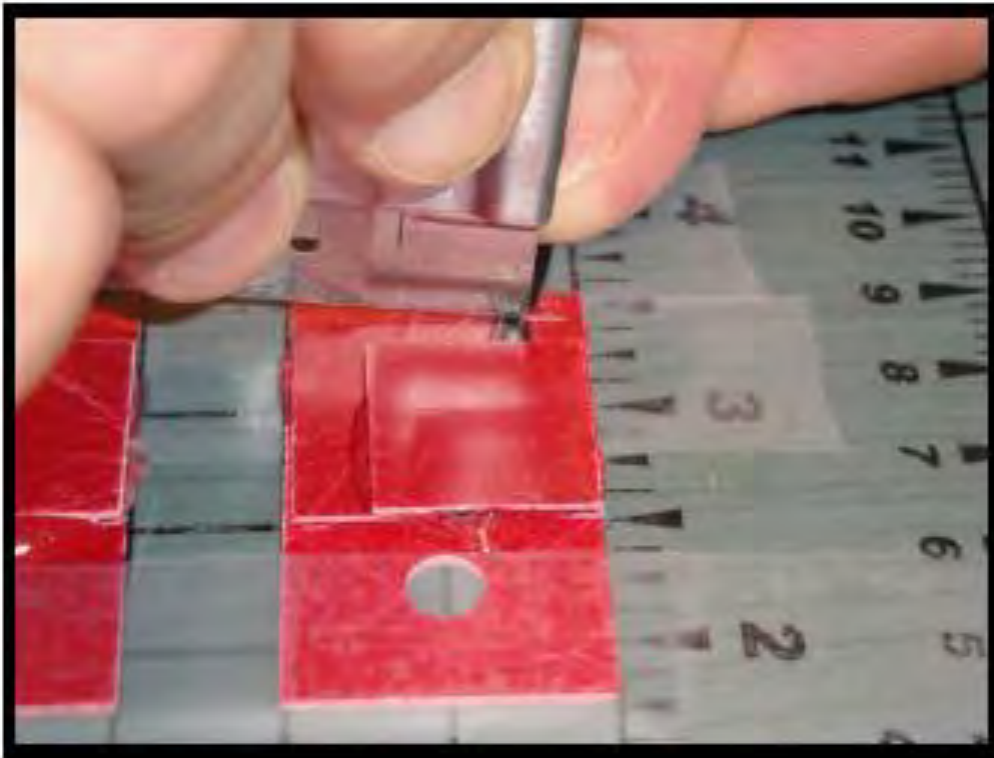
Figure 34 : Cutting excess fiber after epoxy has hardened.

10. <u>MARK THE SPECIMENS</u>

Assign and mark a specimen number to both tabs on each specimen. Date one tab – be consistent because this will later be used as a mark to show orientation during testing.

Figure 35 : Proper markings and storage of the prepared specimens.

Appendix A2

PROCEDURE 2 : Creep Testing with Fiber-Tows on 1 kip MTS 793 Test Equipment

Note: (Starting with a room temperature furnace that has been opened and cleaned)

Note: (If running steam, start the steam generation system about an hour prior and ensure the critical values have been reached. Purge the system with the air bulb and check that steam is being produced.)

1. <u>STAGE DEAD WEIGHT</u> (this is especially important when using large weights)
Install specimen simulator (looped wire section) to upper and lower hooks. This will be used to "balance" the weights on the load train in order to properly load the real fiber tow. Ensure that elevator is in correct position and raise it until the bottom of the load train almost touches the elevator arm. The dead weight will be supported by "Split nut" on elevator arm. Ensure that the slot in the weight is clocked in a way that when lowering the elevator, the operator can visually check that the load train has engaged on the flat washer against the dead weight. Lower the elevator and shift the weights until a balanced state is achieved. **Remember** that the load train should be able to move freely within the stack of weights. Raise the elevator to unload and take out the specimen simulator (looped wire section).
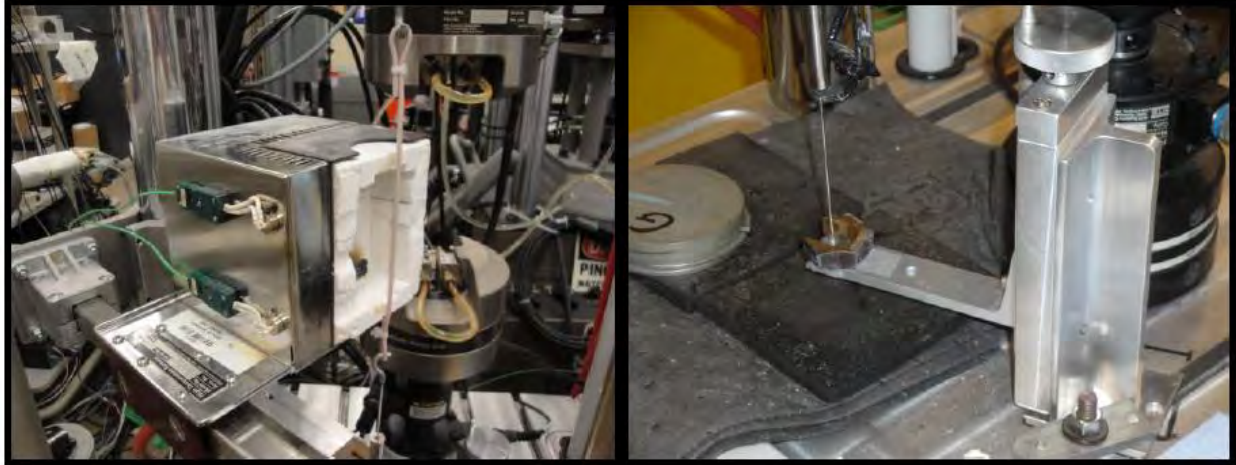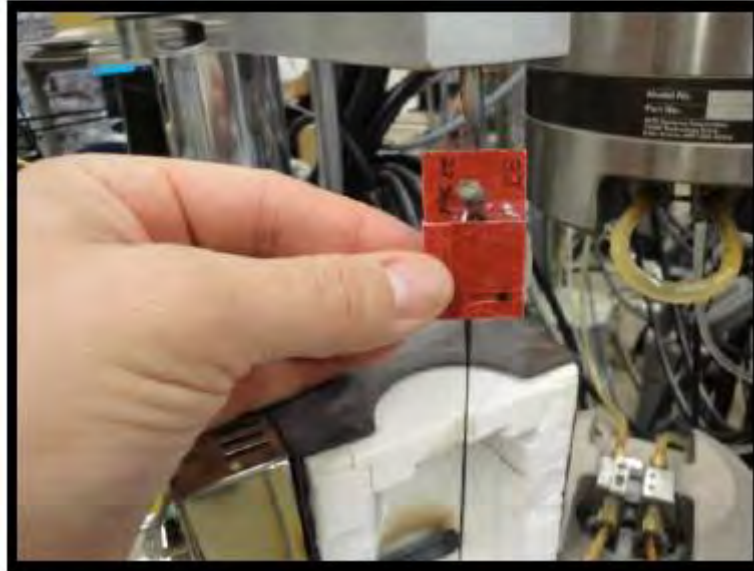
Figure 36 : Specimen simulator mounted and the elevator staged for the weight stack.

Figure 37 : Stacking the weights onto the split-nut and load train staged in weight stack.

2. ATTACH SPECIMEN-UPPER HOOK

Attach a new specimen onto the upper hook, being careful not to the let the fiber-tow be

damaged in any way. The tab marked with the date was used for orientation up.

Figure 38 : Installing the Hi-Nicalon S fiber tow specimen onto the upper hook.

3. ATTACH SPECIMEN-LOWER HOOK

With no weight on the load train, attach the lower hook to the specimen. Let the load
train weight (approx. 10g) pull the fiber-tow taught. Observe that the load train/furnace
alignment is correct. Lower the elevator until the end of the load train has aligned itself
into the lowermost weight as was illustrated in step 1.

Figure 39 : Installing the Hi-Nicalon S fiber tow specimen onto the lower hook.

4. <u>ASSEMBLE SUSCEPTOR</u>

Assemble the susceptor in the furnace with the specimen lying in the middle of the axial cut-outs on the top and bottom inserts. Ensure that the steam port is in proper position for steam tube insertion. If running in steam, use the hollow alumina tube. If running in air, use the plugged alumina tube. Be careful not to damage specimen or drop/damage susceptor.

**Figure 40 : Assembing the susceptor with the specimen passing through the upper and lower plates.**

5. <u>CLOSE FURNACE</u>

Close the furnace leaving a ½" gap between the insulation blocks. Use a dental pick to support the susceptor while doing this. Insert the insulation forms on both sides of the furnace and gently close the furnace halves together. Use a tool to lightly tighten the furnace clamps. Apply remainder of insulation to sides and top.
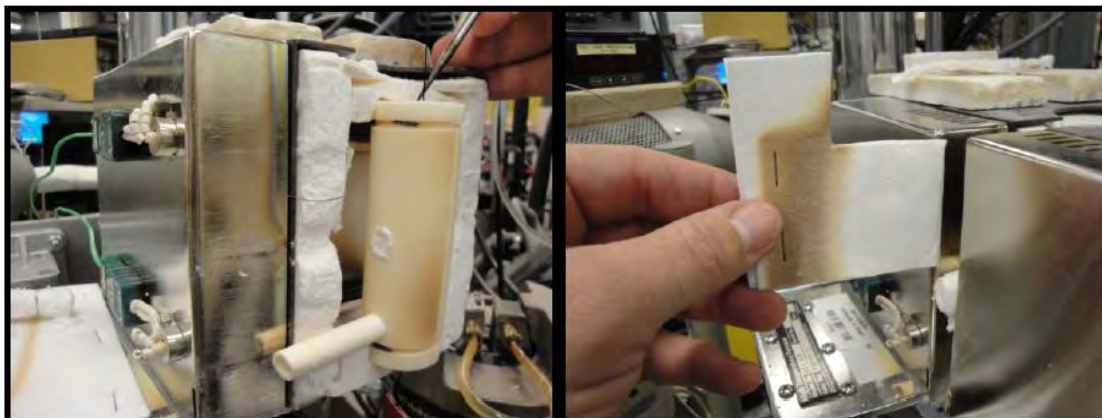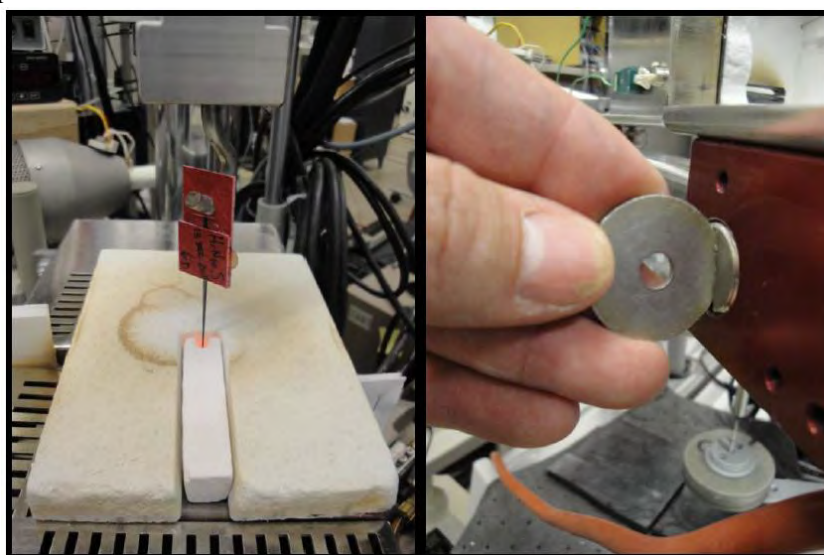
Figure 41 : Securing the susceptor in place with a pick while closing the furnace and installing the preformed insulation on the steam entry side.
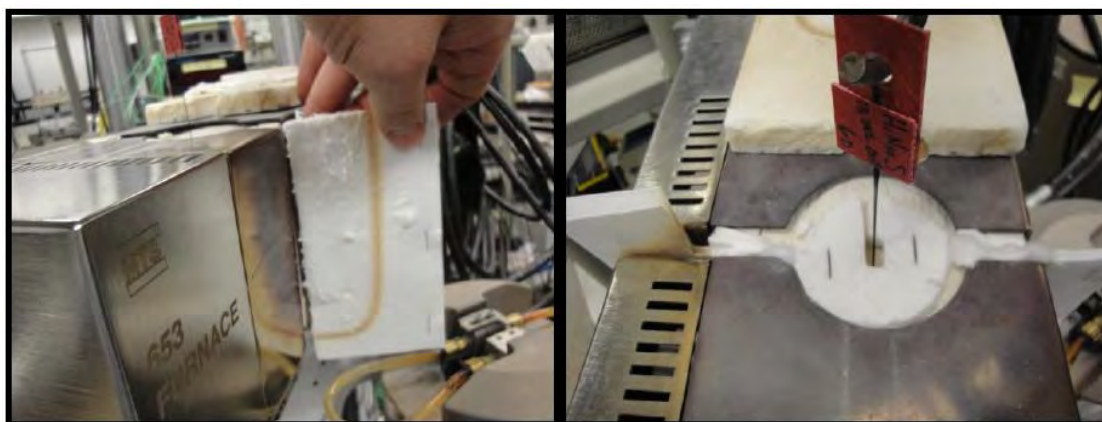
Figure 42 : Installing a second insulation preform on the opposite side and a third perform over the top of the furnace.

`

Figure 43 : Insulation blocks over the top of the furnace and the tool used to tighten the clamps used to secure the two halves of the furnace together.

6. LOAD PROCEDURE

Load or program the appropriate "Procedure" into the MPT/Procedure Editor screen of
the MTS Flextest 40 Controller computer terminal. The procedure file must have a file
extension of ".000" (decimal point, zero, zero, zero). Update the "destination" folders
(contained under each data type tab on the left) in the procedure to send the data to where
you want it. The "heat up data" folder should have an "h" directly after the date. This
differentiates the "heat up data" from the "long term data". Both of these file names
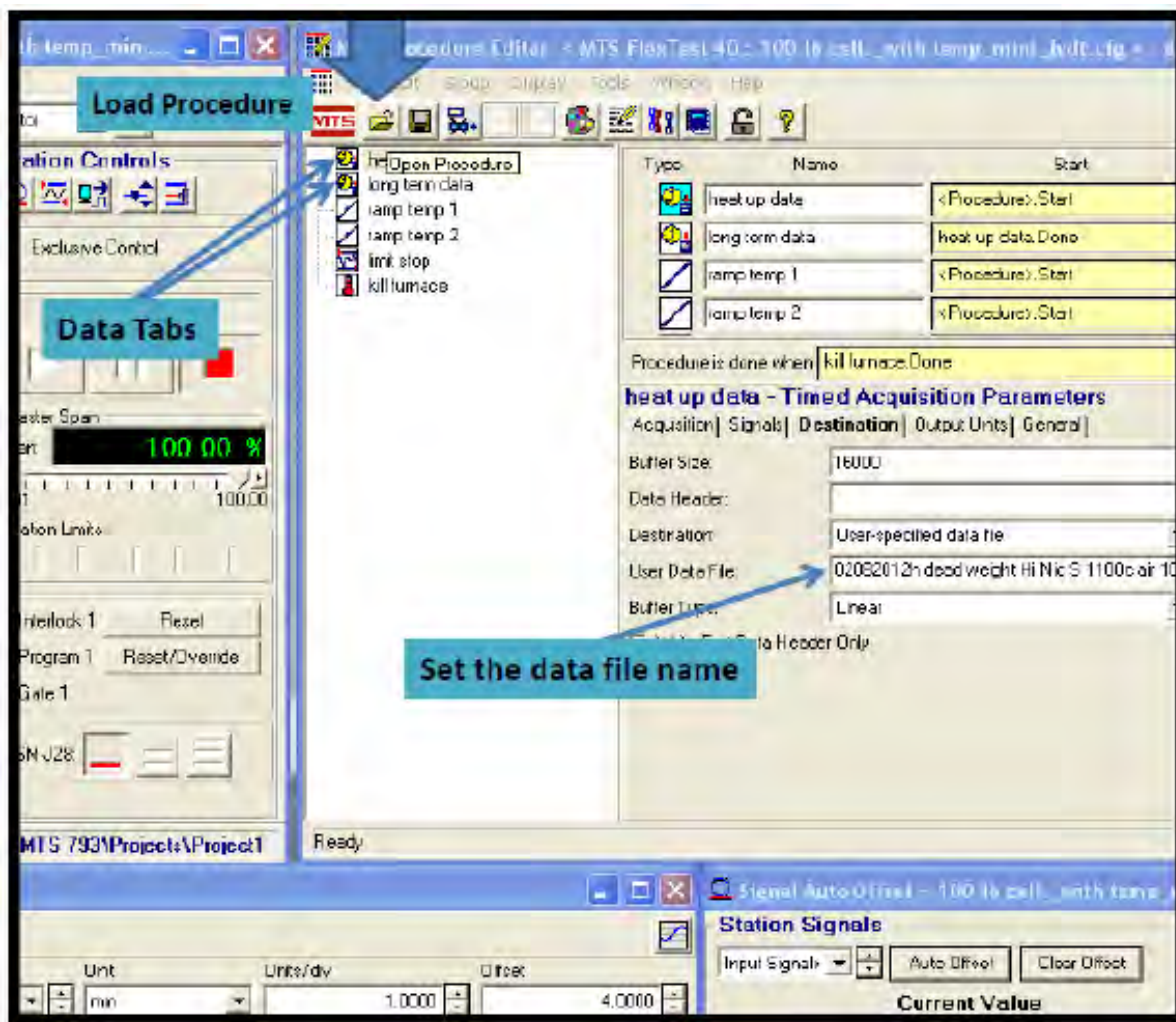should have a ".dat" file extension written at the end of them.

Figure 44 : Load procedure screen.

7. CREATE NEW SPECIMEN

Create a "New Specimen" (click on new specimen tile) on the MPT /Station Manager

screen and name it so that you can identify the file later. This should have no file
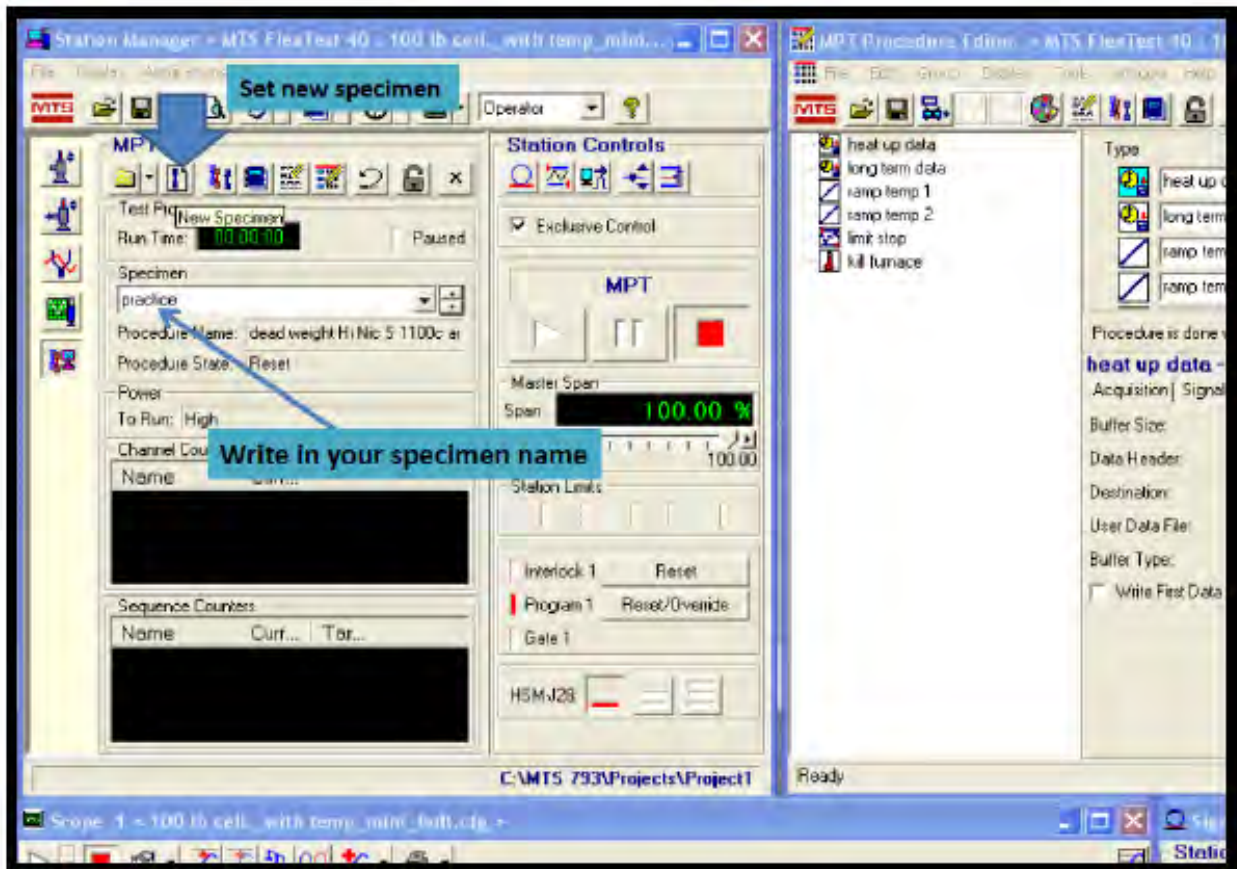
extension.

Figure 45 : Create new specimen screen.

8. ZERO LVDT OFFSET

Zero the offset on the LVDT (Linear Variable Displacement Transducer) on the
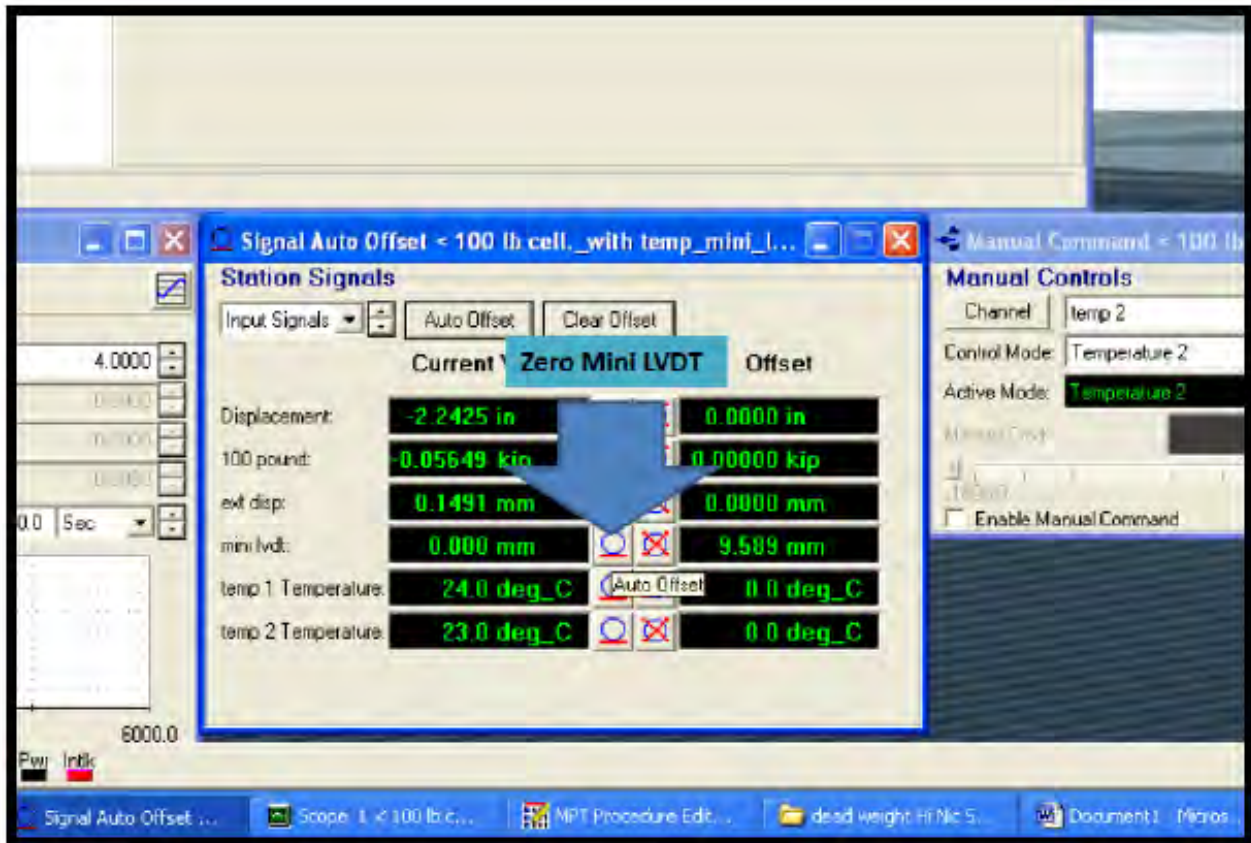
MPT/Signal Auto Offset menu.

Figure 46 : Zero LVDT screen.

9. RUN PROCEDURE-PROCESS

The process will ramp up to temp and dwell. This step will take 45 minutes.
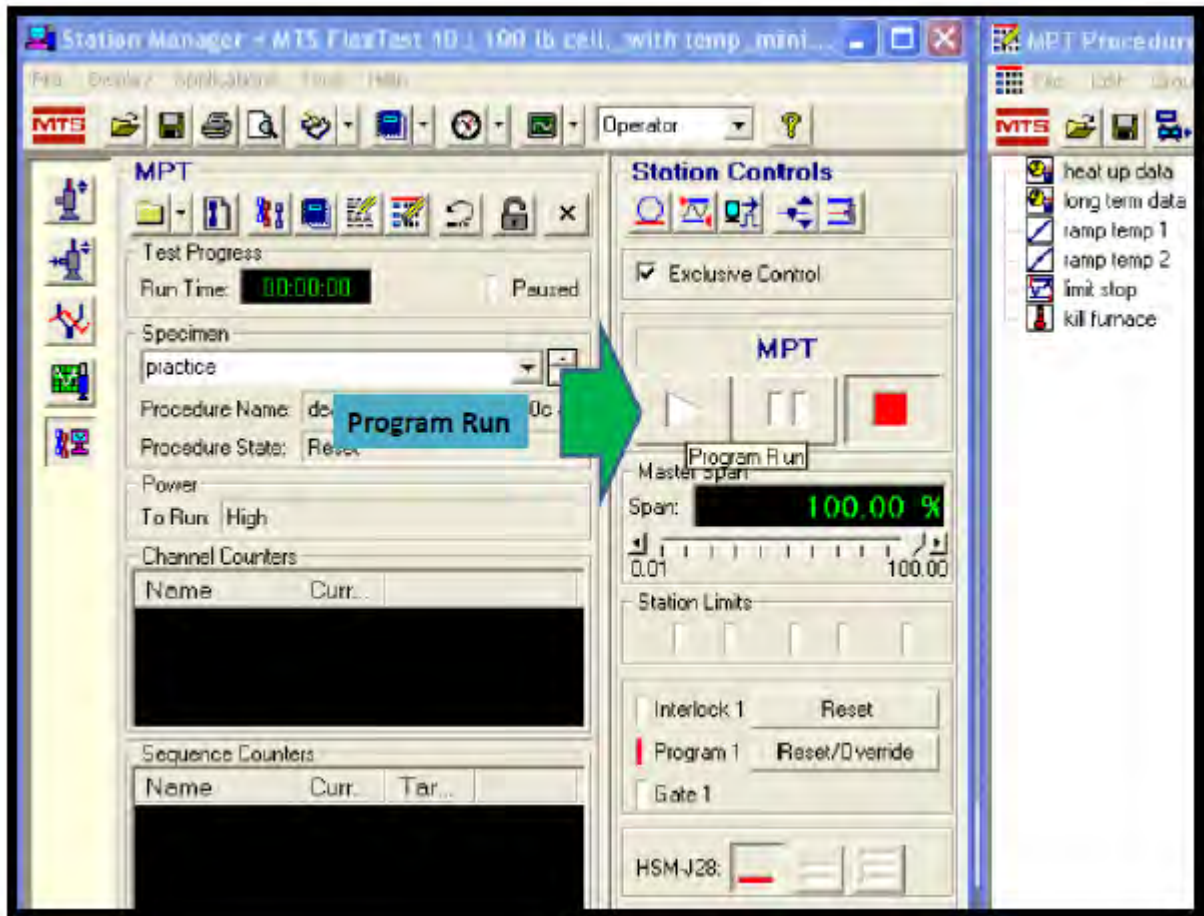


Figure 47 : Run process screen.

10. <u>LOAD SPECIMEN</u>

After 45 minutes have passed on the process timer, **<u>very slowly</u>** (over a time period of approx. 5 sec) load the specimen with the predetermined amount of weight. Use the elevator to do this.   Lower the elevator so that it is completely clear of the load train and weights. Loosen the clamp and move the elevator out of the way and make sure that the rubber mats are under the hanging weights.
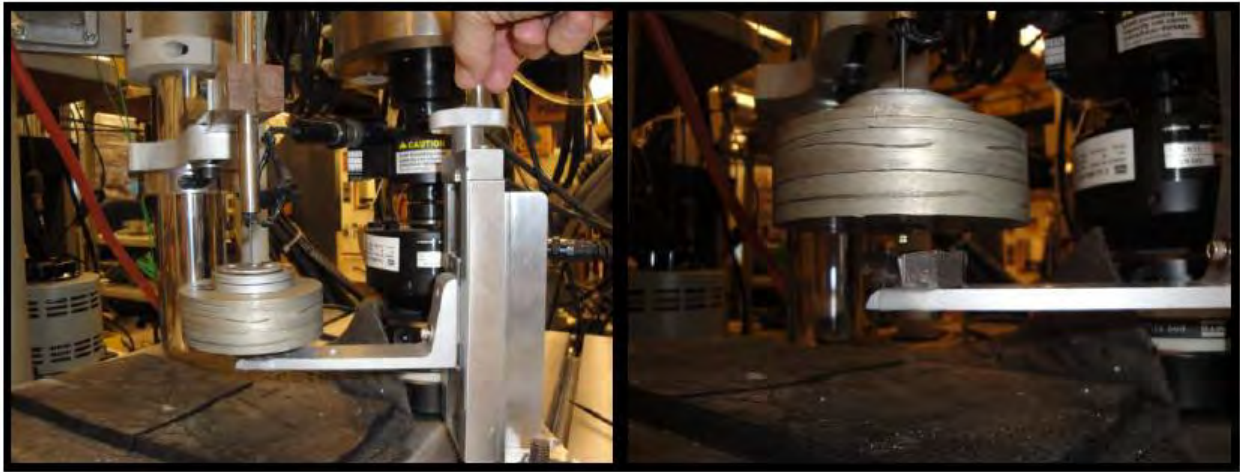
Figure 48 : Lowering the elevator slowly and clearing the split-nut platform.
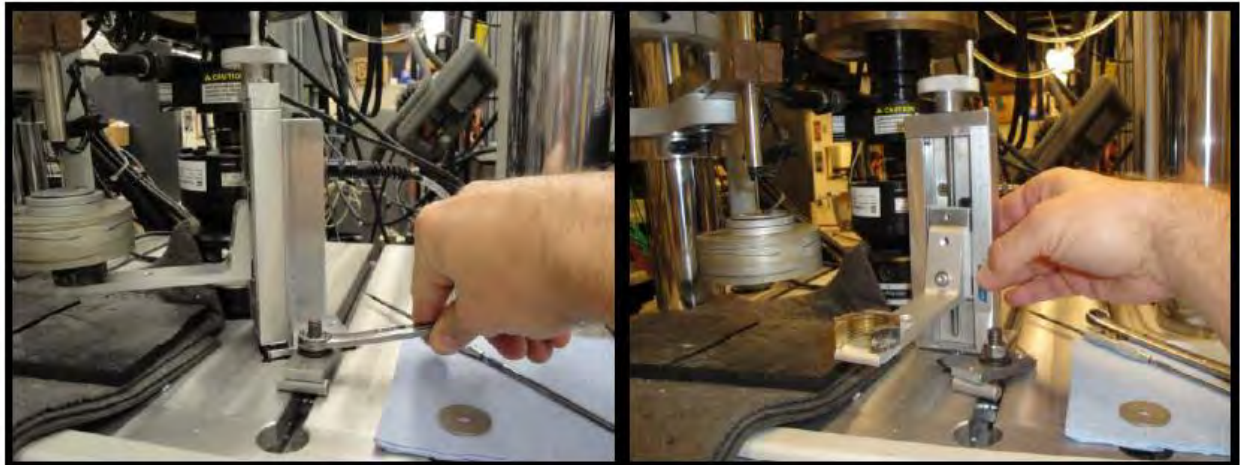
Figure 49 : Unloosing the clamp and moving the elevator out of the way of the weight stack.

11. <u>END RUN</u>

Let the procedure run to completion. After completion of run, go to the folder and find your data file you named previously. **(C:\MTS793\Projects\Project 1\MPT\Specimens\"Your file")**

12. <u>PREP FOR NEXT RUN</u>

After furnace is cool, open up the furnace halves and remove susceptor. Clean all equipment and make ready for next run.

Appendix A3

SPECIFICATION 1 : Stress-Weight Index Table and Equations

Table 4: Stress-weight index table and equations.

Engineering Stress = Force / Cross-sectional Area Total

Hi-Nicalon S Fiber Data

Force =	(Mass) x	(Gravity)
Newtons =	kg	9.81 m/s^2

Avg filament diameter (r) = 0.000012 m
filaments per tow (n)= 500

$$\text{Engineering Stress(Newtons/m}^2) = \frac{\text{Mass(kg) x Gravity(9.81 m/s}^2)}{\text{Cross-sectional Area Total(m}^2)}$$

Cross-sectional Area Total =   n * Cross-sectional Area of filament

Cross-sectional Area of filament =   Pi * r^2

Cross-sectional Area Total =   5.65487E-08 m^2

Engineering Stress		Mass		Sequence of Weights	Mass of Sequence †
5.20	Mpa	0.03 kg		Y, Z, (LT)	0.03 kg
76.33	Mpa	0.44 kg		M, N, R, S, Z, (LT)	0.44 kg
115.36	Mpa	0.665 kg		G, R, T, W, X, Y, (LT)	0.665 kg
138.78	Mpa	0.8 kg		G, M, N, O, (LT)	0.8 kg
154.40	Mpa	0.89 kg		G, M, N, O, T, X, Y, (LT)	0.89 kg
310.53	Mpa	1.79 kg		D, G, N, O, P, T, W, (LT)	1.79 kg
466.66	Mpa	2.69 kg		C, M, N, O, X, Y, Z, (LT)	2.69 kg
622.79	Mpa	3.59 kg		C, F, M, N, O, Y, Z, (LT)	3.59 kg
779.79	Mpa	4.495 kg		C, D, E, M, N, O, Y, (LT)	4.495 kg
935.92	Mpa	5.395 kg		A, G, M, N, O, T, X, Y, (LT)	5.395 kg
1092.05	Mpa	6.295 kg		A, D, G, M, N, O, T, Y, (LT)	6.295 kg
1248.18	Mpa	7.195 kg		A, C, N, O, P, X, Y, (LT)	7.195 kg
1560.44	Mpa	8.995 kg		A, C, D, E, M, N, O, Z, (LT)	8.995 kg

Load Train Weight (LT) =   0.01055 Kg

† - as per Acculab SV-30 (+/- .005 kg)

Weight Cross-Reference Chart

	(kg)		(kg)		(kg)		(kg)
A=	4.505	H=	0.455	O=	0.115	V=	0.02
B=	4.51	I=	0.455	P=	0.115	W=	0.02
C=	2.295	J=	0.455	Q=	0.115	X=	0.02
D=	0.91	K=	0.455	R=	0.1	Y=	0.02
E=	0.915	L=	0.455	S=	0.1	Z=	0.01
F=	0.92	M=	0.113	T=	0.05		
G=	0.455	N=	0.115	U=	0.05		

A-F weighed on Acculab SV-30 (+/- .005 kg)
G-Z weighed on Voyager Pro (+/- .001 kg)

Appendix A4

SPECIFICATION 2 : Tab Fabrication

Note: Prepare ample amounts of the different tabs for specimen prep. Fabricate by cutting fiberglass blanks on the paper shear. Use the heavy-duty hole punch to make the hook hole. After fabrication, store in segmented storage box for later use. Refer to the drawings for dimensions.
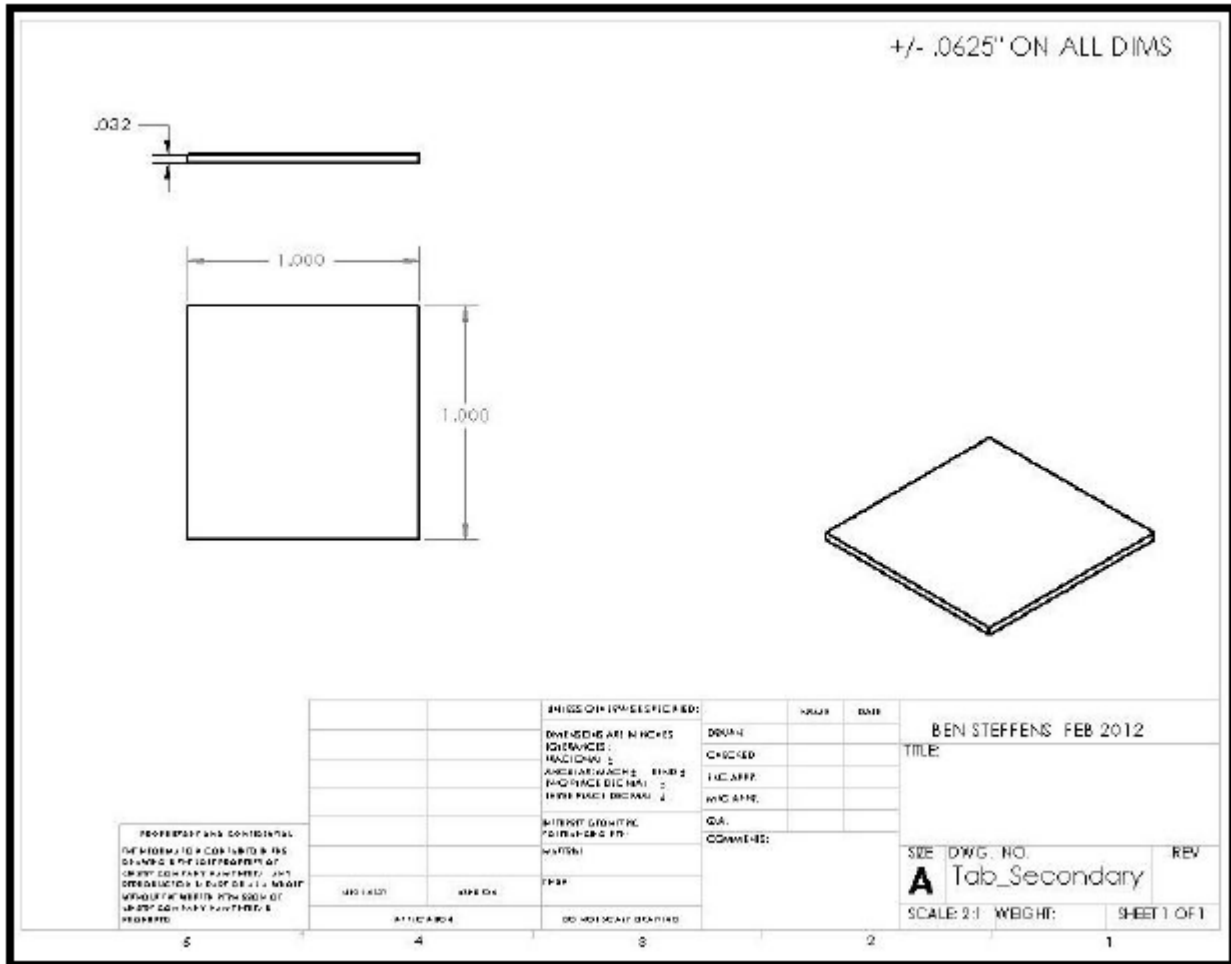

Figure 50 : Tab storage container.
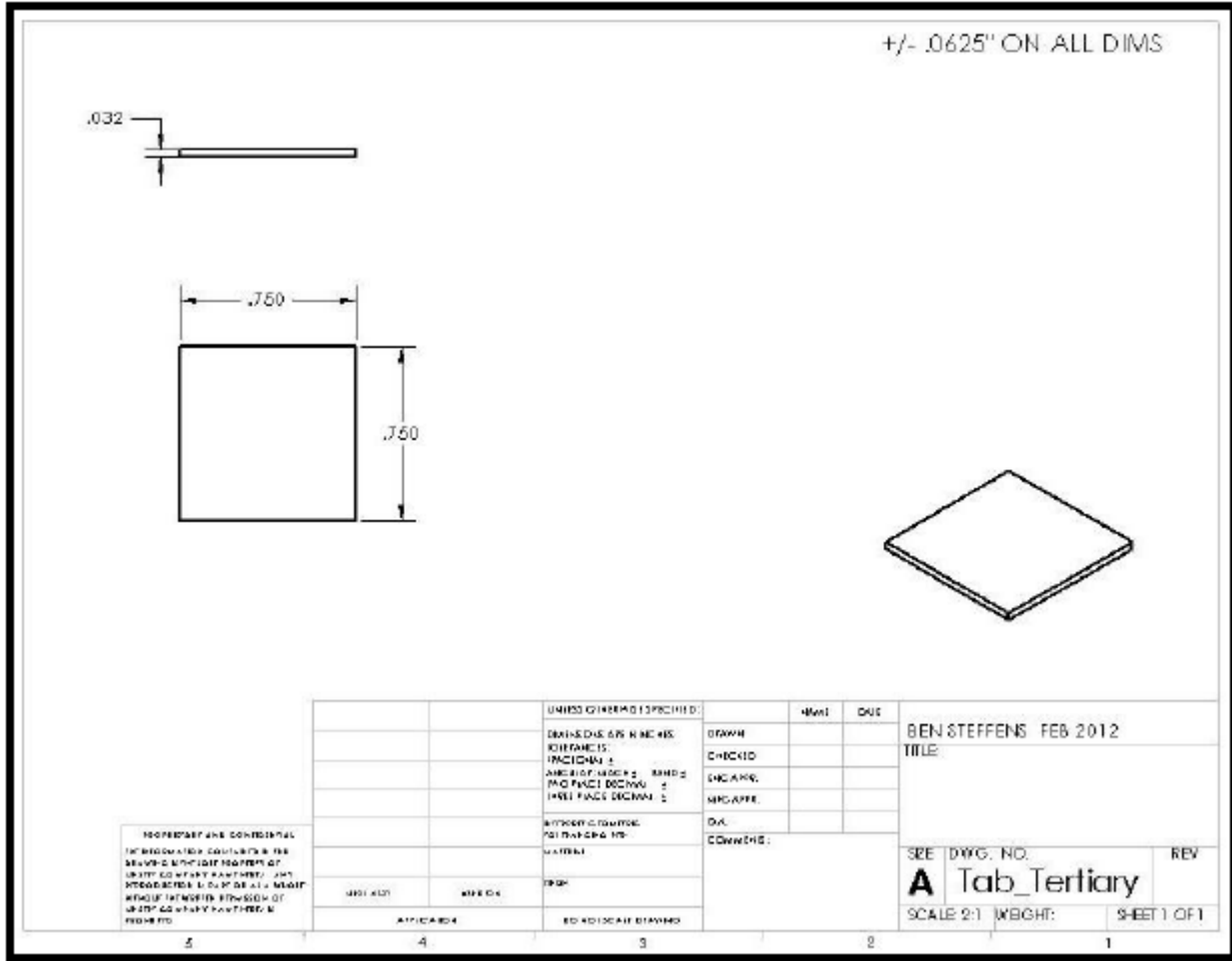
Figure 51 : Technical specifications for Primary Tab

Figure 52 : Technical specifications for Secondary Tab

Figure 53 : Technical specifications for Tertiary Tab

Appendix A5

SPECIFICATION 3 : Furnace and Steam Generator Settings

Table 5: Furnace and Steam Generator Settings

<u>Furnace Temperature Settings</u>

		Air	Steam
800 °C	Upper (1)	801	790
	Lower (2)	804	837
900 °C	Upper (1)	903	892
	Lower (2)	909	939
1000 °C	Upper (1)	1003	994
	Lower (2)	1010	1041
1100 °C	Upper (1)	1102	1097
	Lower (2)	1114	1144
1200 °C	Upper (1)	1205	1200
	Lower (2)	1216	1247

<u>Steam Generator Settings</u>

| Variac	39% ± 1%
Pump	.8 mL/min
Snout T/C	100 °C ± 10 °C
Chamber T/C	240 °C ± 15 °C

Appendix A6

IMAGES : SEM Microscopy
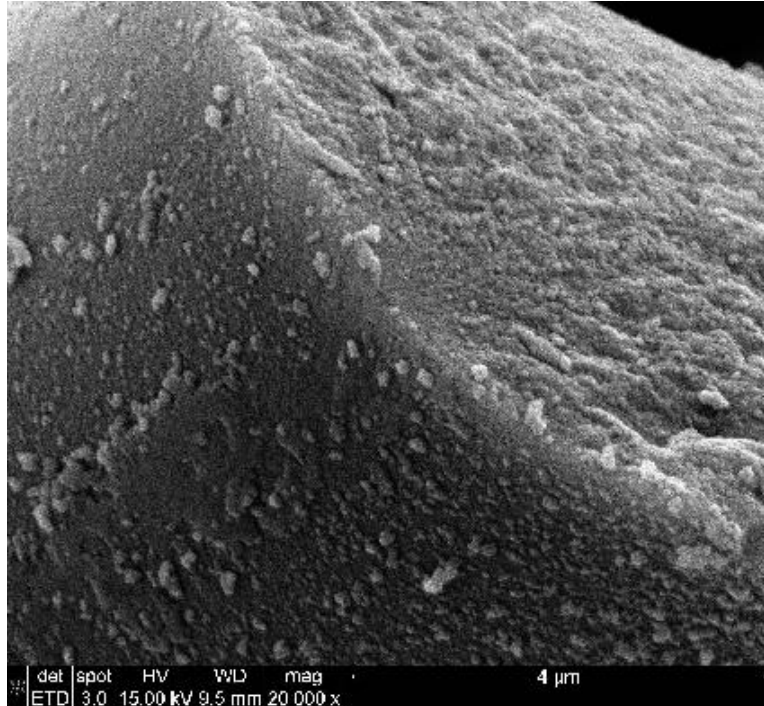
Figure 54 : SEM micrograph of the Hi-Nicalon S fiber tow specimen that achieved run-out during creep test at 800°C in laboratory air (σ_{cr} = 467 MPa, t_f = 100 h).
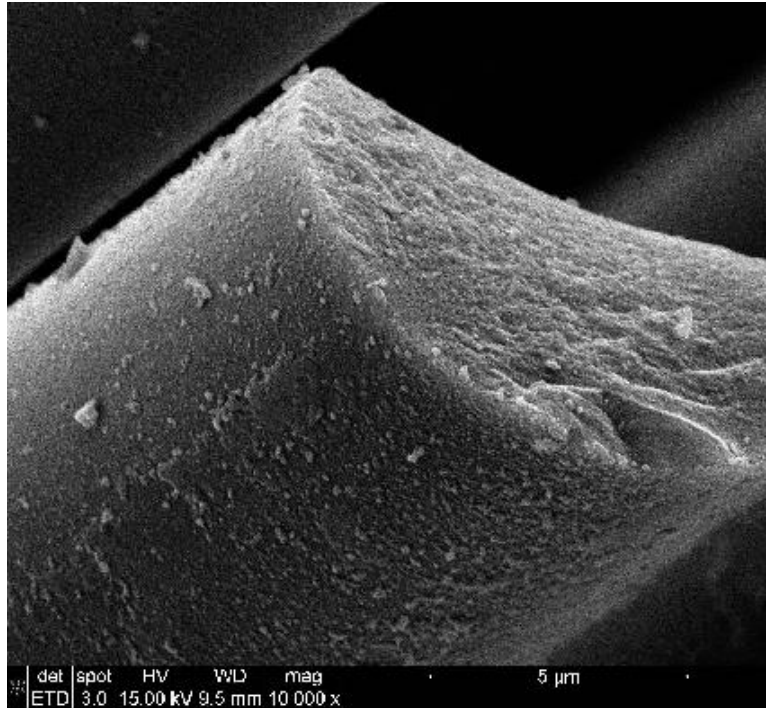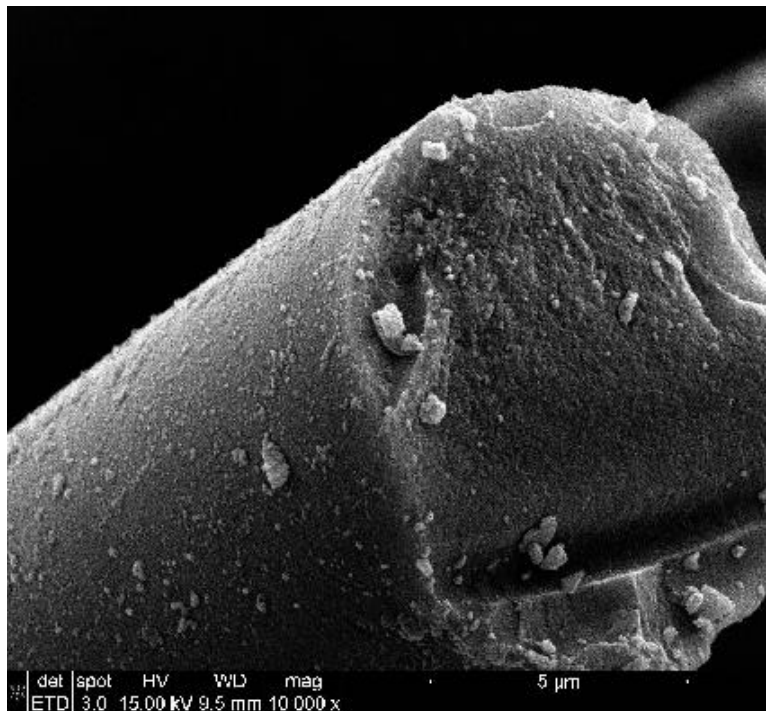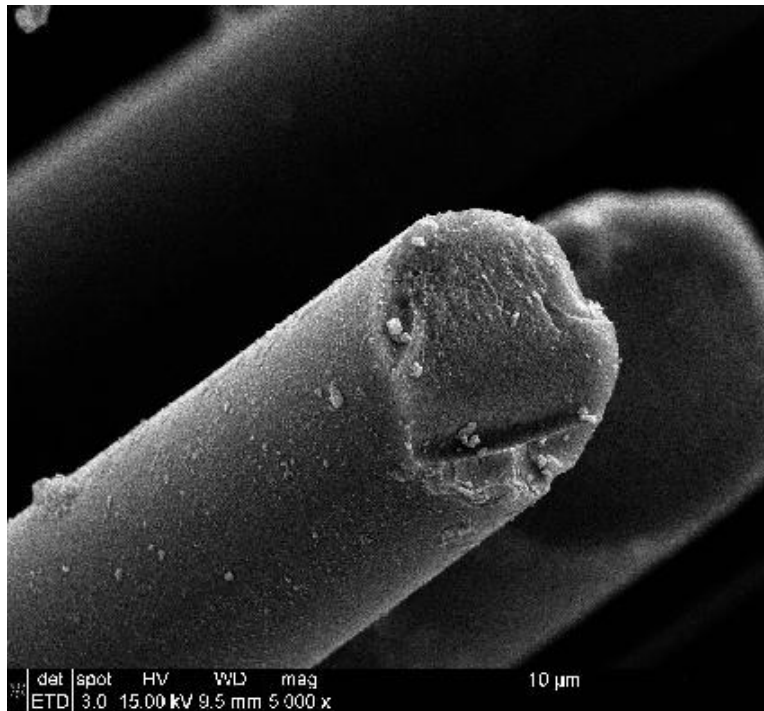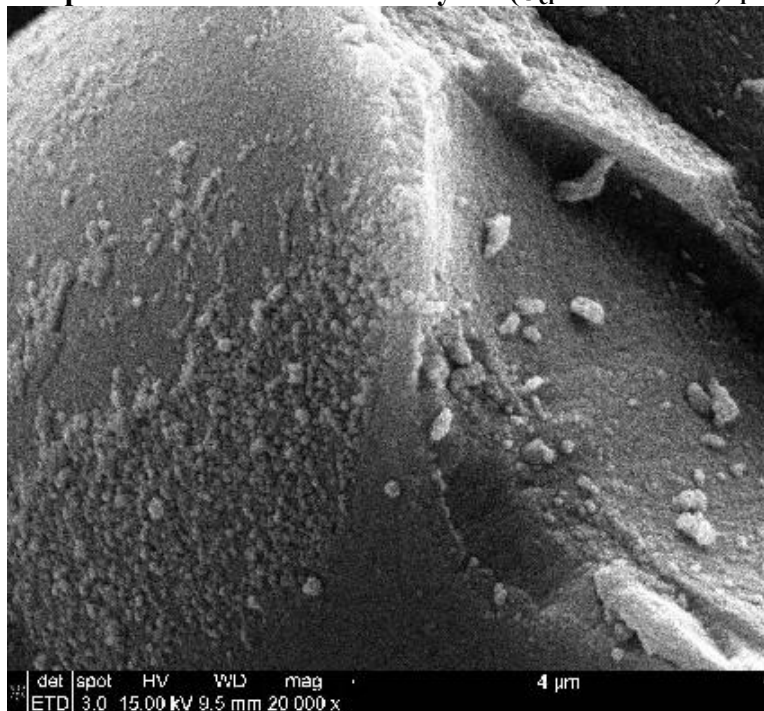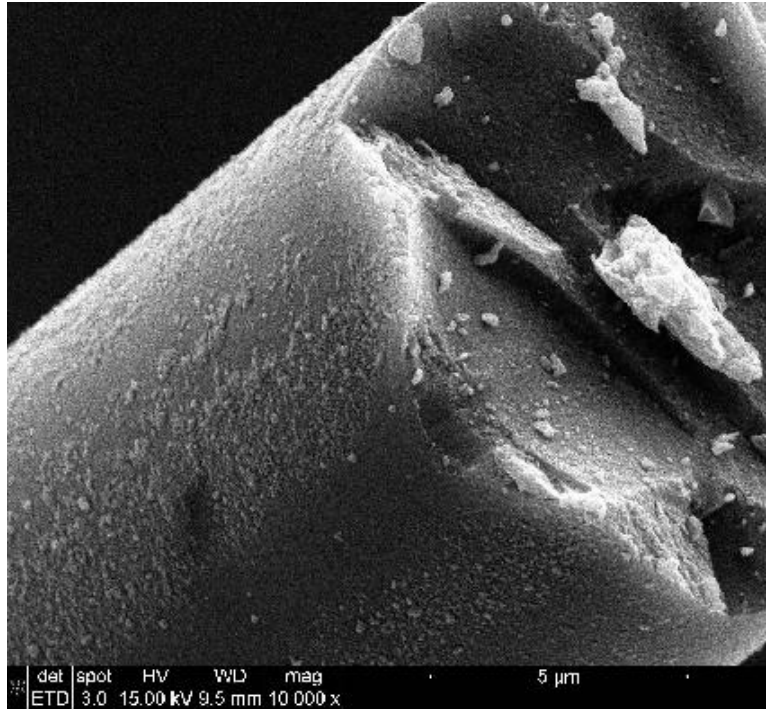
Figure 55 : SEM micrograph of the Hi-Nicalon S fiber tow specimen that achieved run-out during creep test at 800°C in laboratory air (σ_{cr} = 467 MPa, t_f = 100 h).
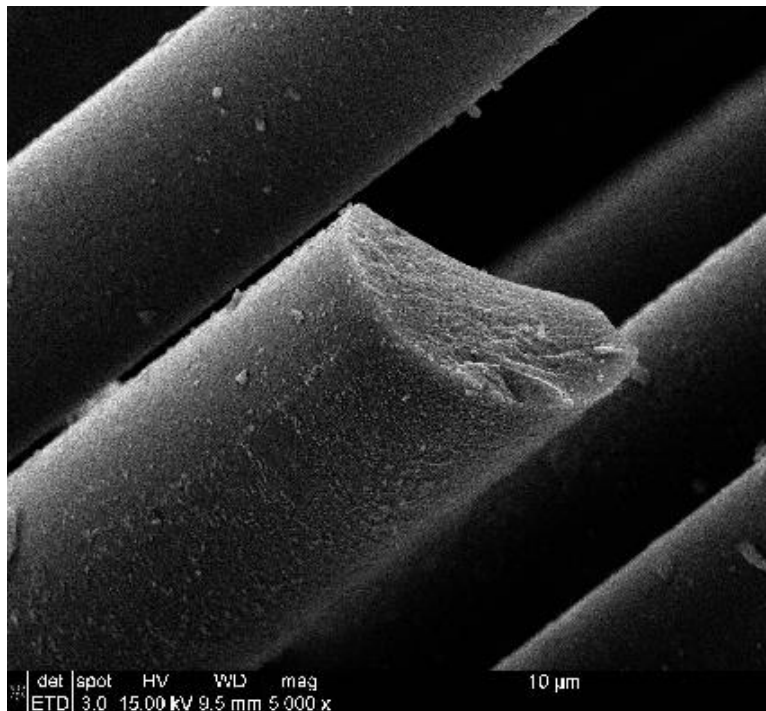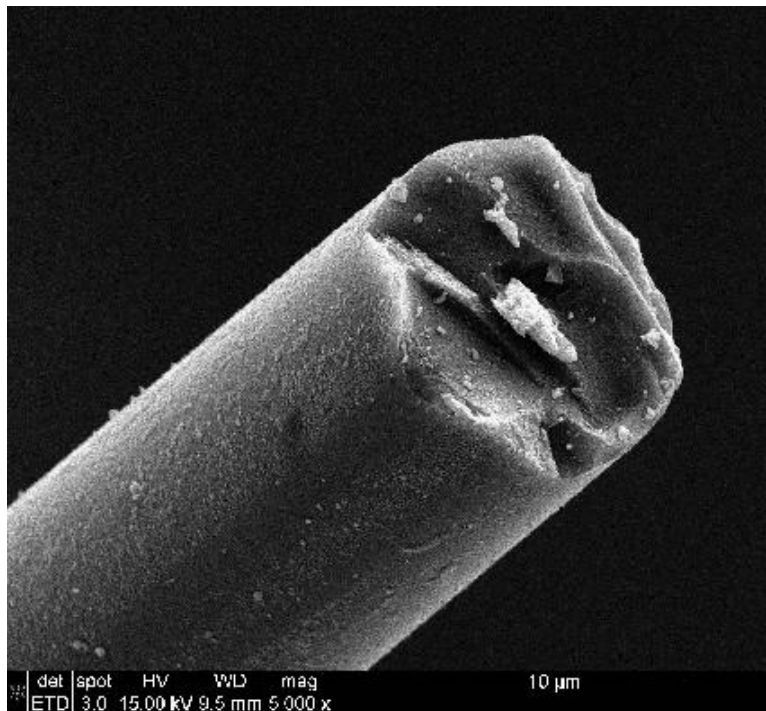

Figure 56 : SEM micrograph of the Hi-Nicalon S fiber tow specimen that achieved run-out during creep test at 800°C in laboratory air (σ_{cr} = 467 MPa, t_f = 100 h).
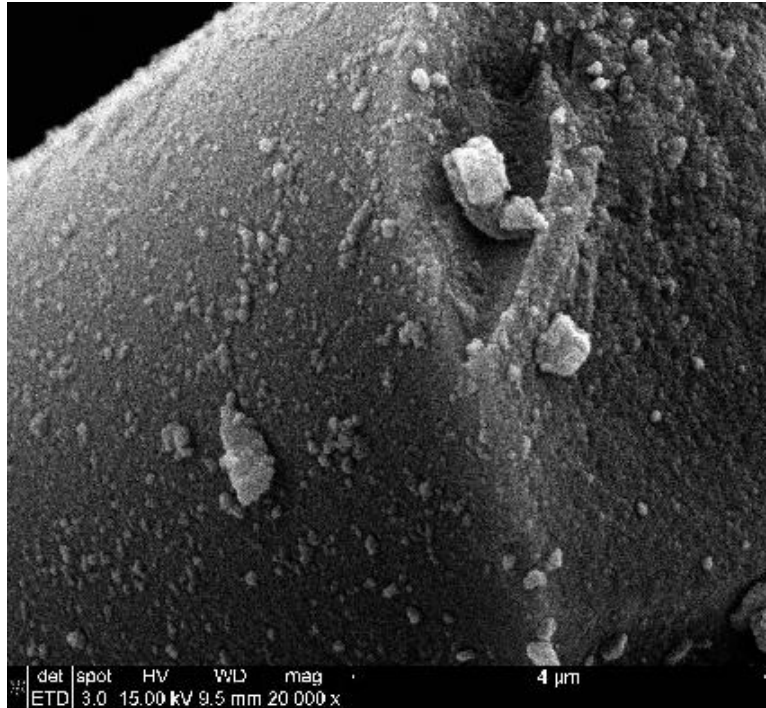
Figure 57 : SEM micrograph of the Hi-Nicalon S fiber tow specimen that achieved run-out during creep test at 800°C in laboratory air (σ_{cr} = 467 MPa, t_f = 100 h).

Figure 58 : SEM micrograph of the Hi-Nicalon S fiber tow specimen that achieved run-out during creep test at 800°C in laboratory air (σ_{cr} = 467 MPa, t_f = 100 h).

Figure 59 : SEM micrograph of the Hi-Nicalon S fiber tow specimen that achieved run-out during creep test at 800°C in laboratory air (σ_{cr} = 467 MPa, t_f = 100 h).

Figure 60 : SEM micrograph of the Hi-Nicalon S fiber tow specimen that achieved run-out during creep test at 800°C in laboratory air (σ_{cr} = 467 MPa, t_f = 100 h).
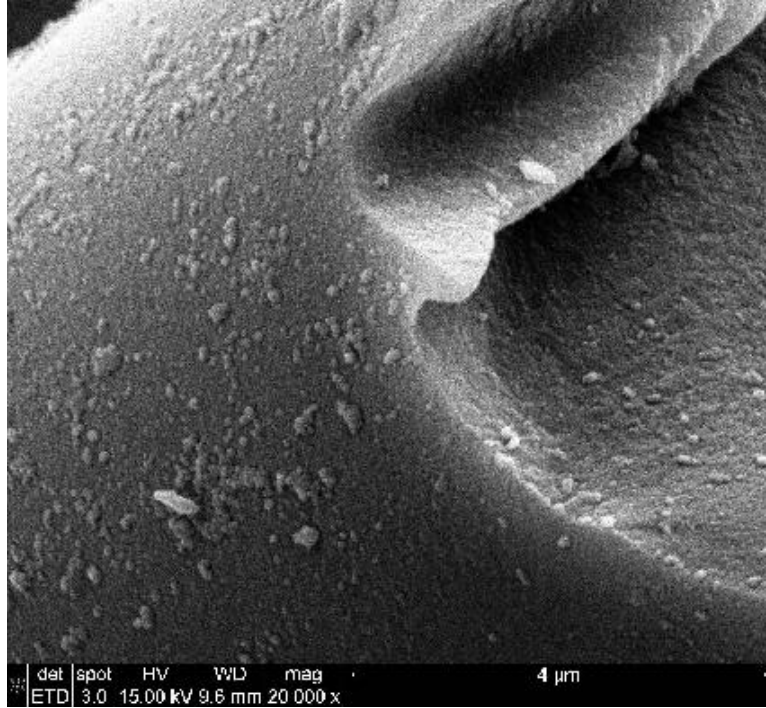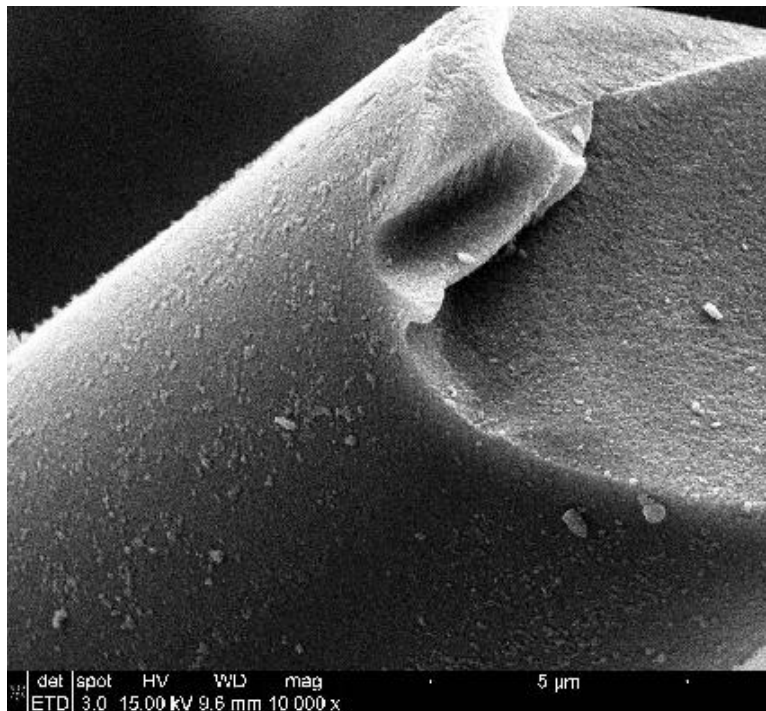
Figure 61 : SEM micrograph of the Hi-Nicalon S fiber tow specimen that achieved run-out during creep test at 800°C in laboratory air (σ_{cr} = 467 MPa, t_f = 100 h).

Figure 62 : SEM micrograph of the Hi-Nicalon S fiber tow specimen that achieved run-out during creep test at 800°C in laboratory air (σ_{cr} = 467 MPa, t_f = 100 h).
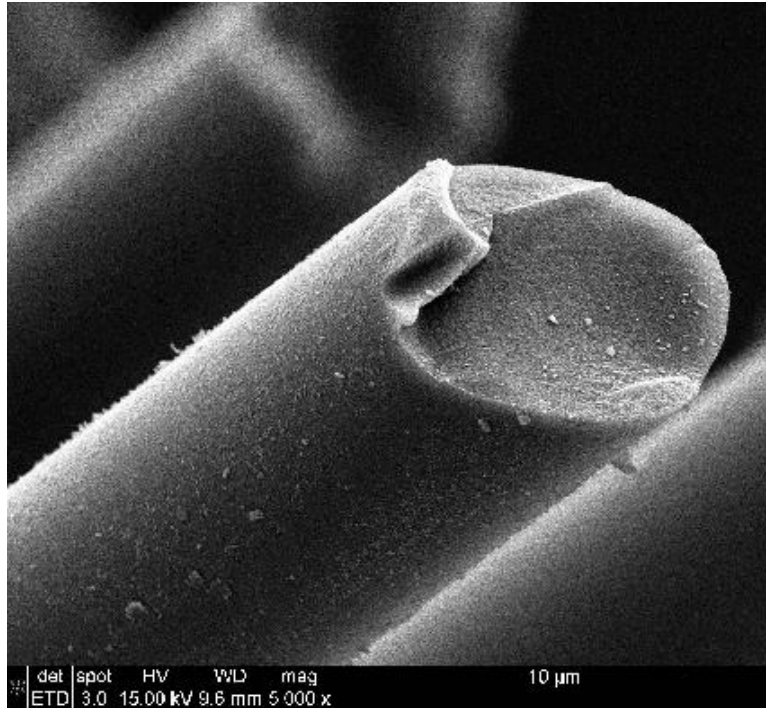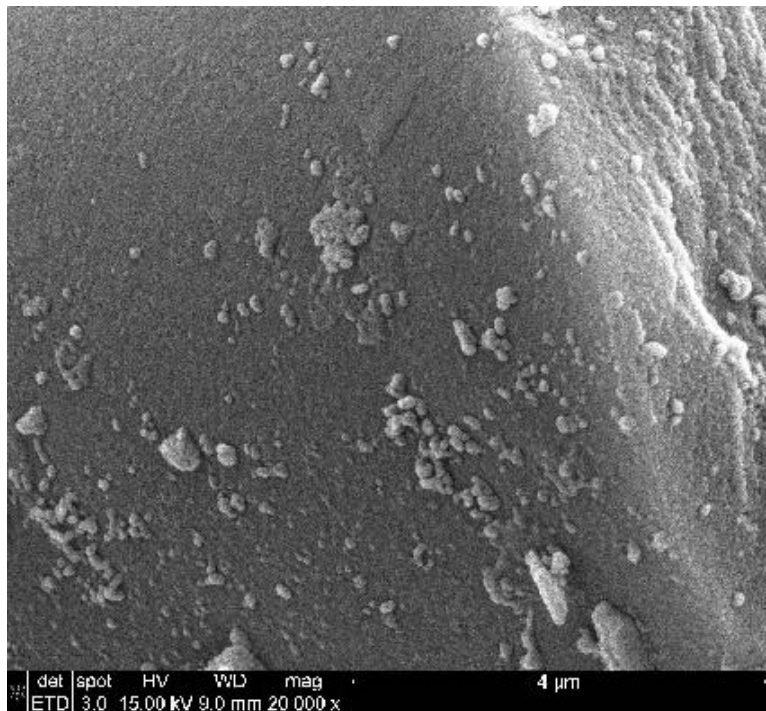
Figure 63 : SEM micrograph of the Hi-Nicalon S fiber tow specimen that achieved run-out during creep test at 800°C in laboratory air (σ_{cr} = 467 MPa, t_f = 100 h).
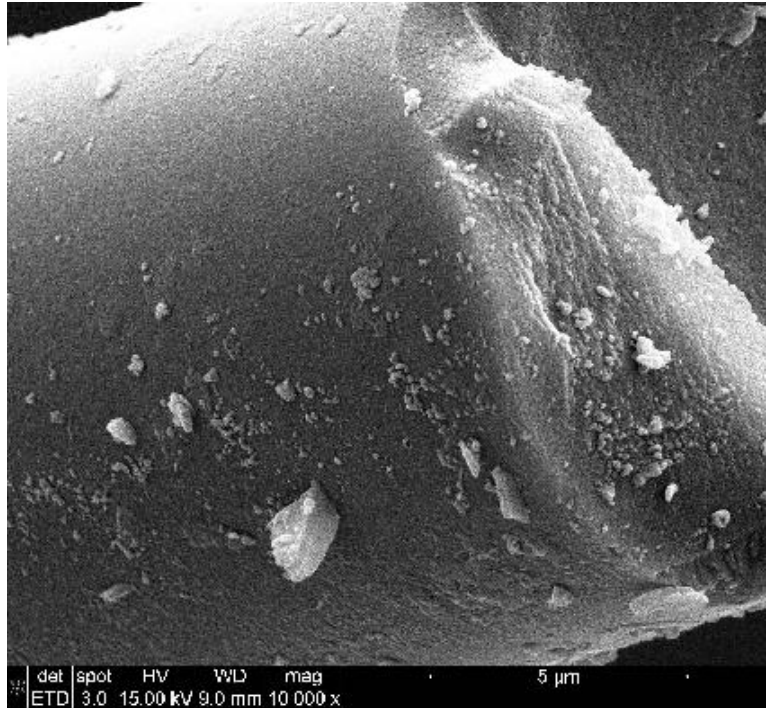

Figure 64 : SEM micrograph of the Hi-Nicalon S fiber tow specimen that achieved run-out during creep test at 800°C in laboratory air (σ_{cr} = 467 MPa, t_f = 100 h).
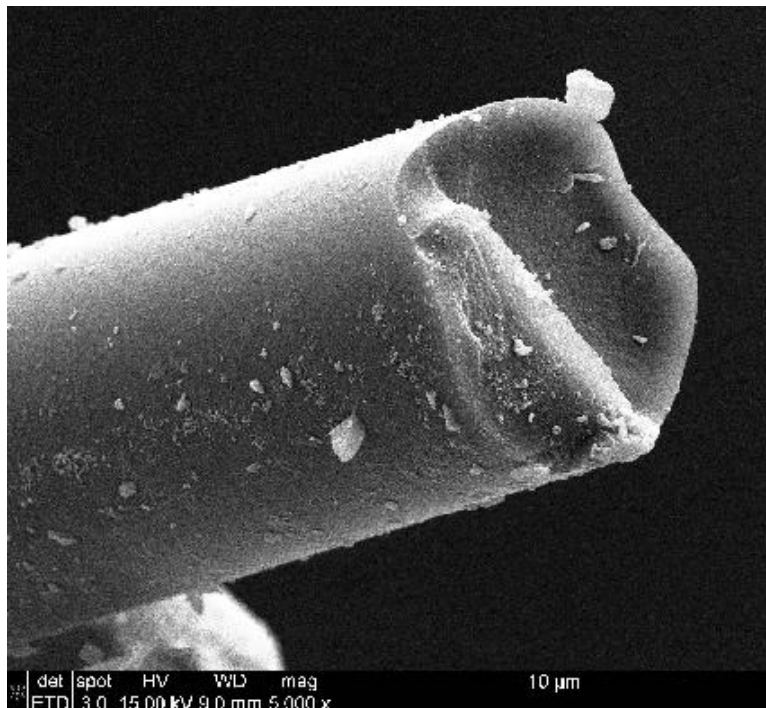
Figure 65 : SEM micrograph of the Hi-Nicalon S fiber tow specimen that achieved run-out during creep test at 800°C in laboratory air (σ_{cr} = 467 MPa, t_f = 100 h).
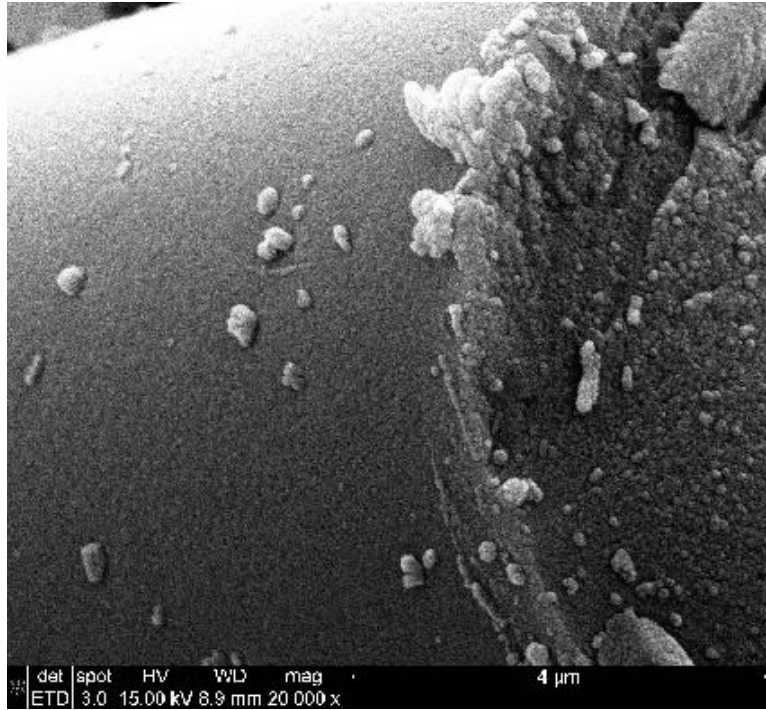

Figure 66 : SEM micrograph of the Hi-Nicalon S fiber tow specimen failed in creep at 800°C in steam (σ_{cr} = 154 MPa, t_f = .82 h).

83

Figure 67 : SEM micrograph of the Hi-Nicalon S fiber tow specimen failed in creep at 800°C in steam (σ_{cr} = 154 MPa, t_f = .82 h).

Figure 68 : SEM micrograph of the Hi-Nicalon S fiber tow specimen failed in creep at 800°C in steam (σ_{cr} = 154 MPa, t_f = .82 h).
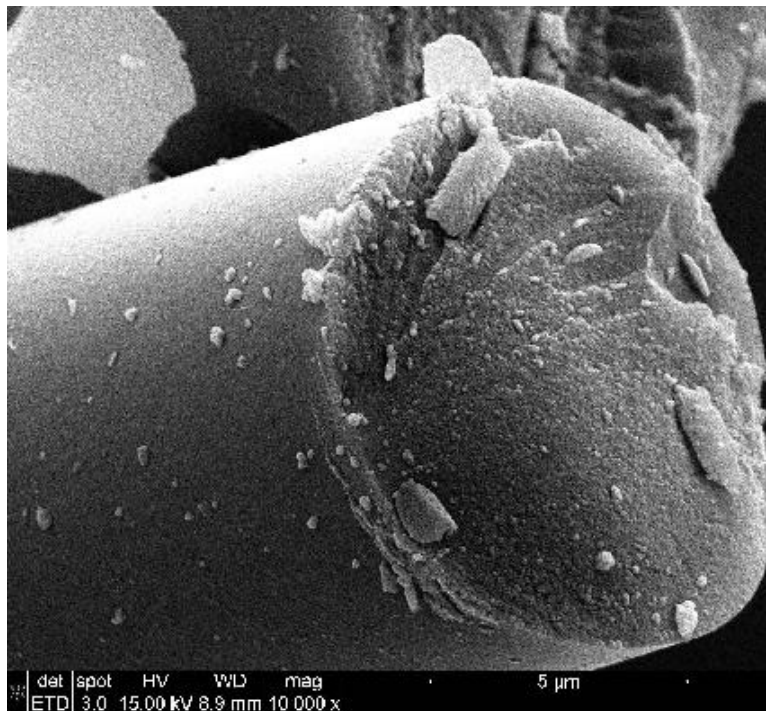
Figure 69 : SEM micrograph of the Hi-Nicalon S fiber tow specimen failed in creep at 800°C in steam (σ_{cr} = 154 MPa, t_f = .82 h).

Figure 70 : SEM micrograph of the Hi-Nicalon S fiber tow specimen failed in creep at 800°C in steam (σ_{cr} = 154 MPa, t_f = .82 h).

Figure 71 : SEM micrograph of the Hi-Nicalon S fiber tow specimen failed in creep at 800°C in steam (σ_{cr} = 154 MPa, t_f = .82 h).

Figure 72 : SEM micrograph of the Hi-Nicalon S fiber tow specimen failed in creep at 800°C in steam (σ_{cr} = 154 MPa, t_f = .82 h).
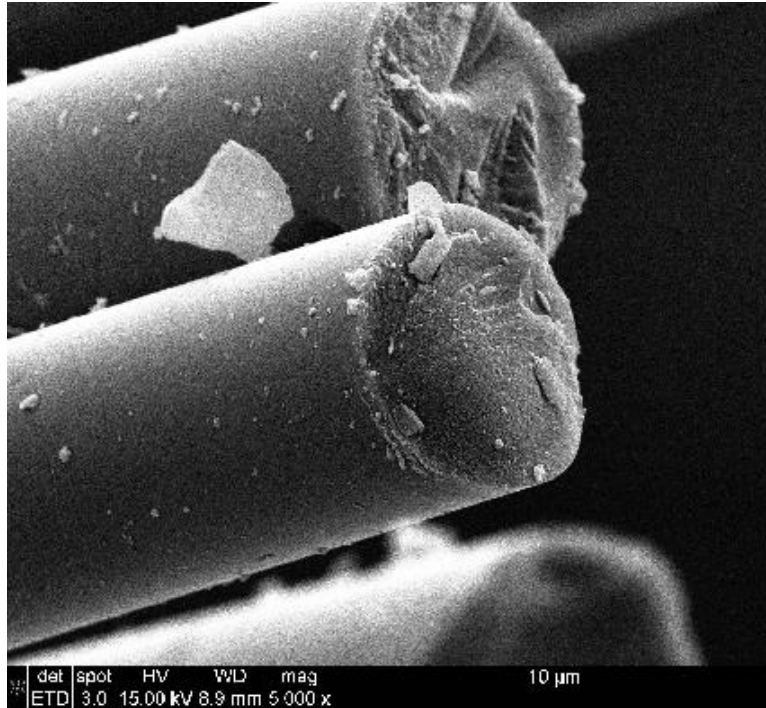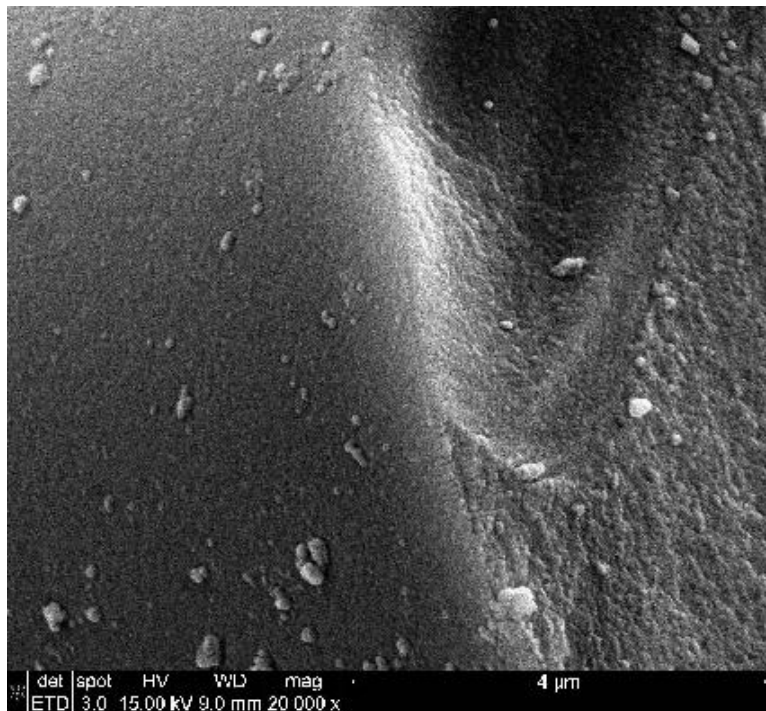
Figure 73 : SEM micrograph of the Hi-Nicalon S fiber tow specimen failed in creep at 800°C in steam (σ_{cr} = 154 MPa, t_f = .82 h).

Figure 74 : SEM micrograph of the Hi-Nicalon S fiber tow specimen failed in creep at 800°C in steam (σ_{cr} = 154 MPa, t_f = .82 h).
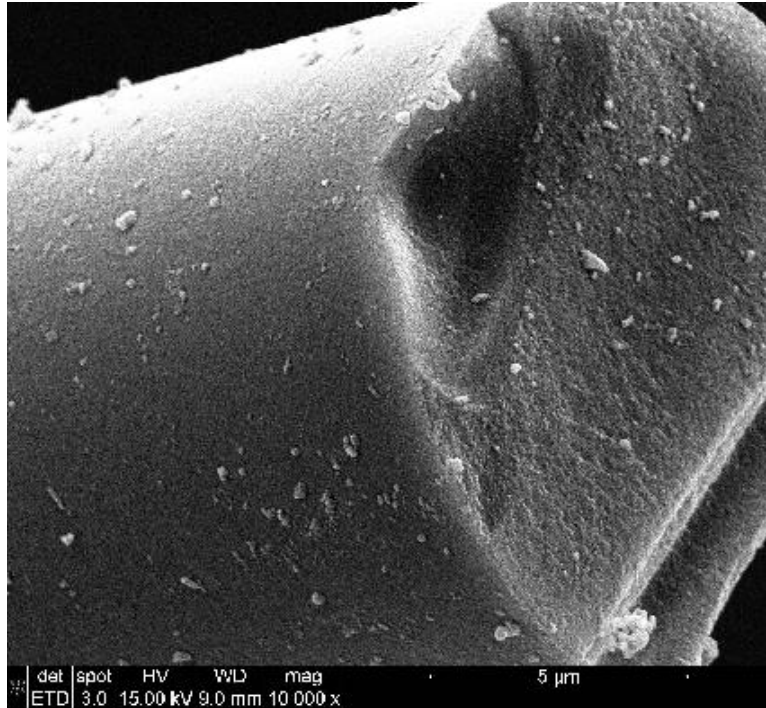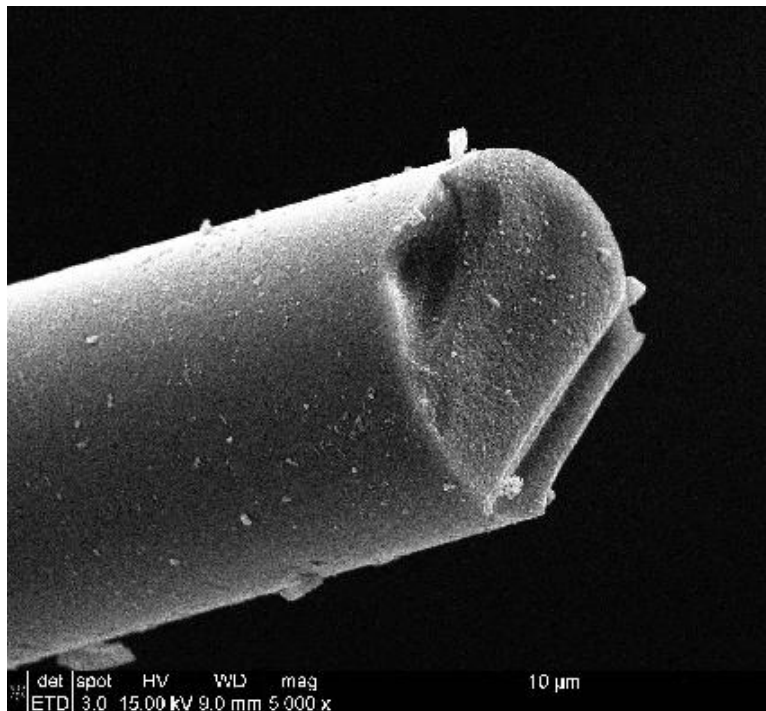
Figure 75 : SEM micrograph of the Hi-Nicalon S fiber tow specimen failed in creep at 800°C in steam (σ_{cr} = 154 MPa, t_f = .82 h).

Figure 76 : SEM micrograph of the Hi-Nicalon S fiber tow specimen failed in creep at 800°C in steam (σ_{cr} = 154 MPa, t_f = .82 h).
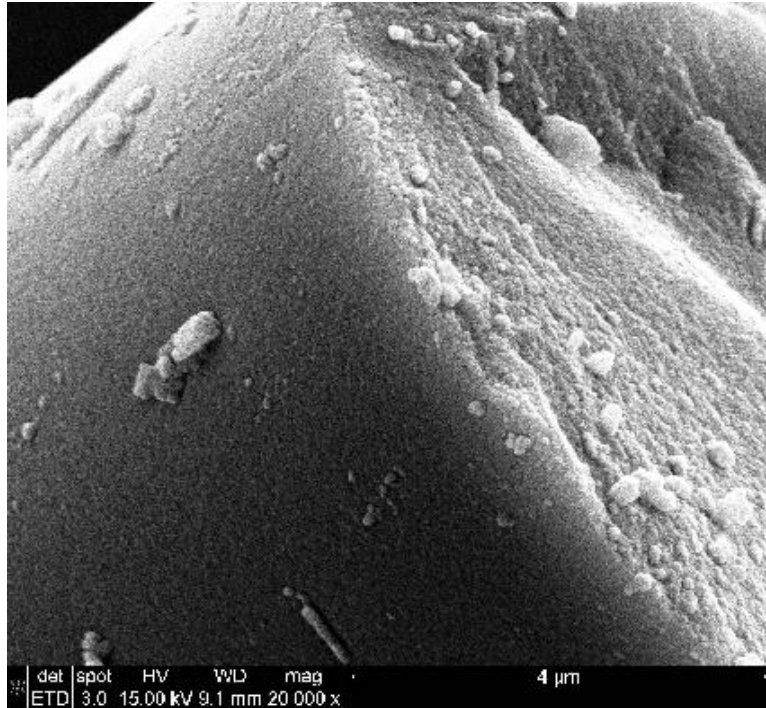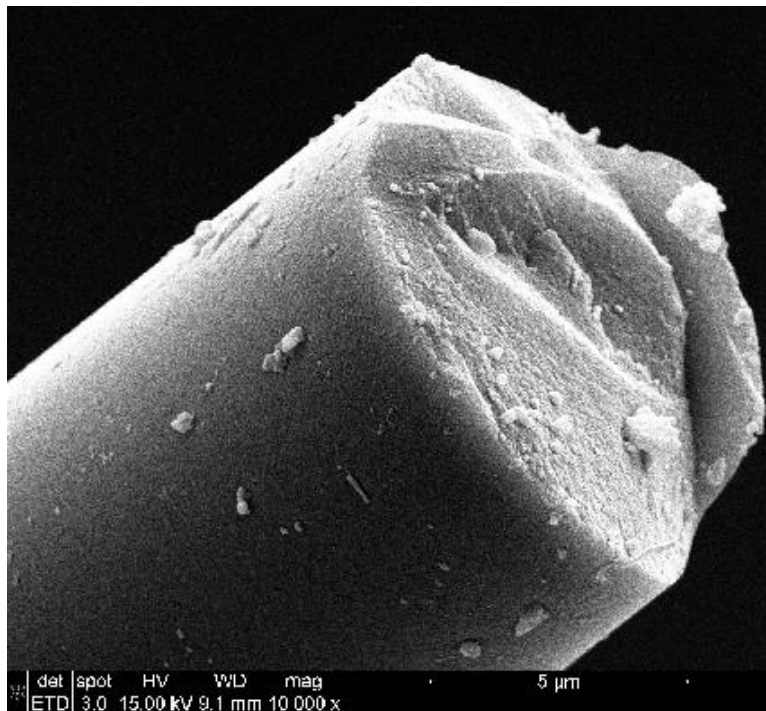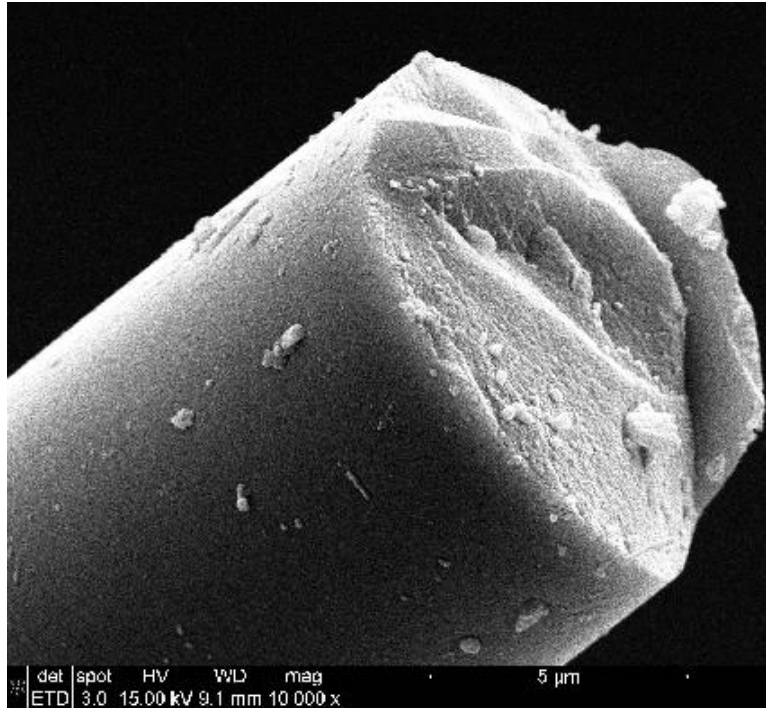
Figure 77 : SEM micrograph of the Hi-Nicalon S fiber tow specimen failed in creep at 800°C in steam (σ_{cr} = 154 MPa, t_f = .82 h).

Figure 78 : SEM micrograph of the Hi-Nicalon S fiber tow specimen failed in creep at 800°C in steam (σ_{cr} = 154 MPa, t_f = .82 h).

Figure 79 : SEM micrograph of the Hi-Nicalon S fiber tow specimen failed in creep at 1100°C in laboratory air (σ_{cr} = 467 MPa, t_f = 17.1 h).

Figure 80 : SEM micrograph of the Hi-Nicalon S fiber tow specimen failed in creep at 1100°C in laboratory air (σ_{cr} = 467 MPa, t_f = 17.1 h).

Figure 81 : SEM micrograph of the Hi-Nicalon S fiber tow specimen failed in creep at 1100°C in laboratory air (σ_{cr} = 467 MPa, t_f = 17.1 h).
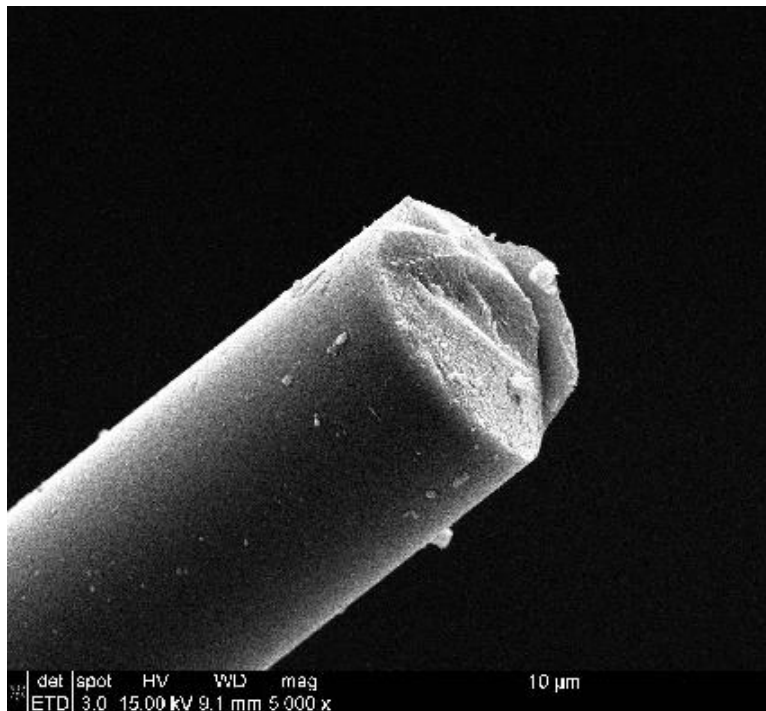

Figure 82 : SEM micrograph of the Hi-Nicalon S fiber tow specimen failed in creep at 1100°C in laboratory air (σ_{cr} = 467 MPa, t_f = 17.1 h).

Figure 83 : SEM micrograph of the Hi-Nicalon S fiber tow specimen failed in creep at 1100°C in laboratory air (σ_{cr} = 467 MPa, t_f = 17.1 h).
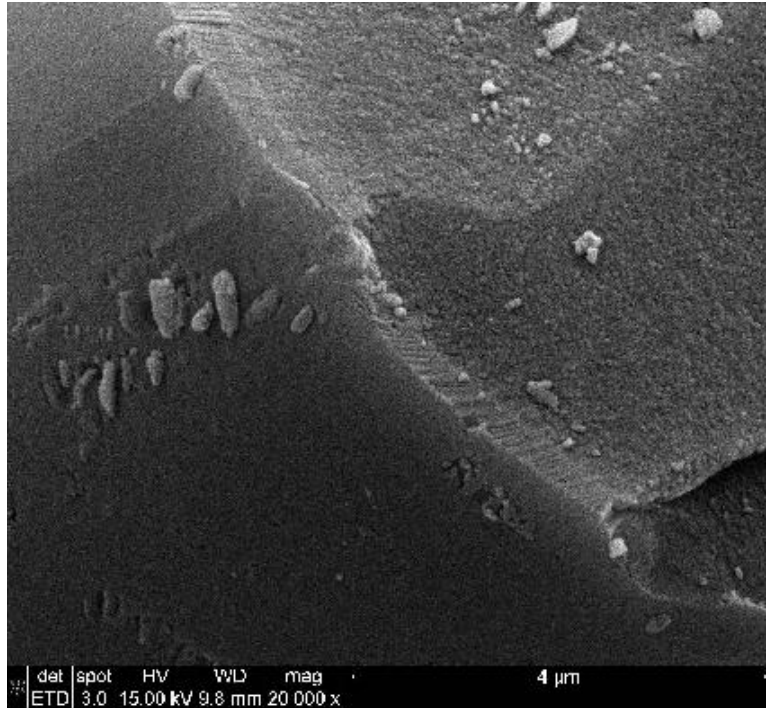

Figure 84 : SEM micrograph of the Hi-Nicalon S fiber tow specimen failed in creep at 1100°C in laboratory air (σ_{cr} = 467 MPa, t_f = 17.1 h).

Figure 85 : SEM micrograph of the Hi-Nicalon S fiber tow specimen failed in creep at 1100°C in laboratory air (σ_{cr} = 467 MPa, t_f = 17.1 h).
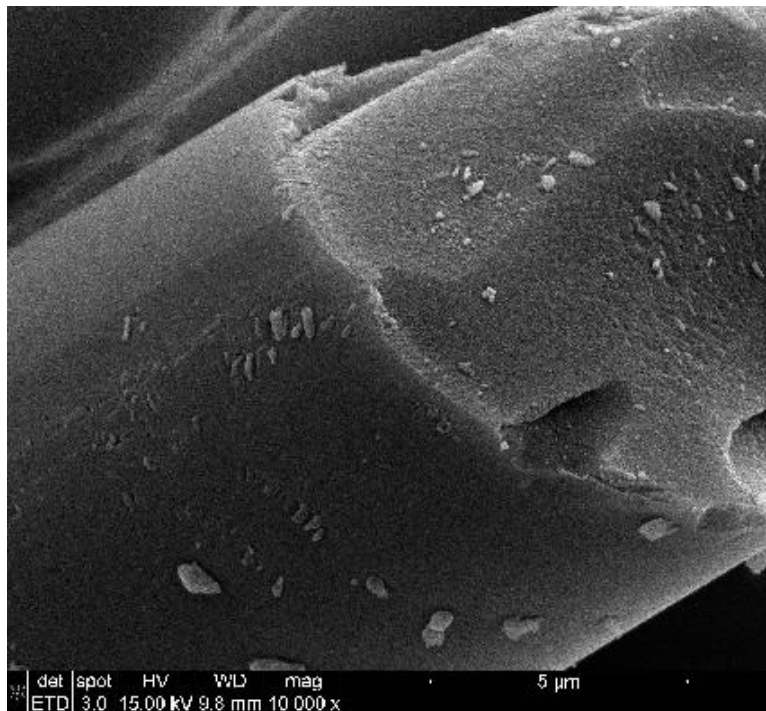

Figure 86 : SEM micrograph of the Hi-Nicalon S fiber tow specimen failed in creep at 1100°C in laboratory air (σ_{cr} = 467 MPa, t_f = 17.1 h).
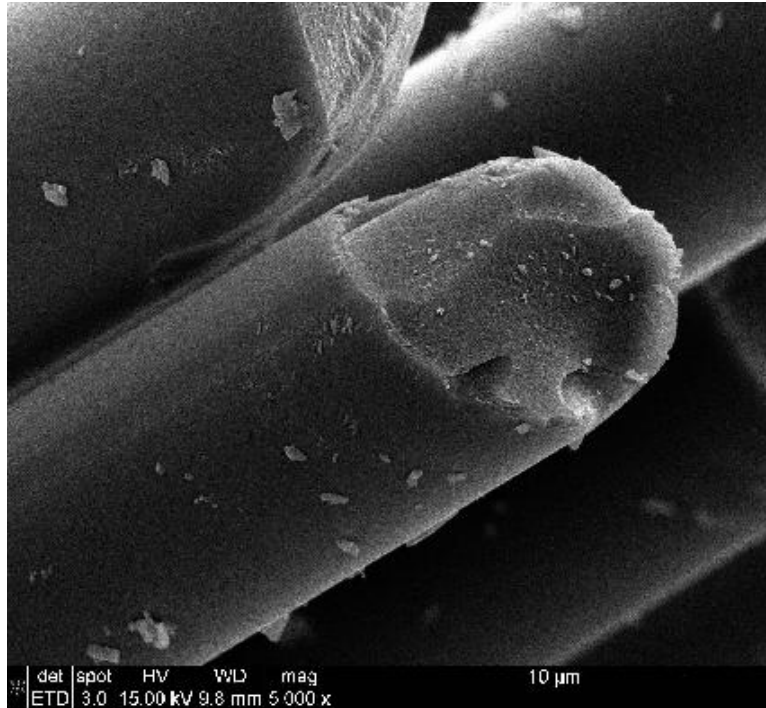
Figure 87 : SEM micrograph of the Hi-Nicalon S fiber tow specimen failed in creep at 1100°C in laboratory air (σ_{cr} = 467 MPa, t_f = 17.1 h).

Figure 88 : SEM micrograph of the Hi-Nicalon S fiber tow specimen failed in creep at 1100°C in laboratory air (σ_{cr} = 467 MPa, t_f = 17.1 h).
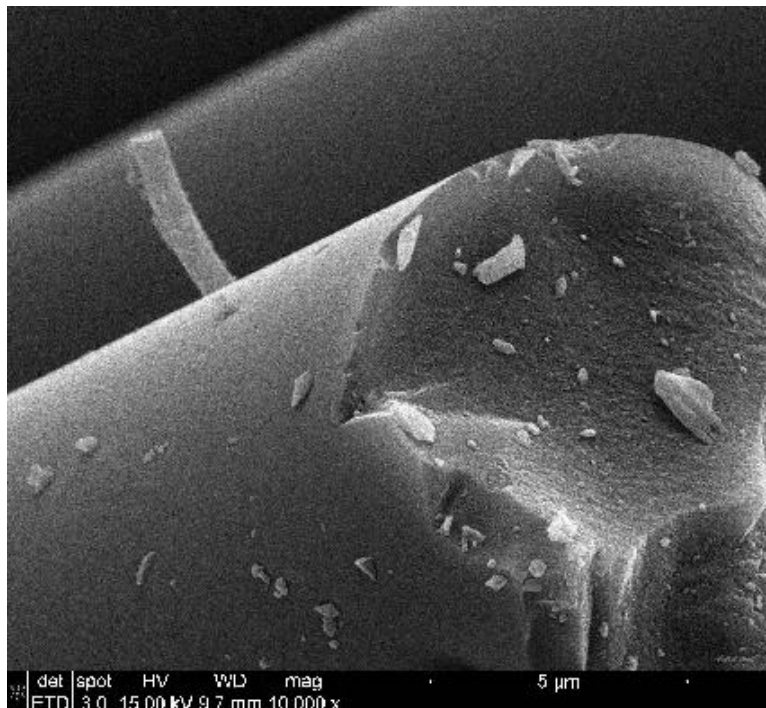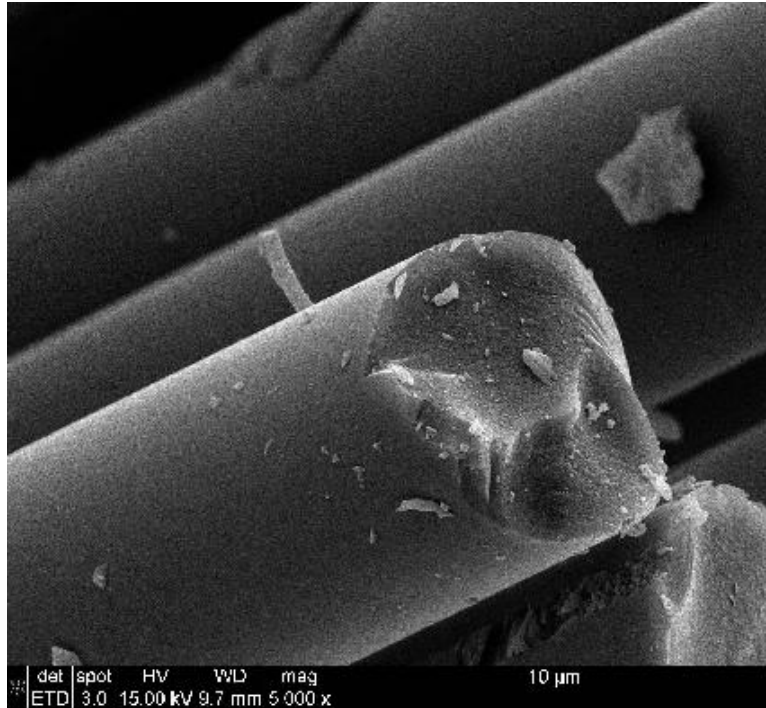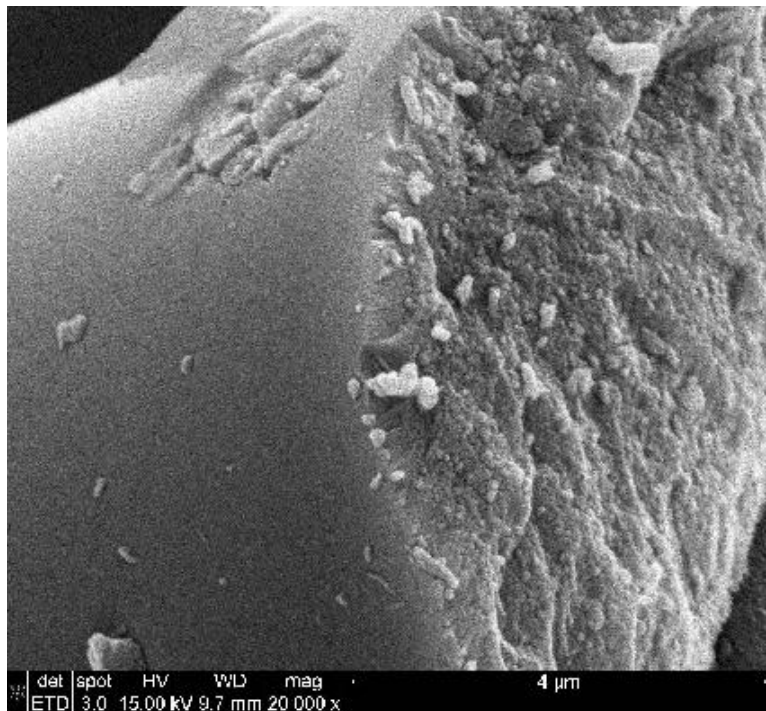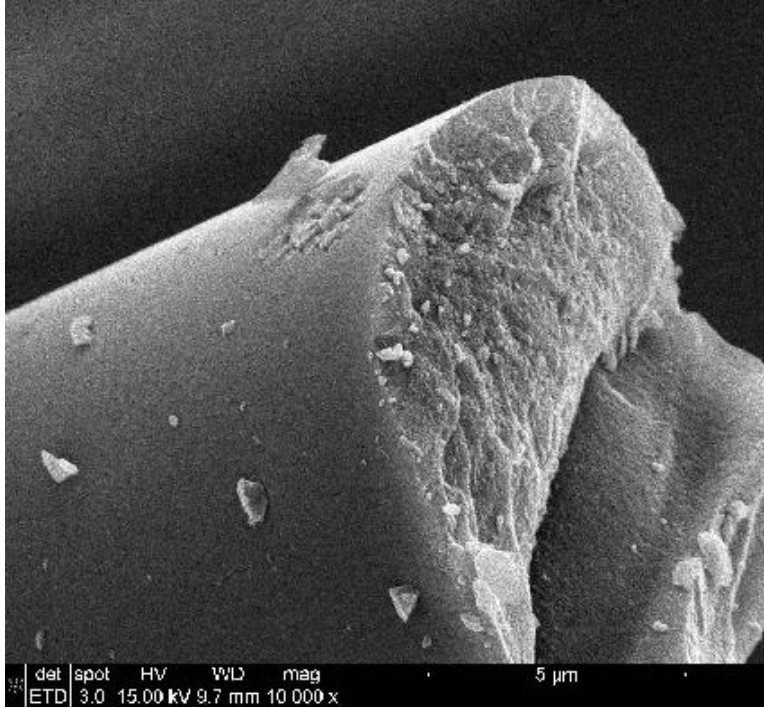
Figure 89 : SEM micrograph of the Hi-Nicalon S fiber tow specimen failed in creep at 1100°C in laboratory air (σ_{cr} = 467 MPa, t_f = 17.1 h).

Figure 90 : SEM micrograph of the Hi-Nicalon S fiber tow specimen failed in creep at 1100°C in steam (σ_{cr} = 154 MPa, t_f = .33 h).

Figure 91 : SEM micrograph of the Hi-Nicalon S fiber tow specimen failed in creep at 1100°C in steam (σ_{cr} = 154 MPa, t_f = .33 h).

Figure 92 : SEM micrograph of the Hi-Nicalon S fiber tow specimen failed in creep at 1100°C in steam (σ_{cr} = 154 MPa, t_f = .33 h).

Figure 93 : SEM micrograph of the Hi-Nicalon S fiber tow specimen failed in creep at 1100°C in steam (σ_{cr} = 154 MPa, t_f = .33 h).

Figure 94 : SEM micrograph of the Hi-Nicalon S fiber tow specimen failed in creep at 1100°C in steam (σ_{cr} = 154 MPa, t_f = .33 h).
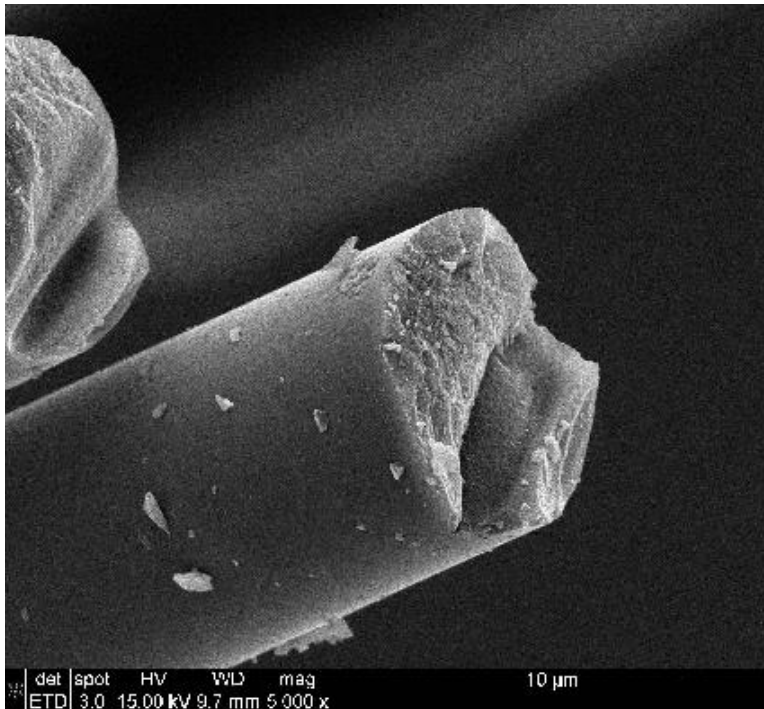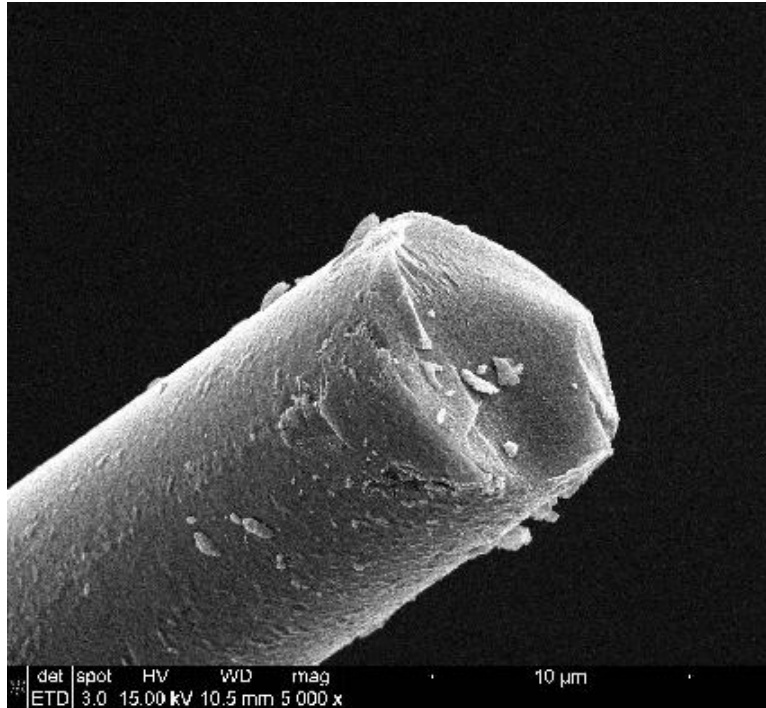
Figure 95 : SEM micrograph of the Hi-Nicalon S fiber tow specimen failed in creep at 1100°C in steam (σ_{cr} = 154 MPa, t_f = .33 h).
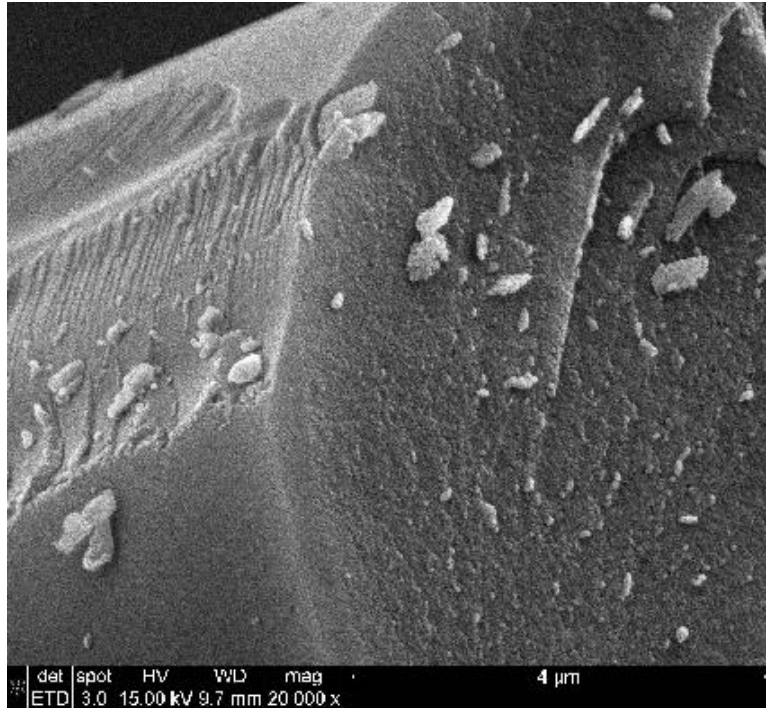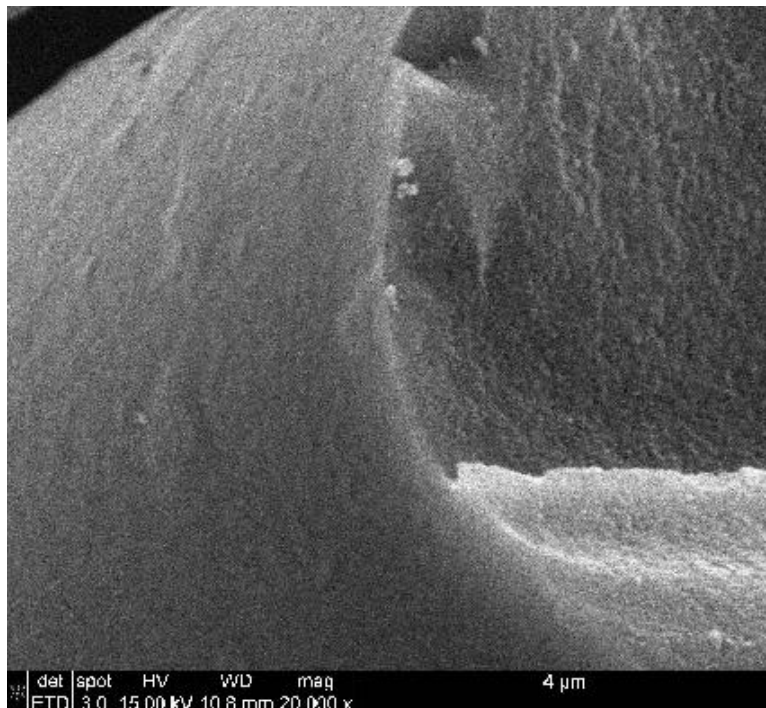

Figure 96 : SEM micrograph of the Hi-Nicalon S fiber tow specimen failed in creep at 1100°C in steam (σ_{cr} = 154 MPa, t_f = .33 h).
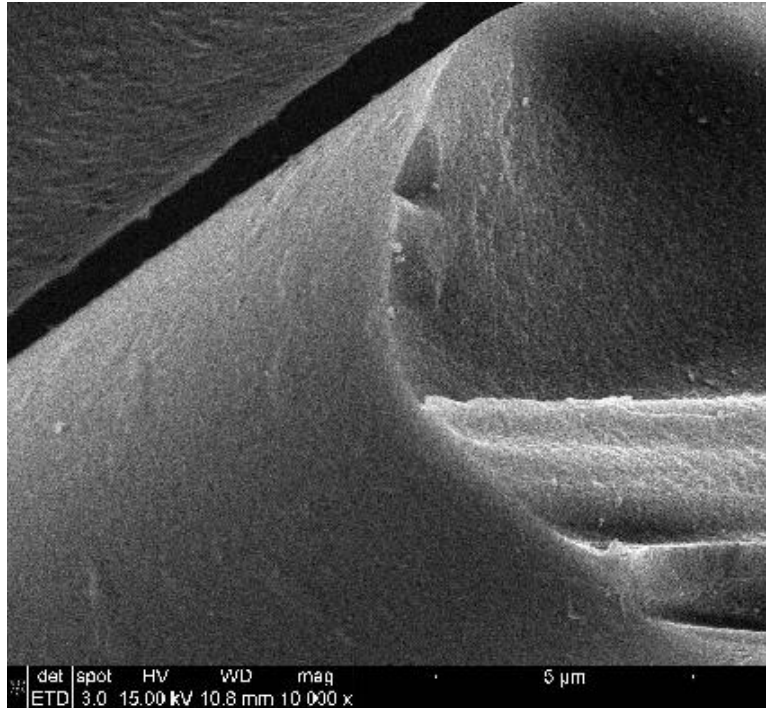
Figure 97 : SEM micrograph of the Hi-Nicalon S fiber tow specimen failed in creep at 1100°C in steam (σ_{cr} = 154 MPa, t_f = .33 h).
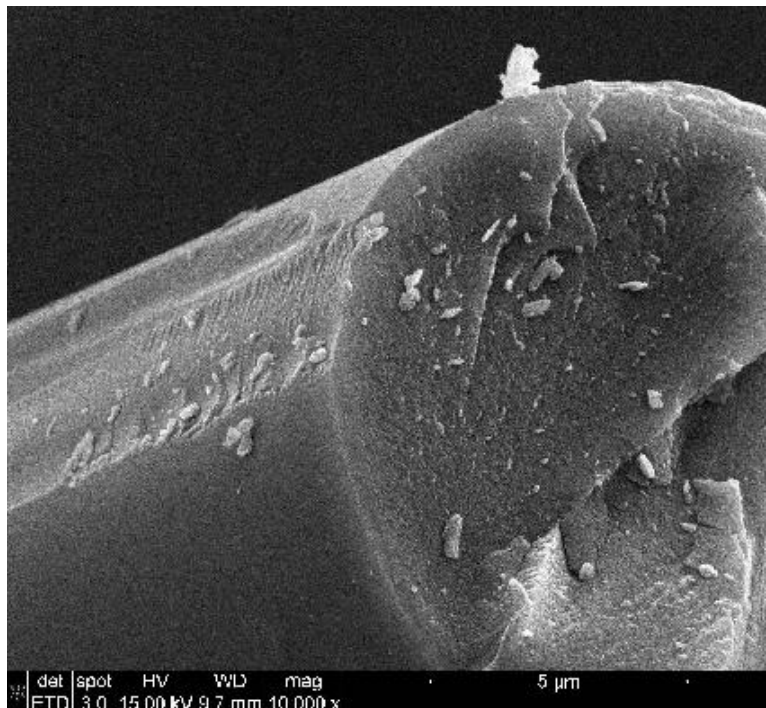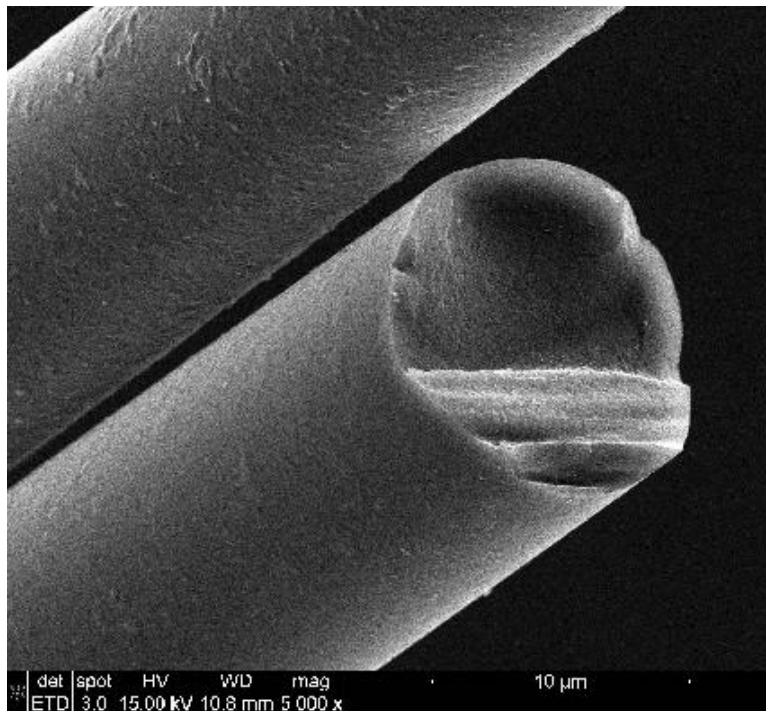

Figure 98 : SEM micrograph of the Hi-Nicalon S fiber tow specimen failed in creep at 1100°C in steam (σ_{cr} = 154 MPa, t_f = .33 h).
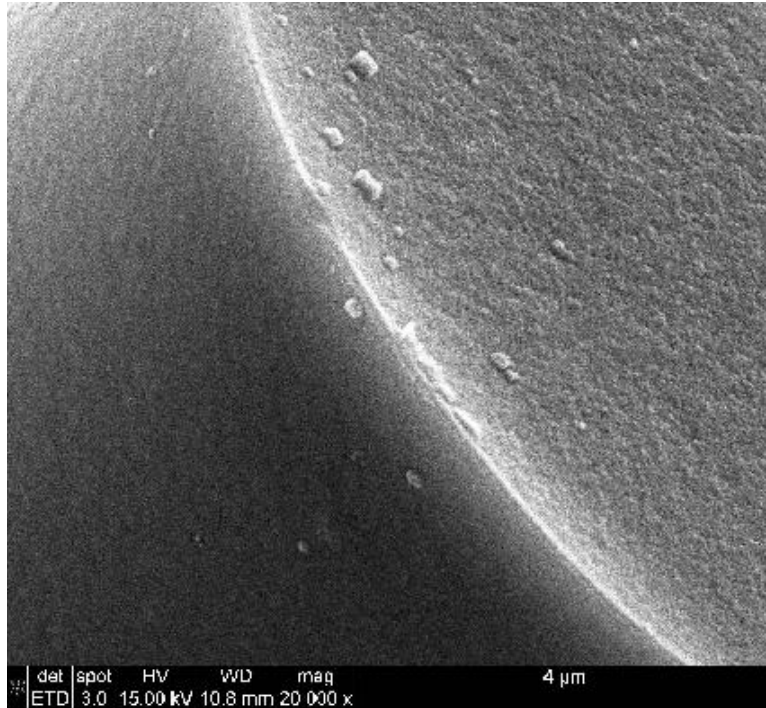
Figure 99 : SEM micrograph of the Hi-Nicalon S fiber tow specimen failed in creep at 1100°C in steam (σ_{cr} = 154 MPa, t_f = .33 h).
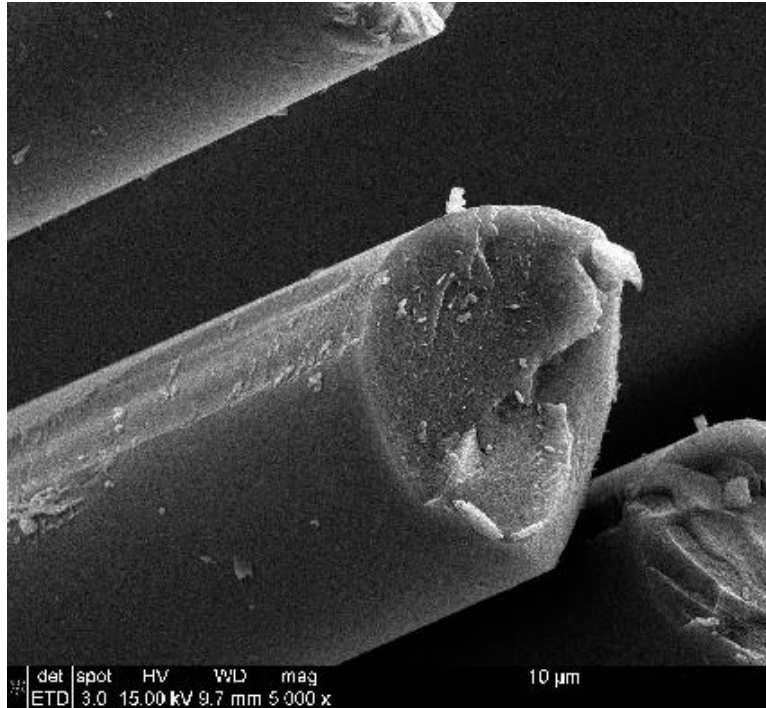

Figure 100 : SEM micrograph of the Hi-Nicalon S fiber tow specimen failed in creep at 1100°C in steam (σ_{cr} = 154 MPa, t_f = .33 h).
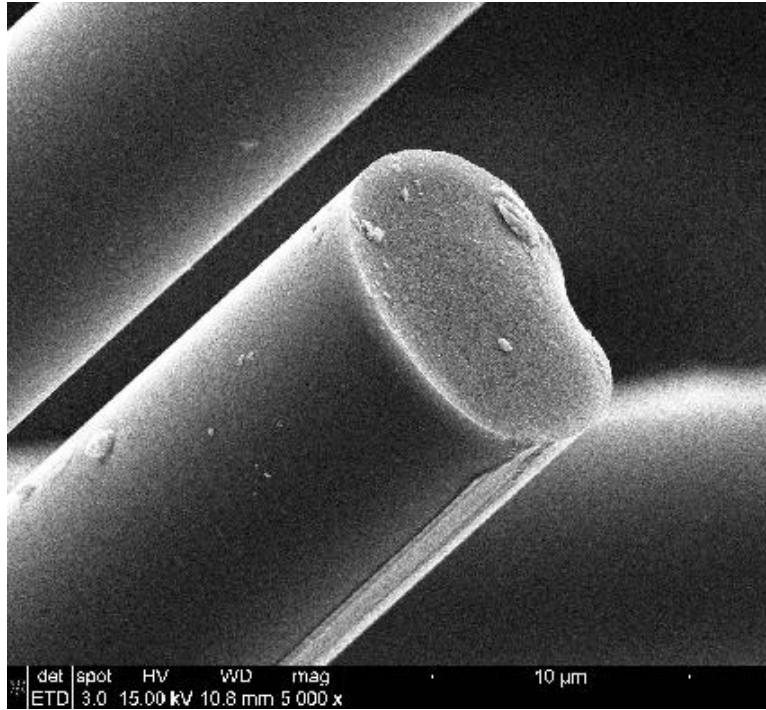
Figure 101 : SEM micrograph of the Hi-Nicalon S fiber tow specimen failed in creep at 1100°C in steam (σ_{cr} = 154 MPa, t_f = .33 h).
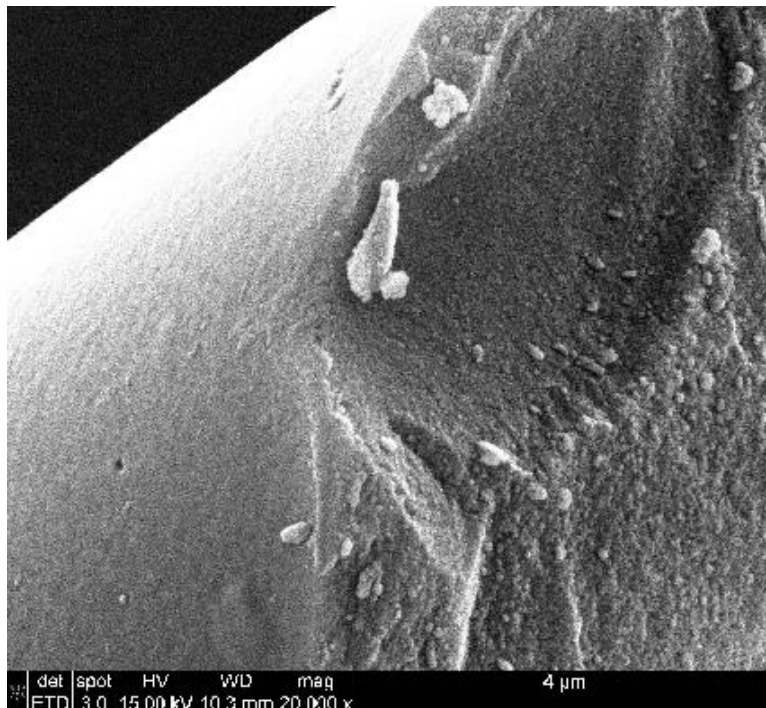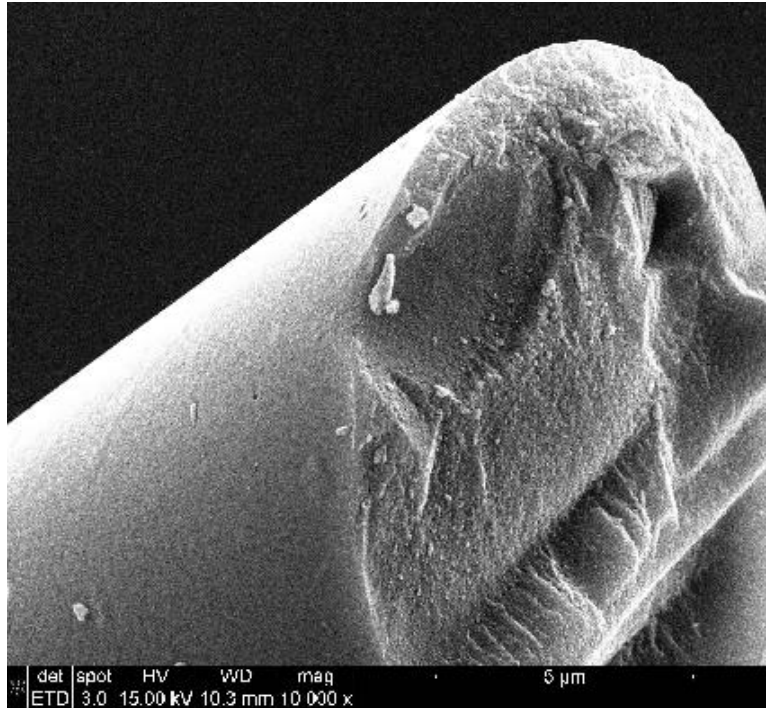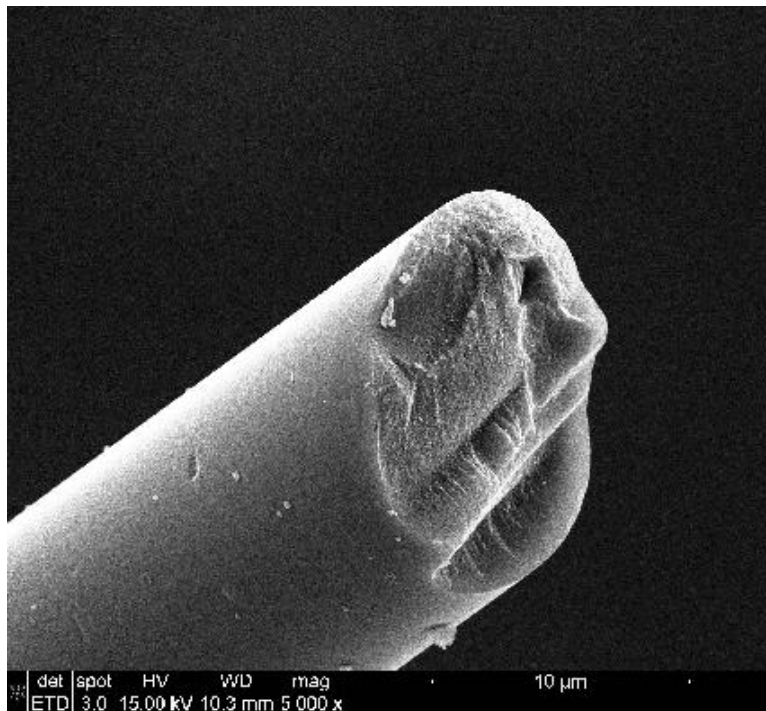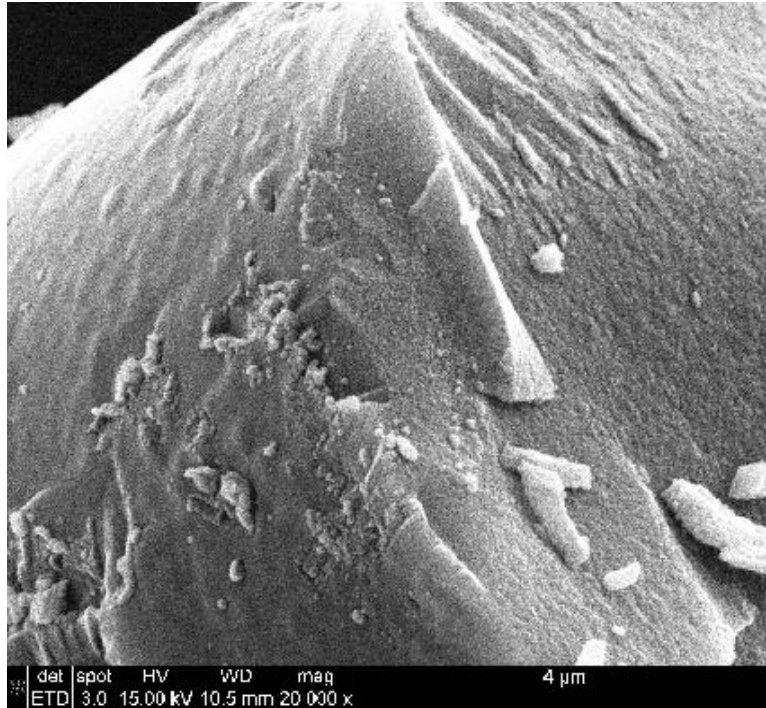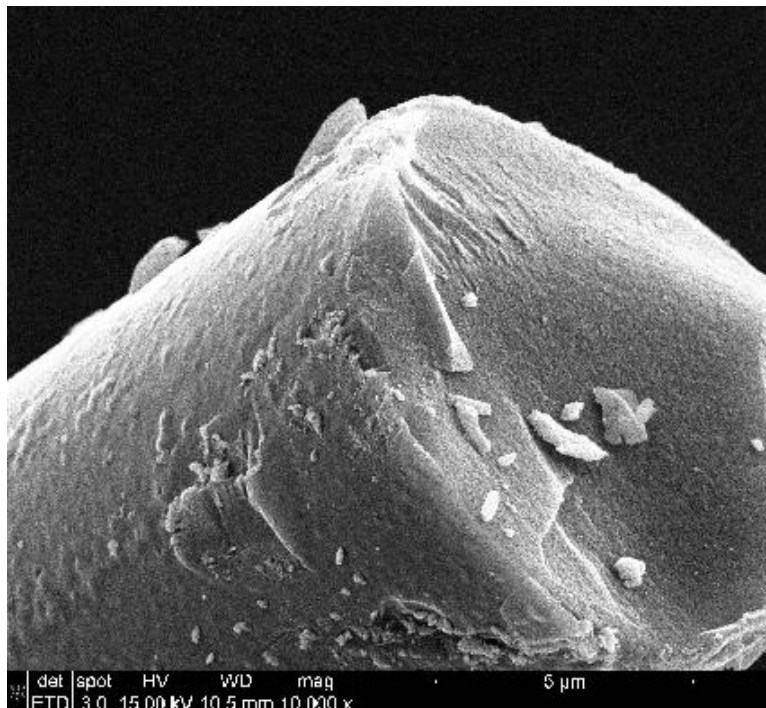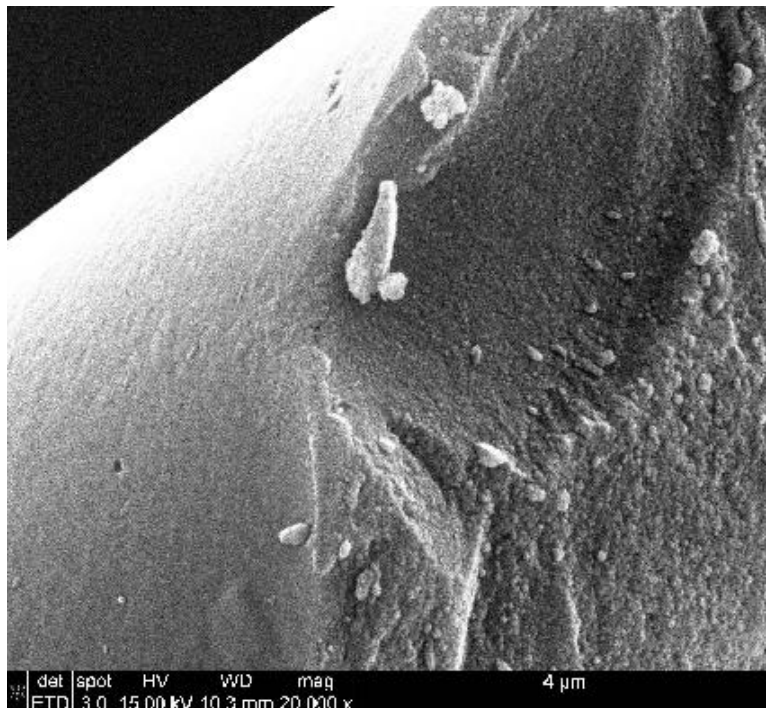

Figure 102 : SEM micrograph of the Hi-Nicalon S fiber tow specimen failed in creep at 1100°C in steam (σ_{cr} = 154 MPa, t_f = .33 h).
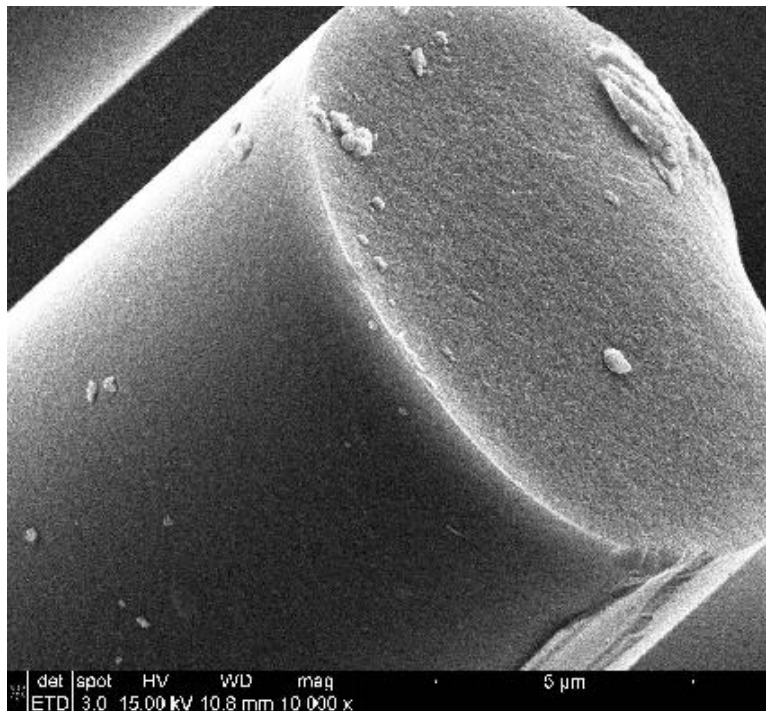
Bibliography

1. "Ceramic Matrix Composites," in Composite Materials Handbook, vol. 5, Department of Defense, 2002.

2. Air Force Link. "Raptor in Flight." U.S. Air Force photograph by Judson Brohmer. n. pag. http://www.af.mil/photos/index.asp?galleryID=40&page=6. 17 January 2005.

3. Armani, Clint . "Creep performance of oxide ceramic fiber materials atelevated temperature in air and in steam." PhD Dissertation, AFIT/DS/ENY/11-02. Graduate School of Engineering and Management, Air Force Institute of Technology (AU), Wright-Patterson AFB OH, March 2011.

4. S. I. Bae and S. Baik, "Sintering and grain growth of ultrapure alumina," Journal of Materials Science, vol. 28, (15), pp. 4197-4204, 1993.

5. A. Bunsell, A. Piant, "A review of the development of three generations of small diameter silicon carbide fibres", J Mater Sci, 41 (2006) 823–839

6. V. Calard and J. Lamon, "Failure of fiber bundles," Composites Science and Technology, vol. 64, (5), pp. 701-710, 2004.

7. H. R. Clauser, "Advanced composite materials," Scientific American, vol. 229, (1), pp. 36-44, 1973.

8. B. D. Coleman, "On the strength of classical fibres and fibre bundles," Journal of the Mechanics and Physics of Solids, vol. 7, pp. 60, 1958.

9. K. G. Dassios, M. Steen and C. Filiou, "Mechanical properties of alumina Nextel™ 720 fibres at room and elevated temperatures: tensile bundle testing," Materials Science and Engineering A, vol. 349, (1-2), pp. 63-72, 2003.

10. DiCarlo, J.A., H-M Yun, G.N. Morscher, and R.T Bhatt. "SiC/SiC Composites for 1200°C and Above." Handbook of Ceramic Composites. 2005.

11. J. A. DiCarlo, "Property goals and test methods for high temperature ceramic fibre reinforcement," Ceramics International, vol. 23, (4), pp. 283-289, 1997.

12. J. A. DiCarlo and H. M. Yun, "Fiber Test Development for Ceramic Composite Thermomechanical Properties," in , vol. Mechanical, Thermal, and Environmental Testing and Performance of Ceramic Composites and Components, ASTM STP 1392, M. G. Jenkins, E. Lara-Curzio and S. T. Gonczy, Eds. West Conshohocken, PA,: American Society for Testing and Materials, 2000.

13. A. G. Evans and F. W. Zok, "The physics and mechanics of fibre-reinforced brittle matrix composites," Journal of Materials Science, vol. 29, (15), pp. 3857-3896, 1994.

14. P. Forio, F. Lavaire, and J. Lamon, ''Delayed Failure at Intermediate Temperatures (600°C–700°C) in Air in Silicon Carbide Multifilament Tows,'' J. Am. Ceram. Soc., 87 [5] 888–93 (2004).

15. W. Gauthier and J. Lamon, ''Delayed Failure of Hi-Nicalon and Hi-Nicalon S Multifilament Tows and Single Filaments at Intermediate Temperatures (500–800°C),'' J. Am. Ceram. Soc., 92 [3] 702–09 (2009).

16. W. Gauthier, F. Pailler, J. Lamon and R. Pailler, "Oxidation of Silicon Carbide Fibers During Static Fatigue in Air at Intermediate Temperatures," J. Am. Ceram. Soc., 92 [9] 2067–2073 (2009).

17. V. H. Hammond, Creep Rupture of an Oxide/Oxide Composite Fiber. PhD Dissertation. University of Virginia, 2001.

18. R. S. Hay, G. E. Fair, "Hi-Nicalon-S oxidation and scale crystallization kinetics," Draft, Air Force Research Lab, Materials and Manufacturing Directorate, WPAFB, OH.

19. C. T. Herakovich, Mechanics of Fibrous Composites. New York: John Wiley & Sons, 1998.

20. H. Ichikawa, K. Okamura, and T. Seguchi, in "High temperature ceramic matrix composites II", edited by A. G. Evans and R. Naslain, Ceramic Transactions 58, (American Ceramic Soc., 1995) p. 65

21. T. Ishikawa, "Advances in Inorganic Fibers," Polymeric and Inorganic Fibers, vol. 178, 2005.

22. F. A. Kandil, "Tensile Creep of Ceramics: the Development of a Testing Facility," Int.J.High Technol.Ceram, vol. 4, (2-4), pp. 243, 1988.

23. R. J. Kerans, R. S. Hay, T. A. Parthasarathy and M. K. Cinibulk, "Interface Design for Oxidation-Resistant Ceramic Composites," J Am Ceram Soc, vol. 85, (11), pp. 2599, 2002.

24. Lamouroux F, Camus G, Thebault J., "Oxidation effects on the mechanical properties of 2D woven C/SiC composites," J Eur Ceram Soc 1994;14:177–88.

25. F. F. Lange, W. C. Tu and A. G. Evans, "Processing of damage-tolerant, oxidationresistant ceramic matrix composites by a precursor infiltration and pyrolysis method," Materials Science & Engineering A (Structural Materials: Properties, Microstructure and Processing), vol. A195, pp. 145-150, 1995.

26. H. H. Moeller, "Tensile testing of ceramic fiber tows," Ceram. Eng. Sci. Proc., vol. 6, pp. 558, 1985.

27. E. H. Moore, T. Mah and K. A. Keller, "3-D composite fabrication through matrix slurry pressure infiltration," Ceram. Eng. Sci. Proc., vol. 15, (4), pp. 113-120, 1994.

28. R. M. Morrell, "A tensile creep-testing apparatus for ceramic materials using simple knife-edge universal joints," Journal of Physics E (Scientific Instruments), vol. 5, (5), pp. 465-467, 1972.

29. R. Naslain, "Ceramic Matrix Composites," in European White Book on Fundamental Research in Materials Science, Max-Planck-Institut für Metallforschung, Stuttgart, Germany, 2001.

30. R. Naslain, "Design, preparation and properties of non-oxide CMCs for application in engines and nuclear reactors: an overview," Composites Science and Technology, vol. 64, (1), pp. 155-170, 2004.

31. Schmidt, S., H. Knabe, H. Immich, R. Mestring, and A. Gessler. "Advanced Ceramic Matrix Composite Material for Current and Future Propulsion Technology Applications." Acta Astronautica, 55, 2004: 409-420.

32. S. M. Sim and R. J. Kerans, "Slurry Infiltration of 3-D Woven Composites," Ceram. Eng. Sci. Proc., vol. 13, (9-10), pp. 632-641, 1992.

33. A. Szweda, M. L. Millard and M. G. Harrrison, "Fiber-reinforced ceramic-matrix composite member and method for making," U.S. Pat. No. 5 601 674, 1997.

34. W. P. Tai, T. Watanabe and N. S. Jacobson, "Delayed failure of Hi-Nicalon and Hi-Nicalon S multifilament tows and single filaments at intermediate temperatures(500°-800°C)," Journal of the American Ceramic Society, vol. 92, (3), pp. 702-709, 2009.

35. W. C. Tu, F. E. Lange and A. G. Evans, "Concept for a damage-tolerant ceramic composite with "strong" interfaces," Journal of the American Ceramic Society, vol. 79, (2), pp. 417-424, 1996.

36. D. J. Vaughan, "Fiberglass Reinforcement," in Handbook of Composites, 2nd ed. G. Lubin and S. T. Peters, Eds. London; New York: Chapman & Hall, 1998.

37. H. M. Yun, J. C. Goldsby and J. A. Dicarlo, "Tensile creep and stress-rupturebehavior of polymer derived SiC fibers," NASA TM-106692, 1994.

38. F. W. Zok and C. G. Levi, "Mechanical properties of porous-matrix ceramic composites," Advanced Engineering Materials, vol. 3, (1), pp. 15-23, 2001.

REPORT DOCUMENTATION PAGE				*Form Approved* *OMB No. 0704–0188*
The public reporting burden for this collection of information is estimated to average 1 hour per response, including the time for reviewing instructions, searching existing data sources, gathering and maintaining the data needed, and completing and reviewing the collection of information. Send comments regarding this burden estimate or any other aspect of this collection of information, including suggestions for reducing this burden to Department of Defense, Washington Headquarters Services, Directorate for Information Operations and Reports (0704–0188), 1215 Jefferson Davis Highway, Suite 1204, Arlington, VA 22202–4302. Respondents should be aware that notwithstanding any other provision of law, no person shall be subject to any penalty for failing to comply with a collection of information if it does not display a currently valid OMB control number. PLEASE DO NOT RETURN YOUR FORM TO THE ABOVE ADDRESS.				
1. REPORT DATE (DD–MM–YYYY) 22-03-2012	2. REPORT TYPE Master's Thesis		3. DATES COVERED (From — To) SEP 10 – MAR 12	
4. TITLE AND SUBTITLE Creep of Hi-Nicalon S Ceramic Fiber Tows at Elevated Temperature in Air and in Steam			5a. CONTRACT NUMBER	
			5b. GRANT NUMBER	
			5c. PROGRAM ELEMENT NUMBER	
6. AUTHOR(S) Steffens, Benjamin R.			5d. PROJECT NUMBER	
			5e. TASK NUMBER	
			5f. WORK UNIT NUMBER	
7. PERFORMING ORGANIZATION NAME(S) AND ADDRESS(ES) Air Force Institute of Technology Graduate School of Engineering and Management (AFIT/ENY) 2950 Hobson Way WPAFB OH 45433-7765			8. PERFORMING ORGANIZATION REPORT NUMBER AFIT/GMS/ENY/12-M03	
9. SPONSORING / MONITORING AGENCY NAME(S) AND ADDRESS(ES) Dr. Geoff Fair 2230 10th St Bldg 655 Rm 177 WPAFB, OH 45433 Geoff.Fair@WPAFB.AF.MIL (937) 255-0384			10. SPONSOR/MONITOR'S ACRONYM(S) AFRL/RXLN	
			11. SPONSOR/MONITOR'S REPORT NUMBER(S)	
12. DISTRIBUTION / AVAILABILITY STATEMENT APPROVED FOR PUBLIC RELEASE; DISTRIBUTION UNLIMITED				
13. SUPPLEMENTARY NOTES This material is declared a work of the U.S. Government and is not subject to copyright protection in the United States.				
14. ABSTRACT Structural aerospace components require materials to have superior long-term mechanical properties that can withstand severe environmental conditions, such as high temperatures, high pressures and moisture, whilst enduring the loads they are designed for. Ceramic-matrix composites (CMCs) are capable of maintaining excellent strength and creep resistance at high temperatures, which make them attractive candidate materials for aerospace applications, particularly in propulsion. Silicon Carbide (SiC) ceramic fibers have been used as constituent materials in CMCs, although oxidation of the SiC to SiO_2 has been a known degradation mechanism. Recently developed near stoichiometric SiC fibers have shown significant improvements in thermochemical stability; however performance of the new fibers at elevated temperatures in steam environments has not been studied thoroughly. The objective of this thesis is to investigate creep of near stoichiometric SiC fiber tows at elevated temperatures in air and in steam environments. The creep response of Hi-Nicalon™-S SiC fiber tows was investigated at 800°C and 1100°C in laboratory air and in steam environments. The creep stresses ranged from 76 MPa to 1560 MPa. Creep run-out was defined as 100 h at creep stress. The presence of steam significantly degraded the creep performance of the fiber tows both at 800°C and at 1100°C. The creep lifetimes of the Hi-Nicalon™-S SiC fiber tows were reduced by approximately an order of magnitude due to steam.				
15. SUBJECT TERMS Hi-Nicalon™-S, SiC fiber tows, ceramic fibers, creep, tension, steam environment, oxidation				
16. SECURITY CLASSIFICATION OF:			17. LIMITATION OF ABSTRACT	18. NUMBER OF PAGES	19a. NAME OF RESPONSIBLE PERSON Dr. Marina Ruggles-Wrenn
a. REPORT U	b. ABSTRACT U	c. THIS PAGE U	UU	120	19b. TELEPHONE NUMBER (Include Area Code) (937)255-3636, ext 4641 (Email: marina.ruggles-wrenn@afit.edu